Université Paris Cité

École doctorale Bio Sorbonne Paris Cité (ED 562)
Centre de Recherche sur l'Inflammation (UMR-S 1149)
Équipe « De l'inflammation au cancer dans les maladies digestives »

Thèse de doctorat en Biologie Cellulaire et Moléculaire

Clinical and molecular characterization of combined hepatocellular-cholangiocarcinoma

Par Elia GIGANTE

Dirigée par le Pr. Valérie PARADIS

Présentée et soutenue publiquement le 06 Décembre 2022

Devant un jury composé de :

Sébastien DHARANCY, PU-PH, Université de Lille, rapporteur
Christophe JUNOT, DR, Université Paris-Saclay, rapporteur
Julien CALDERARO, PU-PH, Université Paris-Est Créteil Val-de-Marne, examinateur
Chiara GUERRERA, PhD HDR, Université Paris Cité, examinatrice
Gérard THIEFIN, PU-PH, Université de Reims Champagne-Ardenne, examinateur
Valérie PARADIS, PU-PH, Université Paris Cité, Directrice

Remerciements



« diffusion non autorisée »

SUMMARY

1 LIST OF ABBREVIATIONS 5

2 ABSTRACTS 6

2.1 Résumé en Français 6

2.2 Abstract in English 8

2.3 Résumé détaillé en Français 10

3 INTRODUCTION 16

3.1 Epidemiology, classification and diagnosis of combined hepatocellular-cholangiocarcinoma 16

3.2 Treatment of cHCC-CCA 34

3.3 Conclusion, clinical aspects. 41

3.4 Heterogeneity of cHCC-CCA 42

3.5 General conclusions (genetics) 48

3.6 Mass spectrometry 51

3.7 MALDI imaging and tumors 63

3.8 Conclusion about MALDI and cancers 74

4 RESULTS FIRST AXIS: Improving the diagnosis of cHCC-CCA 75

Article 1: Combining imaging and tumor biopsy improves the diagnosis of combined hepatocellular-cholangiocarcinoma (Published) 75

5 RESULTS SECOND AXIS: Improving the management of systemic therapy of unresectable or metastatic cHCC-CCAs. 87

Article 2: Systemic treatments with tyrosine kinase inhibitor and platinum-based chemotherapy in patients with unresectable or metastatic hepatocholangiocarcinoma (Published) 87

6 RESULTS THIRD AXIS: Exhaustive molecular characterization of cHCC-CCA by MALDI imaging 102

6.1 Article: MALDI imaging, a multiplex approach without a priori, is a powerful tool for deciphering intra-tumoral heterogeneity: combined hepato-cholangiocarcinomas as proof of concept (In preparation) 102

6.2 MSI on TMAs of cHCC-CCA 119

7 GENERAL CONCLUSIONS 154

8 BIBLIOGRAPHY 155

9 FIGURES AND TABLES LIST 177

10 LISTE DES ÉLÉMENTS SOUS DROITS 179

11 TABLE OF CONTENTS 180

1 LIST OF ABBREVIATIONS

Acetonitrile (ACN)
Artificial intelligence (AI)
Alpha-cyano-4-hydroxycinnamic acid (CHCA)
Alpha-fetoprotein (AFP)
Ammonium bicarbonate (ABC)
Area under the curve (AUC)
Arterial phase hyperenhancement (APHE)
Carbohydrate antigen 19-9 (CA19-9),
cHCC-CCA tumors from cHCC-CCA TMAs (MT-cHCC-CCA)
Cholangiocarcinoma (CCA)
Cholangiolocarcinoma (CLC).
Computed tomography (CT)
Conductive indium tin oxide (ITO)
Contrast-enhanced ultrasound (CEUS)
Cytokeratin 19 (CK19)
Cytokeratin 7 (CK7)
Disease-free survival (DFS)
Desorption Electrospray Ionization (DESI)
Epithelial cell adhesion molecule (EpCAM)
Formalin - Fixed, Paraffin – Embedded (FFPE)
Glypican-3 (GPC-3)
HCC controls (CT-HCC)
HCC from cHCC-CCA TMAs (MT-HCC)
Hepatic venous pressure gradient (HVPG)
Hepatitis B virus (HVB)
Hepatitis C virus (HCV)
Hepatocarcinoma (HCC)
Hepatocellular-cholangiocarcinoma (cHCC-CCA)
Hepatocyte paraffin 1 (HepPar1)
Hierarchical clustering analysis (HCA),
Intrahepatic cholangiocarcinoma (iCCA)
iCCA controls (CT-iCCA)
iCCA from cHCC-CCA TMAs (MT-iCCA)
Immunohistochemistry (IHC)
Intermediate cell carcinoma (INT)
Intratumor heterogeneity (ITH)
Liver transplantation (LT)
Loss of heterozygosity (LOH)
Magnetic Resonance Imaging (MRI)
Mass spectrometry imaging (MSI)
Matrix Assisted Laser Desorption Ionisation (MALDI)
Microvascular invasion (MIV)
Nonalcoholic steato-hepatitis (NASH)
Non-classifiable tumors from cHCC-CCA TMAs (MT-NC)
Overall Survival (OS)
Pancreatic ductal carcinoma (PDAC).
Pancreatic intraductal mucinous neoplasms (IPMNs)
Principal component analysis (PCA)
Primary liver cancers (PLC).
Radioembolization (SIRT)
Receiver Operating Characteristic (ROC)
Root Mean Square (RMS)
Sal-like protein 4 (SALL4)
Score Albumine/bilirubine (ALBI)
Secondary-Ion Mass Spectrometry (SIMS)
Surveillance, Epidemiology, and End Results database (SEER)
Signal-to-Noise Ratio (S/N)
Stochastic t-distributed neighbor embedding (t-SNE)
Time of flight (TOF)
Tissue microarrays (TMA)
Total ion current (TIC)
Transarterial chemoembolization (TACE)
Trifluoroacetic acid (TFA)
Tyrosine kinase (TKI)
World health organization (WHO)

2 ABSTRACTS

2.1 Résumé en Français

Contexte scientifique : Les carcinomes primitifs du foie incluent un large spectre de tumeurs, dont les carcinomes hépatocellulaires (HCC), les cholangiocarcinomes (CCA) et les hépato-cholangiocarcinomes (cHCC-CCA) qui comportent les deux contingents (HCC et CCA) au sein de la même lésion. En raison d'une hétérogénéité intra-tumorale importante, le diagnostic morphologique des cHCC-CCA est difficile. De plus, les études visant à évaluer son pronostic ont fourni des résultats discordants, avec un comportement tantôt plus proche du HCC, tantôt plus proche du cholangiocarcinome intrahépatique (iCCA). De même, la prise en charge thérapeutique des cHCC-CCA n'est pas aussi bien codifiée que pour les HCC ou les iCCA ; le traitement préconisé pour les tumeurs résécables restant la chirurgie. Les chimiothérapies testées sont basées sur les molécules indiquées dans les HCC ou iCCA, sans rationnel scientifique spécifique. Une prise en charge adaptée des patients avec cHCC-CCA repose donc sur une meilleure connaissance et caractérisation morphologique de ces tumeurs composites. Mon travail s'est articulé selon un axe clinique (Projets 1 et 2) et un axe fondamental (Projet 3). Projet 1, diagnostique : Nous avons démontré que la combinaison de caractéristiques morphologiques (macroscopiques *via* l'imagerie et histomoléculaires *via* la biopsie) est plus performante par rapport à chacune des modalités prises séparément. Toutefois, le développement de nouveaux marqueurs tissulaires permettrait d'améliorer son diagnostic pré-opératoire (cf projet 3). Projet 2, thérapeutique : Pour remédier au manque de preuves scientifiques concernant les traitements systémiques du cHCC-CCA métastatique/non résécable, nous avons rapporté dans une cohorte nationale multicentrique que l'efficacité des inhibiteurs de la tyrosine kinase (TKI) ou de la chimiothérapie à base de platine était comparable. En outre, dans notre étude, le score ALBI (Albumine/bilirubine) prédisait la survie des patients atteints de cHCC-CCA. Grâce à une comparaison avec des cohortes de HCC et

CCA métastatiques/non résécables appariés, traités par chimiothérapie, nous avons observé que la médiane de survie après traitements systémiques était superposable dans les trois types tumoraux (cHCC-CCA, HCC et iCCA). Projet 3, analyse moléculaire : Afin d'obtenir une caractérisation moléculaire exhaustive des cHCC-CCA, nous avons utilisé une approche d'imagerie MALDI (spectrométrie de masse *in situ*), permettant l'obtention de profils peptidiques à haute résolution spatiale directement à partir de coupes tissulaires fixées sans étape préalable de marquage. Dans le but d'explorer de façon plus précise l'hétérogénéité intra-tumorale, nous avons analysé en MALDI des lames entières de cHCC-CCA reséqués. Cette analyse a permis d'identifier des zones tumorales supplémentaires non détectées par les techniques conventionnelles. Nous avons aussi construit des tissue micro-arrays (TMA) à partir d'une cohorte de cHCC-CCA reséqués et comparé les profils peptidiques avec des HCC et iCCA. Nous avons ainsi identifié un set de marqueurs moléculaires peptidiques spécifiques des cHCC-CCA. Le potentiel diagnostique et pronostique de ces marqueurs a été également évalué. En conclusion, les travaux présentés, en contribuant à une meilleure description des cHCC-CCA tant sur le plan clinique que moléculaire, permettront d'améliorer la prise en charge des patients.

Mots clés : Hépato-cholangiocarcinomes, carcinomes hépatocellulaires, cholangiocarcinomes, diagnostique, imagerie MALDI, traitements systémiques

2.2 Abstract in English

Scientific background: Primary liver carcinomas include a wide spectrum of tumors, featuring hepatocellular carcinomas (HCC), cholangiocarcinomas (CCA) and hepato-cholangiocarcinomas (cHCC-CCA), which display both contingents (HCC and CCA) within the same lesion. Due to significant intra-tumor heterogeneity, the morphological diagnosis of cHCC-CCA is challenging. In addition, studies aiming at evaluating its prognosis have provided discordant results, with behavior either closer to HCC, either closer to intrahepatic cholangiocarcinomas (iCCA). Similarly, the therapeutic management of cHCC-CCA is not as well codified as for HCC or CCA; the recommended treatment for resectable tumors remaining surgery. The chemotherapies currently used are based on molecules indicated in HCCs or CCAs, without any scientific rationale. Appropriate management of patients with cHCC-CCA is therefore based on better knowledge and morphological characterization of these composite tumors. My project is articulated into one clinical axis (Projects 1 and 2) and one basic axis (Project 3). Project 1, diagnostic: We have demonstrated that the combination of morphological characteristics (macroscopic *via* imaging and histomolecular *via* tumor biopsy) is more performant compared to each of the modalities taken separately. However, the development of new tissue markers would improve its preoperative diagnosis (see project 3). Project 2, Therapeutics: To address the lack of scientific evidence regarding systemic treatments for metastatic/unresectable cHCC-CCA, we reported in a national multicenter cohort that the efficacy of tyrosine kinase inhibitors (TKIs) or chemotherapy platinum-based was comparable. In addition, in our study, the ALBI (Albumin/bilirubin) score predicted the survival of patients with cHCC-CCA. Through a comparison with matched cohorts of metastatic/unresectable HCC and iCCA treated with chemotherapy, we observed that the median survival after systemic treatments was similar in the three tumor types. Project 3, molecular analysis: In order to offer an exhaustive molecular characterization of cHCC-CCA, we used a MALDI imaging approach

(*in situ* mass spectrometry) that provides high resolution spatialized molecular profiles directly from fixed tissue sections without any prior labeling step. To explore more precisely intra-tumor heterogeneity, we analyzed in MALDI-MSI whole slides of resected cHCC-CCA. This analysis made it possible to identify additional tumor areas not detected by conventional techniques. We built then tissue micro-arrays (TMA) from a cohort of resected cHCC-CCAs and compared their peptide profiles with HCCs and iCCAs. We have thus identified a set of peptide markers specific for cHCC-CCA. The diagnostic and prognostic potential of these markers was also evaluated. In conclusion, this work provides further insights in the characterization of cHCC-CCA that will contribute to a better management of patients.

Keywords: Combined hepatocellular-cholangiocarcinomas, hepatocellular carcinomas, cholangiocarcinomas, diagnosis, MALDI imaging, systemic treatments

2.3 Résumé détaillé en Français

Caractérisation clinique et moléculaire des hépato-cholangiocarcinomes

Contexte scientifique : Les carcinomes primitifs du foie englobent un large éventail de tumeurs, notamment les carcinomes hépatocellulaires (HCC), les cholangiocarcinomes (CCA) et les hépato-cholangiocarcinomes (cHCC-CCA) qui présentent les deux contingents (HCC et CCA) au sein de la même lésion. Les données provenant des bases de données indiquent que 0,75% de tous les cancers primitifs du foie (PLC) peuvent être attribués aux cHCC-CCA, avec une incidence estimée à 0,05/100 000 dans la population générale. Selon la classification de l'OMS de 2019, la fréquence est estimée à 2-5% des PLC. Les facteurs de risque associés aux cHCC-CCA sont partagés avec d'autres PLC et comprennent le virus de l'hépatite B (HBV), le virus de l'hépatite C (HCV), la consommation excessive d'alcool et la cirrhose. L'association avec la cirrhose est décrite dans les différentes séries de 26% à 81% ; la plupart des cas rapportés proviennent d'Asie de l'Est et sont liés à l'infection par le HBV. Au fil du temps, plusieurs classifications morphologiques ont été proposées et utilisées successivement dans la littérature, entraînant une certaine confusion. La dernière classification (WHO 2019) définit le cHCC-CCA comme une tumeur composite associant un contingent de HCC et un contingent de CCA parfois accompagnés à des secteurs transitionnels au sein de la même tumeur. Les PLC composés de cholangiolocarcinome sont finalement reclassés dans l'iCCA comme une variante histotypique.

D'un point de vue moléculaire, le cHCC-CCA est probablement monoclonal, dérivé d'une cellule d'origine commune au HCC et à l'iCCA. Les caractéristiques génomiques du cHCC-CCA seraient plus proches du HCC que de l'iCCA, bien que certains cHCC-CCA présentent des caractéristiques génomiques plus proches de l'iCCA. Les facteurs de risque hépatiques, tels que l'infection virale (hépatite B), pourraient être associés à des caractéristiques génétiques

spécifiques dans le cHCC-CCA. Près de 24% des altérations génétiques dans le cHCC-CCA peuvent faire l'objet de traitements ciblés.

En raison d'une importante hétérogénéité intra-tumorale, le diagnostic morphologique du cHCC-CCA est difficile. Celui-ci est basé sur l'analyse histologique de la biopsie tumorale ou de la pièce opératoire. Les marqueurs immunohistochimiques (IHC) ne sont pas obligatoires pour un diagnostic positif, mais sont des arguments en faveur du diagnostic. Dans l'ensemble, la radiologie est essentielle pour guider la biopsie du foie, notamment en assurant des biopsies multiples dans chaque contingent tumoral, et pour évaluer la stadification de la tumeur. Il faut donc reconnaître que les performances diagnostiques de l'imagerie seule ne sont pas suffisantes pour le diagnostic du cHCC-CCA.

De plus, les études visant à évaluer son pronostic ont donné des résultats discordants, avec un comportement tantôt plus proche du HCC, tantôt plus proche du CCA. La prise en charge thérapeutique du cHCC-CCA n'est pas aussi bien codifiée que pour le HCC ou l'iCCA ; le traitement recommandé pour les tumeurs résécables reste la chirurgie. Les résultats après une résection hépatique pour cHCC-CCA semblent plus proches des patients atteints d'iCCA et plus mauvais que pour les patients atteints de HCC, avec une survie réduite. La transplantation hépatique (LT) pour le cHCC-CCA n'a pas encore suffisamment de preuves pour être proposée, mais cette approche est attrayante, surtout pour les petites tumeurs.

Dans l'ensemble, peu de données sont actuellement disponibles pour soutenir la valeur des traitements locorégionaux chez les patients atteints de cHCC-CCA, bien que certaines données rétrospectives suggèrent un rôle pour les traitements intra-artériels chez des patients sélectionnés dont les tumeurs présentent un rehaussement artériel. Les chimiothérapies utilisées chez les patients avec un cancer à un stade avancé sont basées sur les molécules indiquées dans

le HCC ou le CCA, sans justification scientifique spécifique. En ce qui concerne les connaissances actuelles sur le cHCC-CCA, nous pouvons conclure que :

1) Le cHCC-CCA est considéré comme une tumeur rare représentant près de 5% des néoplasies primitives du foie, mais en réalité cette tumeur est probablement largement sous-diagnostiquée.

2) La définition pathologique du cHCC-CCA a considérablement évolué au fil du temps. Un consensus récent a reclassé le cholangiolocarcinome (CLC) dans le groupe des CCA, alors que les cHCC-CCA sont histologiquement caractérisés par la présence de contingents de CHC et de CCA au sein de la même lésion.

3) D'un point de vue moléculaire, le cHCC-CCA dérive d'une cellule d'origine commune au HCC et au CCA. Dans la plupart des cohortes dérivées de patients infectés par une infection virale (HBV), le cHCC-CCA est génétiquement plus proche du HCC que du CCA, bien que certains cHCC-CCA présentent des caractéristiques génomiques plus proches des CCA.

4) La combinaison de l'imagerie et de l'histologie, principalement à l'aide d'une biopsie tumorale, est nécessaire pour le diagnostic du cHCC-CCA avec une performance encore sous-optimale. De nouveaux outils de diagnostic sont nécessaires.

5) La résection hépatique, lorsqu'elle est possible, est le principal traitement du cHCC-CCA.

6) Il n'y a pas de thérapies systémiques ou locorégionales actuellement validées dans le traitement du cHCC-CCA non résécable.

7) Le cHCC-CCA peut être considéré comme une tumeur à faible survie à long terme, qui nécessite des stratégies diagnostiques et thérapeutiques plus appropriées.

Mon projet s'articule selon un axe clinique (projets 1 et 2) et un axe fondamental (projet 3).

Projet 1, diagnostic : notre première étude a évalué la performance de la biopsie hépatique et de l'imagerie pré-opératoire en analysant les cHCC-CCA réséqués avec l'imagerie préopératoire et la biopsie tumorale disponibles. La présence d'un profil de type mixte en imagerie avait une sensibilité de 48% et une spécificité de 81% pour le cHCC-CCA. Alors que le diagnostic de

cHCC-CCA posé sur la biopsie concernait 8/21 patients (38%), la sensibilité était de 48% avec une spécificité de 100% en intégrant des marqueurs immunophénotypiques. Lorsque l'imagerie et la biopsie suggéraient le diagnostic de cHCC-CCA, la sensibilité et la spécificité étaient respectivement de 60% et 82%. Nous avons ainsi démontré pour la première fois qu'une stratégie en deux temps, radiologie et biopsie, améliorait la performance diagnostique. Nos données confirment également l'apport des marqueurs immunophénotypiques à l'histologie conventionnelle. Bien que cela ne soit pas facile à proposer dans la pratique clinique, augmenter le nombre de passages de biopsies guidées par l'image dans les tumeurs nous semble une pratique recommandée pour échantillonner au mieux tous les contingents tumoraux. Enfin, le développement de nouveaux marqueurs tissulaires permettrait d'améliorer le diagnostic préopératoire (voir projet 3).

Projet 2, Thérapeutique : Afin de remédier au manque de preuves scientifiques concernant les traitements systémiques du cHCC-CCA métastatique/non résécable, nous avons évalué l'efficacité des inhibiteurs de tyrosine kinase (TKI) ou d'un traitement de chimiothérapie à base de platine dans une cohorte multicentrique nationale de 83 patients atteints de cHCC-CCA avancé ou non résécable. Les patients atteints de cHCC-CCA ont été comparés à des patients atteints de HCC et d'iCCA avancé traités par chimiothérapie (TKI ou chimiothérapie à base de platine respectivement). La survie globale (OS) des patients avec cHCC-CCA était de 12 mois (13 mois pour les iCCA et 11 mois pour les HCC). Les patients atteints de cHCC-CCA avaient la même survie que le HCC et l'iCCA après ajustement. Le score ALBI, la présence d'ascite et le tabagisme étaient indépendamment associés à l'OS chez les patients atteints de cHCC-CCA. Les patients traités par TKI ont eu une OS médiane de 8,3 mois, contre 11 mois pour les patients traités par chimiothérapie à base de platine ($p = 0,86$). Après ajustement pour le nombre et la taille des tumeurs, l'invasion vasculaire, l'ALBI, le MELD et la cirrhose, le type de traitement n'a pas influencé l'OS et la survie sans progression. En outre, différentes catégories du score

ALBI (albumine/bilirubine) permettaient de prédire la survie des patients. Ces résultats constituent une base pour justifier les attitudes cliniques utilisées empiriquement à ce jour.

Projet 3, analyse moléculaire : Afin d'obtenir une caractérisation moléculaire complète du cHCC-CCA, nous avons utilisé une approche d'imagerie MALDI (spectrométrie de masse in situ), qui permet d'obtenir des profils moléculaires spatialisés à haute résolution directement à partir de coupes de tissus fixés sans étape préalable de marquage. Pour mieux explorer l'hétérogénéité du cHCC-CCA, nous avons utilisé des lames entières de tumeurs et comparé les informations obtenues par les techniques protéomiques aux images histologiques et immunophénotypiques. Grâce à l'analyse non supervisée par segmentation, nous avons identifié des zones de tissu tumoral difficilement caractérisées par l'analyse de routine et décrit avec précision l'hétérogénéité intratumorale du cHCC-CCA. Deuxièmement, par une digestion in silico des différentes protéines utilisées pour caractériser le cHCC-CCA, nous avons développé une liste de peptides dont la distribution morphologique est superposable à celle de l'immunohistochimie conventionnelle. Dans certains cas, l'analyse de la distribution des peptides a permis d'identifier des zones non marquées par l'immunohistochimie (IHC). Notre étude est la première à proposer cette approche d'imagerie, selon laquelle le MALDI pourrait être utilisé de la même manière que l'IHC, en étant capable d'analyser des milliers de marqueurs d'intérêt après une seule acquisition. En théorie, en connaissant la structure d'une protéine, nous pourrions la rechercher même si un anticorps n'est pas disponible. Le MALDI possède toutes les caractéristiques pour améliorer l'analyse histologique standard. Nous avons également construit des TMA à partir d'une cohorte de cHCC-CCA réséqués et avons comparé les profils peptidiques avec ceux des HCC et des iCCA. Nous avons ensuite identifié un certain nombre de marqueurs peptidiques spécifiques aux cHCC-CCA. Le potentiel pronostique de ces marqueurs a également été évalué. Bien qu'il s'agisse d'une technique qui doit encore être

standardisée et validée dans ces applications cliniques, la combinaison des données acquises par différentes machines à différents moments nous a permis de confirmer que les données obtenues peuvent être homogènes entre les plateformes grâce à la synchronisation des spectres et donc être reproductibles. Cette approche nous a permis d'obtenir des signatures moléculaires pertinentes. Malgré les difficultés inhérentes dues à l'hétérogénéité moléculaire des différents tissus dérivés du foie, les TMA sont importantes pour la découverte de biomarqueurs de diagnostic et de pronostic. Cette technique nous a permis de réduire le temps d'analyse et d'assurer une condition expérimentale plus standardisée, permettant l'acquisition de données tant morphologiques que moléculaires. D'un point de vue analytique, nous pouvons affirmer que bien que le cHCC-CCA soit une entité considérée comme étant à cheval sur l'iCCA et le HCC, la présence de multiples nuances morphologiques et moléculaires en fait une entité distincte, difficile à classer, à diagnostiquer et à traiter en raison de son hétérogénéité. Nous pouvons donc suggérer que le cHCC-CCA est moléculairement différent du HCC et de l'iCCA. Dans notre étude, cependant, nous avons signalé plus de similitudes avec l'iCCA. Par conséquent, grâce au MALDI, une liste étendue de peptides différentiels d'intérêt a été développée qui pourrait permettre l'identification pré-thérapeutique de différents histotypes de foie. La nature monocentrique de notre étude MSI nécessite pourtant une validation externe pour affirmer sa validité à grande échelle. En conclusion, notre travail a contribué à améliorer les connaissances sur le cHCC-CCA en combinant des approches conventionnelles et innovantes.

3 INTRODUCTION

3.1 Epidemiology, classification and diagnosis of combined hepatocellular-cholangiocarcinoma

3.1.1 Epidemiology

Hepatocellular carcinoma (HCC) and cholangiocarcinoma (CCA) together make up almost 95% of all primary liver cancers (PLCs). HCC alone accounts for 85% of PLCs, while CCA accounts for about 10%. The remaining PLCs correspond to combined hepatocellular cholangiocarcinoma (cHCC-CCA) which is defined histologically by the coexistence of HCC and intrahepatic CCA (iCCA) in the same lesion. (Allen et Lisa 1949)(Koster et Kasman 1932).

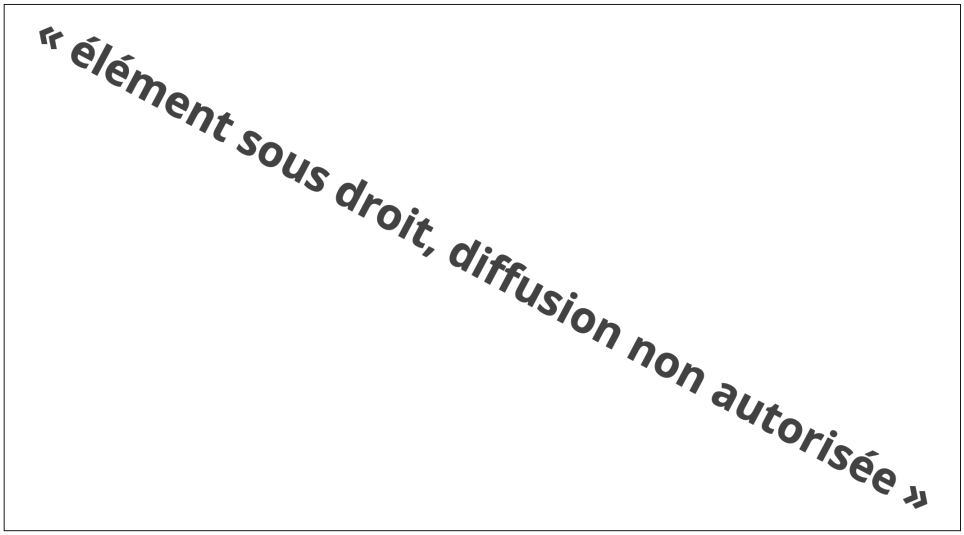


Figure 1: Prevalence and macroscopical appearance of cHCC-CCA

Adapted from Paradis et al (Paradis et Zucman-Rossi 2022)

3.1.1.1 Incidence and prevalence

Data from large databases indicate that a proportion of 0.75% of all PLCs could be attributed to cHCC-CCAs with an estimated incidence of 0.05/100 000 in the general population (Garancini et al. 2014; Ramai et al. 2019)(Kudo et al. 2020). The incidence in the various cohorts based on single-center studies of resected or autopsy patients is variable, ranging from 2.4% to 5.3% of PLCs. According to the 2019 WHO classification, the reasonable frequency is estimated to be between 2% and 5% of PLCs (E. Brunt et al. 2018; Sempoux, s. d.)(Goodman et al. 1985)(Ng et al. 1998)(Allen et Lisa 1949)(Jarnagin et al. 2002)(Lee et al. 2006)(Edmondson et Steiner 1954). However, these studies have limitations that potentially lead to an inaccurate assessment of the true incidence of cHCC-CCA; firstly, because they included a limited number of patients with confirmed histology according to anatomopathological classifications. Furthermore, when available, histology is based on surgical specimens included in retrospective studies. In some studies, also based on social security data, the diagnosis of cHCC-CCA was obtained from the discordance between histology and serum markers (e.g. diagnosis of HCC with elevated CA 19-9 or positive histology for CCA and elevated alpha-fetoprotein) or histology (e.g. positive histology for HCC and presence of histological markers of CCA). Adding to the confusion is the fact that the definitions have changed several times over the years, changing the inclusion criteria for different studies (Gigante et al. 2021).

3.1.1.2 Risk factors

All PLCs share similar risk factors and thus include the known causes of chronic liver disease, cHCC-CCA are associated with: chronic hepatitis B virus (HBV) infection, chronic hepatitis C virus (HCV) infection, excessive alcohol consumption, with a male predominance (up to 79% of men) (Table 1)(Gigante et al. 2021). The association with cirrhosis is reported with different frequencies. For example, it is described in the different surgical series from Eastern countries

as ranging from 26 to 81%; the majority of cases from these geographical areas are related to HBV infection (E. Brunt et al. 2018)(Ng et al. 1998; Lee et al. 2006; Taguchi et al. 1996; C.-L. Liu et al. 2003; Gentile et al. 2020; Y.-M. Zhou et al. 2014). In Western countries, the rate of cirrhosis ranges from 0% to 52% with HCV as the leading cause in Spain (43%) and the United States (23%), while excessive alcohol consumption appears as the main etiology in France (40%) (Jarnagin et al. 2002)(G. Sapisochin et al. 2014)(M. L. Wells et al. 2015). These data are consistent with a systematic review of the literature that assessed how the prevalence of cirrhosis in patients with cHCC-CCA reaches up to 51.7% based on histological examination of liver explants or surgical specimen (Gentile et al. 2020). Thus, from a numerical point of view, it appears that cHCC-CCA straddles the line between iCCA (which is associated with a low rate of cirrhosis and HBV/HCV infection) and HCC (associated with a high rate of cirrhosis and HBV/HCV infection).

Table 1: Risk factors of hepatocholangiocarcinoma. Adapted from (Gigante et al. 2021)

Author and year	*Country*	*N histologically confirmed*	*Advanced fibrosis*	*HCV*	*HBV*	*Alcohol*	*Metabolic Syndrome*
Sasaki et al. 2017	*Japan*	*53*	*14/24 (58%)*	*9/19 (47%)*	*9/44 (21%)*	*2/19 (11%)*	*3/19 (16%)*
Xue et al. 2019	*China*	*121*	*54/115 (47%)*	*2/115 (2%)*	*89/115 (77%)*	-	-
Zhou et al 2017	*China*	*144*	*91/144 (63.2%)*	-	*101/144 (70%)*	*29/144 (20%)*	-
Okamura et al 2020	*Japan*	*89*	*30/89 (34%)*	*29/89 (33%)*	*37/89 (43%)*	-	-
Gentile et al 2019	*Systematic Review*	*437*	*226/437 (52%)*	*39/437 (9%)*	*264/437 (60%)*	-	-
Welles et al 2015	*USA*	*39*	*12/39 (31%)*	*9/39 (23%)*	*0/39*	*3/39 (8%)*	*2/39 (5%)*
*De Martin et al 2020**	*France*	*31*	*31/31 (100%)*	-	-	*40/75 53%*	-
Holzner et al 2020	*USA*	*47*	*20/47 (43%)*	*15/47 (32%)*	*22/47 (47%)*	-	-
Nguyen et al. 2022	*France-Vietnam*	*96*	*54/96 (56.3%)*	*22/93 (23.6%)*	*20/90 (22.2%)*	*37/82 (45.1%)*	*11/ 80 (13.7%)*
Calderaro et al. 2022	*Multicentrique*	*280*	*117/263 (44.5%)*	*58/280 (20.7%)*	*60/280 (21.4%)*	*59/280 (21.1%)*	*55/280 (19.6%)*

Only cHCC-CCA histologically confirmed were included (Goodman transitional type (type II)/Allen and Lisa type B or C/WHO classical type tumors and stem cell type with exception of CLC.

3.1.2 Pathological characterization of cHCC-CCA

As anticipated below, the diagnosis of cHCC-CCA requires at the microscopic evaluation the presence of both HCC and CCA areas, whatever their respective extent (Figures 2 and 3).

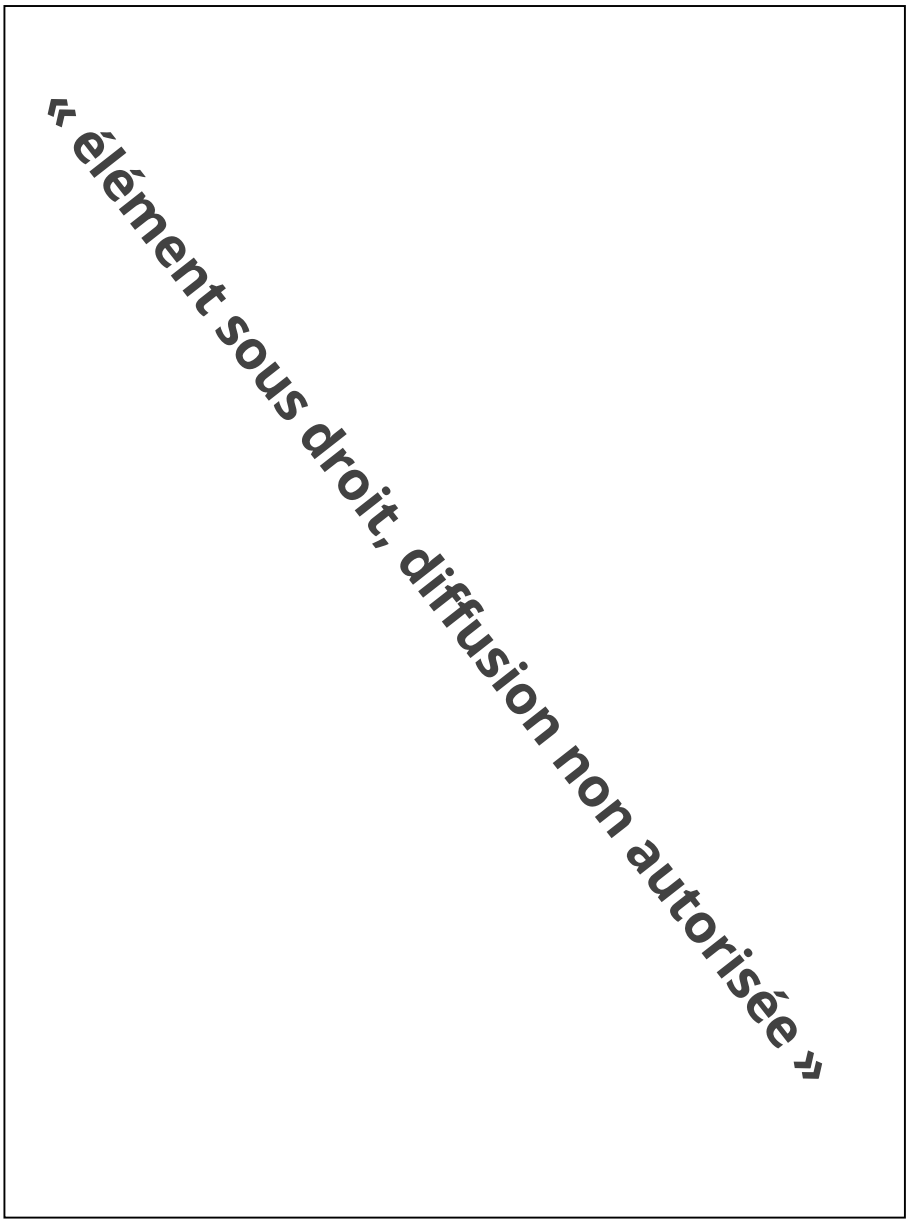


Figure 2: Macroscopic and microscopic features of iCCA and HCC.

Adapted from Beaufrere et al (Beaufrère, Calderaro, et Paradis 2021).

~~*(A-C) Macroscopic and microscopic features of iCCA: (A) Macroscopic features: white fibrous tumor developed in a non-cirrhotic liver, (B) Microscopic features: tumor glands embedded in a fibrous stroma, (C) Expression of cytokeratin 7 by tumor cells, (D) Masson's trichrome staining showing discrete portal fibrosis. (E-H) Macroscopic and microscopic features of HCC: (E) Macroscopic features: well-delimitated encapsulated tumor developed in a cirrhotic liver, (F) Microscopic features: neoplastic cells organized in cords (trabeculae) of separated by sinusoidal spaces, (G) expression of Hepar-1 by tumor cells in HCC, (H) Masson's trichrome staining: cirrhotic liver parenchyma. HCC, hepatocellular carcinoma; iCCA, intrahepatic cholangiocarcinoma.*~~

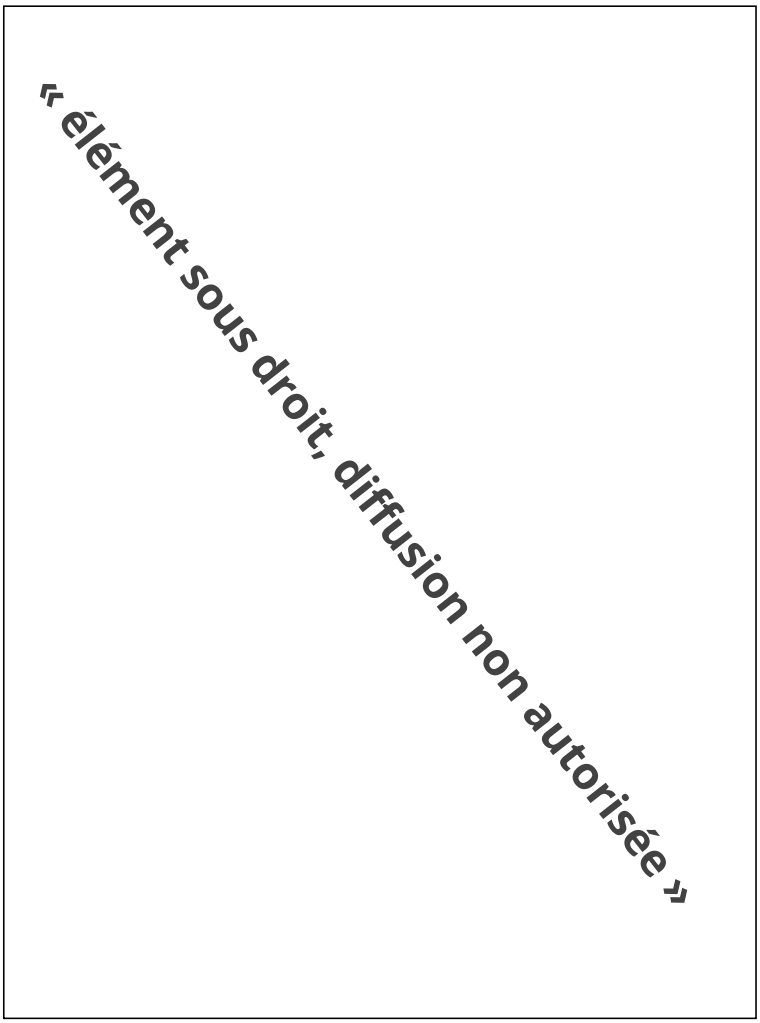


Figure 3: Macroscopic and microscopic features of cHCC-CCA.

Adapted from Beaufrère et al (Beaufrère, Calderaro, et Paradis 2021).

~~*(A) Fibrous well-demarcated tumor developed in a cirrhotic liver in macroscopic examination; (B) Unequivocal cholangiocytic (arrow) and hepatocytic area (star) of cell differentiation (Hematein and eosin staining x100); (C) Hepatocytic area showing tumor cells organized in trabeculae (H&E staining x200); (D) Expression of HepPar-1 by tumor cells in hepatocytic area (x200); (E) No expression of CK7 by tumour cells in hepatocytic area (x200); (F) Cholangiocytic area showing tumour glands embedded in a fibrous stroma (H&E staining x200); (G) No expression of HepPar- 1 by tumour cells in cholangiocytic area (x200); (H) Expression of CK7 by tumour cells in cholangiocytic area (x200). cHCC-CCA, combined hepatocellular carcinoma-cholangiocarcinoma; CK7, cytokeratin 7.*~~

In order to fully understand this tumor, it is necessary to report the fact that several morphological classifications have been proposed over time (Table 2), which have been used sequentially in the literature, generating a considerable amount of confusion over the definitions adopted. Indeed, the pathological definition of cHCC-CCA has evolved significantly over time. Despite the description of this entity under different names at the beginning of the last century, the nomenclature of cHCC-CCA has evolved significantly over time (H. G. Wells 1903) (mixed

tumors, duplex type, intermediate type, carcinoma of dual origin, cholangiohepatoma), the first attempt of classification was developed in 1949 from Dr. Raymond A. Allen and Dr. James R. Lisa from the Pathology department of City Hospital, New York, which identified three different subtypes (Allen et Lisa 1949).

Type A: characterized by the presence of HCC and CCA in two different areas of the liver.

Type B: characterized by the presence of HCC and CCA in adjacent areas.

Type C: characterized by the presence of HCC and CCA within the same lesion.

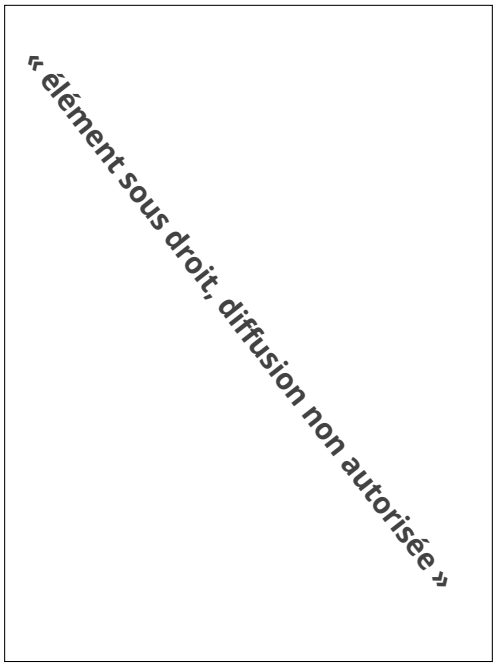


Figure 4: Combined liver cells and bile ducts carcinoma

From Allen et al (Allen et Lisa 1949).

~~*1. Case 3. A nodule showing chiefly a neoplasm of liver cell type. At the periphery, some groups have a zone of more opaque cells suggestive of the bile duct type.*~~
~~*2. Case 3. A duct is lined partly by large cuboidal opaque cells and partly by large granular cells of hepatic parenchymal character. Cells of the two types apparently have transitional forms. X 400.*~~



Figure 5: Combined liver cells and bile ducts carcinoma.

From Allen et al (Allen et Lisa 1949).

~~*3. Case 4. A nodule surrounded by a fibrous wall has an intimate mingling of ducts and cords. X 45.*~~
~~*4. Case 4. The ducts are lined chiefly by large cuboidal or columnar opaque cells, a more granular cell occasionally being present, as in the duct on the left. Other small nests are composed of large granular cells only, some of giant size. X 400.*~~

A few years later, in 1985, an analysis of 24 cases proposed a further classification defining 3 main types. Type I referred to “collision tumor”, which was characterized by the presence of HCC and CCA in the same liver. Type II or transitional was characterized by the presence in the same lesion of an area with an intermediate differentiation between HCC and CCA. Type III identified as a fibrolamellar tumor and was typical of young patients without cirrhosis, and similar to the type of fibrolamellar HCC presenting pseudo-glands that produce mucin *(Goodman et al. 1985).*



Figure 6: Type I combined Hepatocellular-choangiocarcinoma

From Goodman et al (Goodman et al. 1985).

~~*Type I or "collision tumor." There is no transition from the trabecular hepatocellular carcinoma (top) to the tubular scirrhous cholangiocarcinoma (bottom) (X60).*~~

In 2010, cHCC-CCA WHO classification has been revisited, and described, mainly based on morphological features, two main histologic types, including the classic type and the type with stem cell features further subdivided into 3 subtypes (typical, intermediate and cholangiolocellular) (Theise 2010). Although considerable and repeated efforts have been made to arrive at a consensus definition, the accurate diagnosis and characterization of cHCC-CCA, and consequently its subtyping, remain complex, even for experienced pathologists, mainly because of the great heterogeneity of this entity as well as its relative rarity(Akiba et al. 2013; Ikeda et al. 2013). The discussion on terminology allowed by the development of knowledge to exclude certain PLC types from cHCC-CCA, such as collisional tumors, hepatoblastoma, typical HCC with immunohistochemical expression of CK19 or EpCam progenitor cells, typical iCCA with immunohistochemical expression of hepatocyte markers. One of the most heated discussions in the field of histologic classification has been the validity of including

intermediate cell carcinoma (INT) and cholangiolocellular carcinoma (CLC) as subtypes of cHCC-CCA. Mainly due to the results of various studies focusing on molecular analysis, it was possible to make a revision of the classification and definitively establish that CLC is not a subtype of cHCC-CCA, but a subtype of iCCA(Nagtegaal et al. 2019). INT, despite its classification as another histological entity, different from cHCC-CCA, is nevertheless discussed in the same session as tumor classification (Sempoux, s. d.).

To ensure greater commonality in the language used by all professionals involved in the management of liver cancer, an attempt was made to make classifications uniform with a proposed consensus terminology on PLCs that could not be included in either HCC or iCCA. This group was divided into three classes:

1. Tumors with the presence of mixed hepatocytic and cholangiocytic histology with transitional or separate areas within the same tumor are considered combined HCC-CCA. (cHCC-CCA).

2. PLC fully composed of “intermediate cells” (intermediate cell carcinoma), defined as cells of intermediate size between stem cells and hepatocytes with transient morphology between hepatocytes and cholangiocytes, considered as a subtype of cHCC-CCA (E. Brunt et al. 2018; Sempoux, s. d.).

3. PLC composed of pure CLC. This diagnosis can be made if more than 80% of PLC is composed of cholangiolocarcinoma subtype. CLC is then considered as a morphological variant of iCCA (E. Brunt et al. 2018).

According to this classification, the concept of "stem cell" phenotype based on immunohistochemistry (EpCAM, K19 and CD56 positivity) is no longer considered a sub-category *per se*, but is rather an additional element used to better characterize the histological report, and which can be present in different types of PLCs (Motoko Sasaki et al. 2015). Moreover, all subtypes of PLC could be associated in the same lesion with minor histological

components; they were observed in more than a half of cHCC-CCA (Motoko Sasaki et al. 2015; Akiba et al. 2013). If different subtypes are recognized, a precise description is recommended and the percentage of each tumor type represented should be assessed in surgical specimens.

The current theorical approach of classification is synthetized in Fig.7. The different classifications are summarized in Table 2.

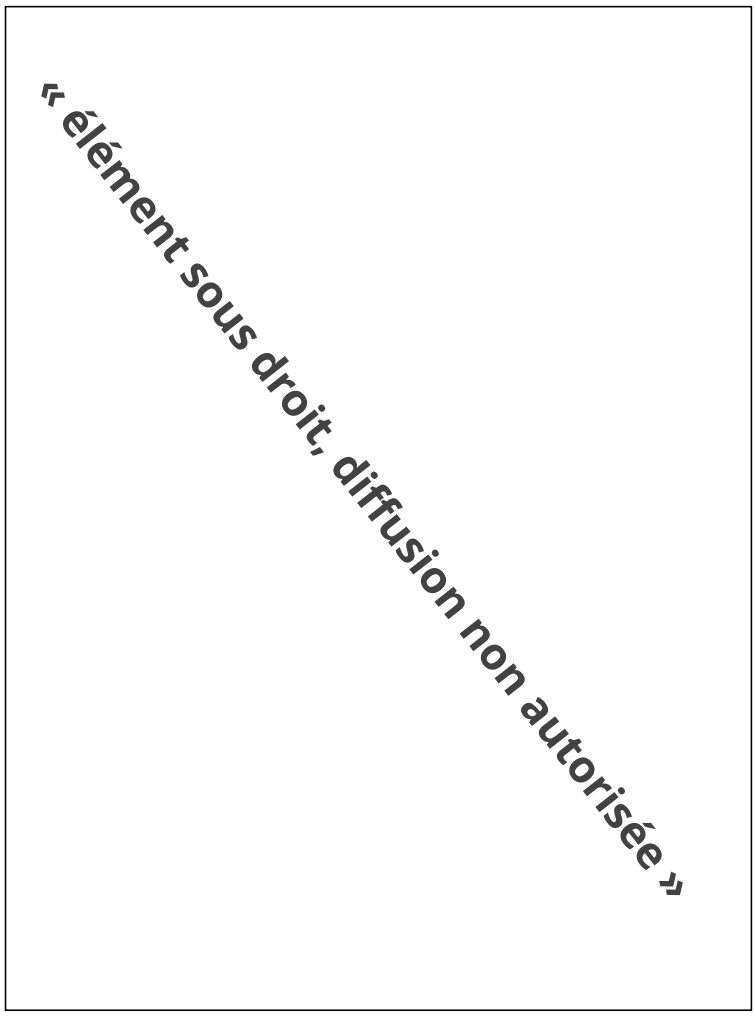


Figure 7: Histological relationships between PLCs.

From Brunt et al.(E. Brunt et al. 2018)

~~*PLCs show an array of differentiative states from hepatocytic(left) through combined types (middle) to cholangiocytic (right). In the middle are the cHCC-CCAs - these are histologically partly morphological HCC and partly morphologically iCCA; immunophenotyping of such lesions can be helpful in confirming the histological impression, but morphology remains the primary criterion.*~~

~~*CLC is a separate form of generally lower grade biliary malignancy.*~~

~~*Intermediate cell carcinoma is also distinctive: For this tumor, the morphology is neither that of HCC nor that of iCCA, but the mixture of cholangiocytic and hepatocytic features is observed on a cell-by-cell basis on the basis of immunophenotyping. Thus, for this tumor type alone, morphology requires confirmatory immunophenotyping to demonstrate the mixture of differentiation markers*~~

~~*SCf/p: stem cell features*~~

Table 2: Different classifications of hepatocholangiocarcinoma

Adapted from Gigante et al.(Gigante et al. 2021)

Allen et Lisa 1949(Allen et Lisa 1949)	*(A) Double tumor with distance between the two lesions.* *(B) Combined type in which both HCC and iCCA show proximity with fusion.* *(C) Mixed type in which the two tumors show close contact with origin from the same site.*
Goodman et al. 1985 (Goodman et al. 1985)	*Type I or "collision tumor," separate lesions of HCC and iCCA* *Type II or "transitional tumors" elements of HCC and iCCA in the same tumor with transition.* *Type III or "fibrolamellar tumors" similar to the fibrolamellar variant of HCC*
WHO 2010 (Theise 2010)	*Classic type, consisting of HCC and iCCA with the presence of transition zones.* *The stem cell type is further subdivided into:* *-Typical: Presence of foci of mature hepatocytes surrounded by peripheral groups of progenitor cells.* *-Intermediate: Presence of characteristics intermediate between hepatocytes and cholangiocytes* *-CLC: Presence of cells imitating cholangioles enveloped by a sclerotic stroma and displaying progenitor cell markers.*
Consensus terminology 2018 (E. Brunt et al. 2018)	*Combined HCC-CCA (cHCC-CCA): presence of hepatocytic and cholangiocytic histology mixed within the same tumor.* *Intermediate cell carcinoma: small cells of size between stem cells and hepatocytes and morphology between hepatocytes and cholangiocytes* *Pure cholangiolocarcinoma reclassified in CCA*

3.1.2.1 Histological diagnosis

The diagnosis of cHCC-CCA is based on histology obtained from liver biopsies or surgical specimens derived of liver resections or explants (E. Brunt et al. 2018; Sempoux, s. d.). Histologically, cHCC-CCA tumor cells are arranged in various HCC patterns (trabecular, pseudoglandular or acinar) and iCCA pattern (glandular). The two components may be intimately mixed or more distinctly separated within the same cancerous lesion. Typical areas of iCCA form glands or cords of small cells with little cytoplasm usually enveloped in fibrous stroma. In contrast, areas of HCC are composed of variously pleomorphic hepatocyte-like cells, often with aberrant growth compared to normal liver parenchyma, such as thickened trabeculae or massively dilated canaliculi (showing a 'pseudoglands' or 'pseudoacini' shape). The liver carcinoma-like component may present with one or more of the findings common to pure liver carcinoma, such as steatosis, ballooning with Mallory-Denk bodies and accumulation of intercellular or intracellular bile (E. M. Brunt et al. 2015; Gigante et al. 2021).

3.1.2.2 Pathological tools useful for diagnosis

Immunohistochemical (IHC) markers are not mandatory elements for the positive diagnosis of cHCC-CCA, but are rather considered as helpful makers to better characterize PLC. It is important to keep in mind that the diagnosis can be made regardless of the percentage of each tumor component. Given the high degree of intratumor heterogeneity of cHCC-CCA, extensive tumor sampling is highly recommended: sampling of all different histologic components identified macroscopically on operative findings (at least 1 block/cm), and multiple biopsy sampling in case of atypical imaging suggestive of cHCC-CCA (Beaufrère, Calderaro, et Paradis 2021).

The most common IHC markers used in routine include hepatocytic markers (HepPar1, AFP and glypican-3); cholangiocytic markers (CK19, CK7) and “stem cells” markers (EpCAM, CK19, CD133) (E. Brunt et al. 2018; Gigante et al. 2019). These markers should always be

considered in the context of morphological analysis and not as *per se* data. This is especially true for "stem cell markers" because they could potentially be expressed by all PLCs. It is also important to note that no consensus has been reached on the necessary cut-off of positive cells undergoing immunostaining to indicate their positivity.

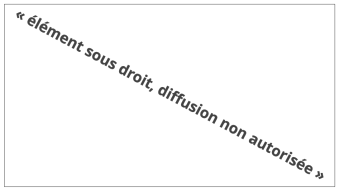


Figure 8: Immunohistochemistry.

Adapted from Moeini et al (Moeini et al. 2017)

~~*Representative morphological and positive immunohistochemical staining features observed for each mixed HCC-CCA subclass.*~~

Recently, the diagnostic and prognostic value of Nestin in cHCC-CCA has been reported (Calderaro et al. 2022a).

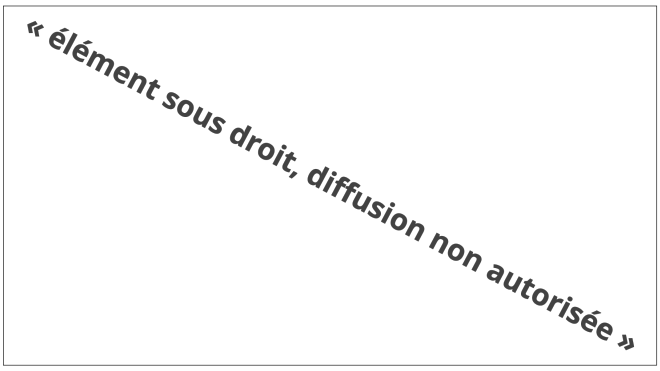


Figure 9: Nestin as a diagnostic marker.

From Calderaro et al (Calderaro et al. 2022)

Some studies performed on limited numbers of patients already suggested that Nestin could be a diagnostic marker of cHCC-CCA (Xue et al. 2019; M Sasaki, Sato, et Nakanuma 2022; Malvi et al. 2020). Nestin is a class IV intermediate filament that has also been shown to be a central regulator of cellular maintenance of cells in a stem state, which may favor the formation of

neoplastic clones(Tschaharganeh et al. 2016; Gleiberman et al. 2005). A recent study used to assess the diagnostic value of Nestin a comparison of 461 cHCC-CCA, 221 iCCA, and 368 HCC from various centers around the world. Nestin was analyzed by immunohistochemistry on tissue samples derived from liver surgery specimens or biopsies. Nestin's diagnostic value for cHCC-CCA was comparable between surgical and biopsy samples. Nestin was much less effective in distinguishing mixed tumors from iCCA. The already known marker CK19 was also able to effectively distinguish cHCC-CCA from HCC, and thus, the composite score combining Nestin and CK19 reached an AUC of 0.92 (Calderaro et al. 2022). While tumor biopsy achieves a very good diagnostic performance for HCC or iCCA in a pre-surgical setting, the performance of liver biopsy for the diagnosis of cHCC-CCA is estimated to be lower due to misdiagnosis of HCC or iCCA. For a long time, although biopsy was considered necessary, its diagnostic accuracy was not established. This fact is certainly attributable to the intratumoral heterogeneity of cHCC-CCA. We should say that before our study reported below in the results session (Gigante et al. 2019), no study has specifically evaluated the diagnostic performance of biopsy in cHCC-CCA patients. In the study by Nishie et al., the diagnostic concordance calculated between histological analysis from the surgical specimen (taken as gold standard for diagnosis) and radiology was reported as low as 44.4% (Nishie et al. 2005). More data are required to improve the performance of histological diagnosis on liver biopsy.

3.1.3 Main clinical manifestations of cHCC-CCA

cHCC-CCAs usually present with non-specific symptoms that could be shared by HCC and iCCA. The major features includes fatigue, abdominal pain, weight loss, pruritus, ascites, hepatomegaly; and in advanced states, jaundice, acute cholangitis related to biliary compression or invasion (Gigante et al. 2021; Cutolo et al. 2022).

3.1.4 Biochemical elements of the characterization of cHCC-CCA

3.1.4.1 Alpha-phoetoprotein and CA 19.9

Serum markers classically associated with liver tumors are alpha-fetoprotein for HCC and CA19-9 for CCA (Johnson et al. 2022; Kubo et al. 2022). Sometimes, the discordance between imaging and serum tumor markers (HCC with increased CA19-9 or hypovascular nodule suggestive of ICCA with increased AFP) could rise the suspicion of a cHCC-CCA (Ng et al. 1998; C.-L. Liu et al. 2003). However, serum biomarkers are not reliable for the diagnosis of cHCC-CCA with elevation of serum CA19-9 and AFP observed only in 45% of the cases and a limited specificity of 75% for the combination of des-gamma-carboxyprothrombin, AFP and CA-19-9 (M. L. Wells et al. 2015)(J. Chen, Li, et Yu 2020).

3.1.5 cHCC-CCA characterization by imaging

Even though histology remains the gold standard for the diagnosis of cHCC-CCA, radiology may suggest the diagnosis in some cases. Therefore, given the fundamental need to be able to establish a diagnosis before surgery, various strategies have been developed over time. One of the fundamental elements in determining the radiological behavior of mixed tumors is the relative percentage of the two tumor classes that compose it, respectively CCA and HCC, which have specific features on imaging. According to the distribution of the prevailing histological type, the lesion will therefore have a behavior more suggestive of HCC or CCA (Cutolo et al. 2022).

3.1.5.1 Computed tomography (CT) and Magnetic Resonance Imaging (MRI)

The criteria currently used for the characterization of HCC in cirrhotic patients are the so-called LI-RADS, a system based on the interpretation of some elements derived from the analysis of computed topographies (CT) and Magnetic Resonance Imaging (MRI). In LI-RADS system, key elements and ancillary characteristics are evaluated, allowing the categorization of the

lesions in various classes. Imaging of untreated lesions without histological examination can be classified as LI-RADS-1, LI-RADS-2, LI-RAD -3, LI-RADS-4, LI-RADS-5, LI-RADS-M, LI-RADS-TIV. There is also a LI-RADS-NC category assigned to images that cannot be categorized due to the absence of important sequences or image degradation. The most suggestive features for the diagnosis of cHCC-CCA are the enhancement in the arterial phase, the diameter of the tumor, the washing, the presence of a capsule and others. Accessory criteria for HCC are hypointensity in the hepatobiliary phase in MR with contrast media, the hypointensity in the transitional phase, the moderate hyper intensity in the T2 phase, diffusion restriction, mosaic architecture, presence of fat in the lesion, the presence of iron in the lesion and other criteria (Cutolo et al. 2022; Marrero et al. 2018)(Figure 10).

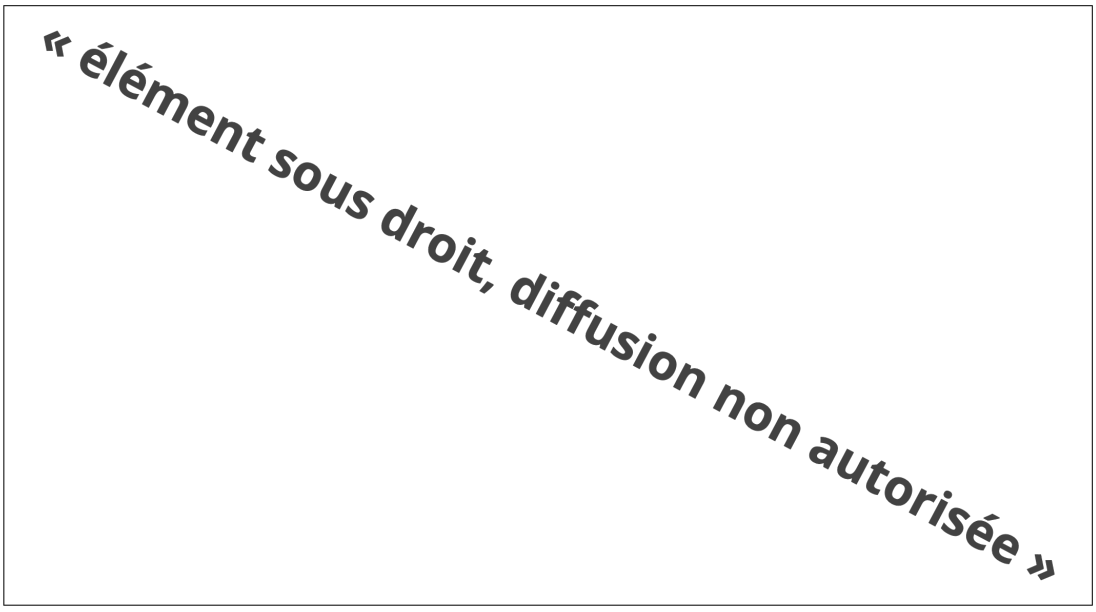


Figure 10: Imaging features of cHCC-CCA

Adapted from Gigante et al (Gigante et al. 2021)

~~*Radiological features of hepatocholangiocarcinoma. An example of an MRI of cHCC-CCA with a well-delineated heterogeneous lesion with capsular retraction. The lesion harbored progressive delayed enhancing areas mixed with areas with arterial enhancement and washout.*~~

Hallmarks of HCC (i.e. arterial phase hyperenhancement [APHE] and washout) are observed in a minority of cHCC-CCA (M. L. Wells et al. 2015; Gigante et al. 2019; Potretzke et al. 2016). Nevertheless, recent studies using LI-RADS have reported misclassification of cHCC-CCA as HCC in 26% to 54% of cases when using major radiological features (Mitchell et al. 2015)(Jeon et al. 2019). Noticeably, 88% of these patients could be reclassified as malignant tumors but "non-HCC" (LI-RADS M category) after addition of auxiliary features based on rim/peripheral arterial phase hyperenhancement, progressive central enhancement, portal venous and delayed phase images, predominantly peripheral washout appearance, liver surface retraction, biliary obstruction, and marked diffusion restriction (Mitchell et al. 2015). The depiction of these features explain why the main differential diagnosis is often iCCA, and why performance of imaging is often insufficient (Hwang et al. 2012; Nishie et al. 2005; Willekens et al. 2009; de Campos et al. 2012; Potretzke et al. 2016) (Fowler et al. 2013). The association of features of HCC with other of iCCA (e.g. appearance of iCCA with portal venous invasion, or appearance of HCC with biliary dilation or enlarged lymph nodes) may also be suggestive of the diagnosis. The influence of the presence of chronic liver disease or cirrhosis, and of the possible associated etiologies on diagnostic performance are not established. In a study of 300 cirrhotic patients with HCC, CCA and cHCC-CCA using the Li-RADS criteria revised in 2018, the LR-M category had a sensitivity of 63% a specificity of 90% in distinguishing HCC lesions from other lesions (CCA and cHCC-CCA). Moreover, the LR-M demonstrated a higher specificity (93.8%) and sensitivity (73.8%) for diagnosing non-HCCs (CCA and cHCC-CCA) smaller than 20 mm. Unfortunately, in the study, in the non-HCC group, iCCAs were considered together (Xinai Liu et al. 2022). The specificity of the LR-M category has been questioned by a recent study by Zou et al. conducted in the different subtypes of primary hepatic cancer (HCCs, iCCAs, and cHCC-CCAs) through the LI-RADS v2018 classification. In fact, in this study, LI-RADS v2018 criteria showed a high specificity but a low sensitivity in

distinguishing HCC from non-HCC malignant lesions. Most iCCAs were classified as LR-M or LR-TIV, but about half of the cHCC-CCAs were identified instead as LR-5. The latter category generally suggests with a high specificity the diagnosis of HCC, suggesting a low performance of the system in terms of specificity for cHCC-CCAs (Zou et al. 2021).

3.1.5.2 Contrast-enhanced ultrasound

Finally, even contrast-enhanced ultrasound (CEUS) has insufficient specificity for the diagnosis of cHCC-CCA, as the tumors show a non-specific association of various degrees of heterogeneous hyperenhancement of the arterial phase with washout (R. Li et al. 2016; Sagrini et al. 2019). A recent Eastern multicenter study conducted on 55 patients with cHCC-CCA compared to 55 patients with HCC, proposed some composite diagnostic criteria based on CEUS and CT/MR LI-RADS. The authors proposed the positive diagnosis of cHCC-CCA if one of the following criteria were present: (1) presence of APHE on CEUS and LR-M on CT/ MRI; (2) LR-5 diagnosis on both CEUS and CT/MRI with elevated levels of CA19-9; (3) LR-M on both CEUS and CT/MRI with presence of elevated AFP. Patients and controls were mostly affected by HBV while patients with cHCC-CCA were less affected by cirrhosis than patients with HCC. The reported sensitivity, specificity were 64.8% and 84.4%, respectively with an accuracy of 76.1%. The authors proposed that the discrepancy between contrast-enhanced models of CEUS and CT / MRI can be a good diagnostic element for cHCC-CCA(Y. Zhou et al. 2022).

3.1.5.3 Artificial intelligence in radiology

The performance of a radiomic approach was tested on ultrasound-based artificial intelligence (AI) model that tried to identify different types of PLC. This approach, although original, unfortunately yielded a modest result. In fact, the comparison of the radiomic model applied to the distinction between iCCA vs cHCC-CCA reported AUC value of 0.728 in the test cohort

(Peng et al. 2020). Again, the same type of methodological approach was used by a recent study on ultrasound radiomics using the 2017 CEUS LI-RADS criteria. In the design of the study, the authors chose the LR-M category as reference for cHCC-CCA diagnosis, despite the fact that category includes also other malignant tumors of the liver and is not specific of cHCC-CCA. Despite the choice of such a broad category as LR-M, the performance of the eco-radiomic model was not significantly more effective than the simple LI-RADS criteria (C.-Q. Li et al. 2022).

These results, despite having been obtained through the use of the most-modern data processing and interpretation techniques provided by AI, confirm again the limited diagnostic performance of imaging alone for the diagnosis of cHCC-CCA. Nevertheless, radiology is fundamental to guide liver biopsy (especially possible multiple biopsies in such heterogeneous tumors) and to assess tumor staging.

3.2 Treatment of cHCC-CCA

Randomized controlled trials are widely available for HCC and CCA, and solid multicentric cohort studies have guided the drafting of international guidelines for clinical management. In contrast, in the cases of rare PLC, such as cHCC-CCA, well-designed prospective studies and clinical trials are not possible due to their scarcity. The available literature is therefore generally derived from retrospective studies with small number of patients.

3.2.1 Surgery

3.2.1.1 Liver resection.

Liver resection is currently the most effective curative-intent therapy for cHCC-CCA. According to the state of the art, the principle of oncological liver surgery is based on the fact that liver resection aims to completely remove the lesion with adequate margins, and ensure

sufficient residual liver volume(Agrawal et Belghiti 2011). In the case of liver surgery for HCC, a resection margin >10 mm has been associated with prolonged disease-free survival in some studies (40% versus 0% at 1 year) (Ma et Chok 2017). Major hepatectomy can be proposed, providing that sufficient residual liver volume is granted(> 20% of total liver volume in non-fibrotic patients and > 40% in patients with cirrhosis) in order to limit the risk of post-operative liver failure (Agrawal et Belghiti 2011). In patients with cirrhosis, evaluation of the degree of portal hypertension should also be routinely performed according to the standards of care. In this setting, it is generally considered that clinically significant portal hypertension (defined as a HPVG > 10 mm Hg or to the existence of indirect signs of portal hypertension) represent absolute contra-indications to major hepatectomy (Cucchetti et al. 6). Furthermore, lymphatic pattern of tumor spread in cHCC-CCA suggests that hilar lymphadenectomy should be routinely undertaken. However, this needs particular care in the setting of cirrhosis given its associated increased morbidity (Bagante et al. 2018). Finally, the need for routine lymphadenectomy should currently restrict the use of the laparoscopic approach only to centers with extensive expertise both in liver surgery and laparoscopy (Yoh, Cauchy, et Soubrane 2020). Surgical series reported survival rates of 17 to 32 months for cHCC-CCA, lower than those reported in patients with HCC (46–52 months) and CCA (26–37 months) with a survival rate lower than 30% at 5 years due to early tumor recurrence (Jarnagin et al. 2002; C.-L. Liu et al. 2003)(J. H. Kim et al. 2010). A systematic review of 13,613 patients with PLC, including 437 cHCC-CCA (3.2%), described a disease-free survival (DFS) after resection of 14.2 months in cHCC-CCA compared to 17.8 months in iCCA and 43.1 months in HCC, with an overall survival (OS) of 37, 32 and 67 months (in cHCC-CCA, iCCA and HCC, respectively) (Gentile et al. 2020). Outcomes after liver resection for cHCC-CCA seems closer to patients with iCCA and worse than patients with HCC (Gigante et al. 2019; « EASL Clinical Practice Guidelines: Management of hepatocellular carcinoma » 2018)(Jarnagin et al. 2002) even if a recent study

identified no difference of outcomes after adjustment on cirrhosis and tumor size (Holzner et al. 2020).

A recent Chinese study sought to create a radiological nomogram to predict survival in patients resected for cHCC-CCA. Patients were divided into a training group and an evaluation group. The radiological features were collected starting from CT scanners at the portal venous phase. The nomogram was then created by inserting the radiological criteria and clinical factors and analyzed with a Cox regression. Factors independently associated with survival were the radiomic score, vascular invasion, anatomic resection, total bilirubin and the presence of satellite lesions. A further nomogram including clinical and radiological factors subsequently demonstrated a stronger association with survival. The two categories created (low-risk and high-risk patients) were found to have a highly different survival (81.6 months vs 6.1 months, $p < 0.001$). The median OS of the study cohort was 21.6 months, and OS rates were 61.0%, 48.3%, and 37.4% at 1, 3 and 5 years, respectively. The AUC of the nomogram for 1-year OS was 0.878 in the training set, and 0.937 in the validation set. Despite the limits of this monocentric cohort based on patients affected by viral hepatitis and with high degree of liver fibrosis, the study proposed an original approach, which needs to be validated on an external and more heterogenous cohort (Tang et al. 2021). In a large cohort of patients that underwent surgery, the role of Nestin as a prognostic marker was explored by Calderaro et al. In Multivariable analysis, Nestin was an independent prognostic factor for both disease-free and OS in association with usual factors (tumor size, microvascular invasion). Interestingly, Nestin was associated with worse DFS in iCCA patients without difference in OS (Calderaro et al. 2022).

3.2.1.2 Liver transplantation

The role of liver transplantation (LT) for the treatment of small iCCA or cHCC-CCA remains controversial. A systematic review of retrospective studies for LT for cHCC-CCA reported a mean DFS and OS rates at 1 year were 69% and 84%, respectively (Gentile et al. 2020). The median 5-year OS rate was 49.4% for cHCC-CCA patients compared to 80.3% for HCC patients. Although, as reported above, the overall survival of resected patients was 37 months, with a 5-year survival rate of 32%, it must be considered that resected and transplanted patients differed in baseline characteristics (tumor size, age, comorbidities). These results were discouraging, below the results of LT for HCC, and, in many countries, cHCC-CCA is still a contraindication for LT (Gigante et al. 2021).

In contrast, recent studies with similar inclusion criteria reported more positive outcomes. The first study conducted in Spain on 42 patients undergoing LT for HCC with an incidental diagnosis of HCC-CC or iCCA and stratified according to tumor size and number. The 1-, 3-, and 5-year survival rates were similar between cHCC-CCA and HCC controls (93%, 78%, and 78% vs 97%, 86%, and 86% respectively). Patients with multinodular or uninodular tumors larger than 2 cm had obviously the worst outcomes (G. Sapisochin et al. 2014). The second retrospective study analyzed patients treated by resection (n=26) or LT (n=95) for iCCA and cHCC-CCA less than 5 cm developed on cirrhosis. Overall survival (67% at 5 years) and recurrence-free survival (75% at 5 years) were higher in patients treated by LT than in patients treated by resection and small tumor has a better outcome. iCCA and cHCC-CCA patients had comparable survival (De Martin et al. 2020).

Recent retrospective data suggest that cirrhotic patients transplanted have a better survival than patients resected if tumor size is <5 cm (De Martin et al. 2020; G. Sapisochin et al. 2014)(Lunsford et al. 2018). In a recent multicenter study conducted in North America, the authors compared the results of LT in patients with HCC and cHCC-CCA. The results were

particularly encouraging, reporting a similar overall survival at 5-year (cHCC-CCA 70.1% vs HCC 73.4%, p = 0.806), despite higher cHCC-CCA recurrence rates (23.1% vs 11.5% at 5 years, p <0.001). The authors also compared patients transplanted for cHCC-CCA with patients resected for cHCC-CCA, describing a better survival associated with liver transplantation. Unfortunately, these data must be taken with caution, as only 5.3% of the patients enrolled in the study had a preoperative diagnosis of cHCC-CCA (Dageforde et al. 2021). A propensity score matching analysis conducted in China on 223 patients with cHCC-CCA derived from Surveillance, Epidemiology, and End Results database (SEER), described that the LT recipients had better outcomes than controls who underwent hepatectomy or local destruction (p<0.05). The post-LT survival was similar to those with HCC (p>0.05) but better than those with iCCA (p<0.05). The authors developed a score based on vascular invasion, tumor size, multiple tumors that could divide patients into two prognostic subgroups: the low- and the high-risk, patients in the low-risk group were more likely to benefit from LT (X. Chen et al. 2022).

One of the main drawbacks of these retrospective studies is that cHCC-CCA was identified incidentally on the explant, and data on intention-to-treat analysis of LT for cHCC-CCA diagnosed before inscription on the waiting list are lacking. A consensus on LT for CCA and cHCC-CCA concluded that there is not enough evidence to propose LT for cHCC-CCA but that this approach should be explored in clinical trials (Gonzalo Sapisochin et al. 2020).

3.2.2 Locoregional treatments

3.2.2.1 Intra-arterial treatments and percutaneous ablations.

The effectiveness of transarterial chemoembolization (TACE) on cHCC-CCA was analyzed in retrospective studies including a limited number of patients. TACE tested in 50 patients induced a partial response or stable disease in 70% of the cases, mainly observed in tumors showing arterial phase hyperenhancement (APHE) with a median overall survival of 12.3 months (J. H.

Kim et al. 2010). Better outcomes were reported in a cohort of patients treated by TACE for recurrence after liver resection. Interestingly, and as expected, cHCC-CCAs with a with non-rim APHE pattern at imaging have a better radiological response rate (36% vs 0%) and survival (52.8 months vs 12.4 months) compared to patients with rim APHE (Yoon et al. 2016; Na et al. 2018). One study reported that the frequency of cHCC-CCA was more frequent in explant of patients treated by TACE than untreated patients suggesting that TACE could induce modification of tumor phenotype (Zen et al. 2011). Radioembolization (SIRT) has been rarely studied on cHCC-CCA. Data about SIRT and chemotherapy on unresectable iCCA were encouraging, reporting that 22% of patients could be down-staged to surgical intervention suggesting a possible role of SIRT on cHCC-CCA (Edeline et al. 2019). In the only study available, SIRT was associated with a 55% radiological response rate, 65% disease control rate with a median overall survival of 9.3 months in 21 patients (Malone et al. 2020). The use of other locoregional treatments such as radiofrequency and microwave has been described episodically and is not currently based on solid literature data (Renzulli et al. 2021; Gigante et al. 2021). Altogether, only few data are currently available to support the value of intra-arterial treatments in patients with cHCC-CCA, even if some retrospective data suggest a role in selected patients with tumor showing APHE.

3.2.3 Treatment of advanced or metastatic cHCC-CCA

Data about systemic treatments in unresectable cHCC-CCA are limited to few retrospective series testing the first-line treatment approved for advanced HCC (Sorafenib) and CCA (gemcitabine/platinum regimens) (Llovet et al. 2008; Rizvi et al. 2017).

3.2.3.1 Platinum based chemotherapy

A multicentric Japanese study on 36 patients with unresectable cHCC-CCA analyzed different first-line systemic treatments. The median overall survivals of the gemcitabine/cisplatin, fluorouracil/cisplatin and sorafenib were 11.9, 10.2 and 3.5 months, respectively, suggesting that sorafenib (only 7 patients included) was associated with a reduced survival (Kobayashi et al. 2018). A French multicentric study included 30 patients treated by gemcitabine combined either with oxaliplatin or cisplatin +/- bevacizumab. Eight patients (28.6%) had a partial response and 14 (50%) stable disease with a median progression free survival was 9.0 months and overall survival 16.2 months. The limitation of this study remains the absence of histology in more than 25% of the patients (Salimon et al. 2018). The largest series available is a monocentric cohort of 68 histologically confirmed cHCC-CCA who received systemic therapy for unresectable disease mainly using gemcitabine-based regimen (57/68) with 23.5% gemcitabine +/- fluoropyrimidine and 60.3% gemcitabine with platinum. Overall survival was 11.5 months in patients receiving gemcitabine/platinum therapy and 9.6 months in the 7 patients treated with sorafenib alone (Trikalinos et al. 2018). To recapitulate, systemic treatment based on the gemcitabine/platinum regimen is the most widely used chemotherapy. This attitude stems more from clinical practice and recommendations for the treatment of iCCA, as the use of this chemotherapy in cHCC-CCA has only been reported from small retrospective studies (Gigante et al. 2021).

3.2.3.2 Oral targeted therapies

Finally, in a recent monocentric study from Korea including patients affected by cHCC-CCA predominantly infected by hepatitis B infection, treatment with TKI or cytotoxic chemotherapy with platinum-based regimes had similar outcomes. The treatment outcomes were not significantly different between patients who received TKI and those who received cytotoxic chemotherapy (median PFS, 4.2 vs 2.9 months, p= 0.52; median OS, 10.7 vs 10.6 months,

p=0.34). Interestingly, in multivariable analysis, the factors associated with worse outcome were tumor size, ≥30% of total liver volume, bilirubin value and TKI first- line chemotherapy (E. J. Kim et al. 2021). Thus, it is evident that the role of TKI in the treatment of advanced cHCC-CCA is still poorly explored as is the general attitude toward the use of systemic chemotherapy.

3.3 Conclusion, clinical aspects.

Despite several advances in the last decades mainly in the field of physiopathology, rare PLCs such as cHCC-CCA suffer from their condition of orphan diseases with pitfalls in term of diagnosis, availability of dedicated prospective clinical data and clinical trials. Moreover, grants dedicated to these cHCC-CCA are lacking and pharmaceutical companies are rarely interested in the development of new drugs for these patients. In order to bypass these limitations, large international consortiums are needed in the future to rise grant to run large prospective cohort and better define rare PLC in term of physiopathology and clinical behavior. We can conclude:

1) Recent consensus has reclassified pure CLC as CCA whereas cHCC-CCA are characterized histologically by the presence of two distinct morphological patterns in the same lesion.
2) Combination of suggestive imaging followed by histological evidence, mainly using tumor and non-tumor biopsy, is required for the diagnosis of cHCC-CCA with sub-optimal performances. New diagnostic tools are needed.
3) Liver resection, when feasible, is the main treatment of cHCC-CCA.
4) No systemic or locoregional therapies are currently validated in the treatment of unresectable cHCC-CCA.
5) Liver transplantation is still an area of research for small and not advanced cHCC-CCA.
6) We must consider cHCC-CCA as a cancer with poor long-term survival that needs more adapted diagnostic-therapeutic strategies.

3.4 Heterogeneity of cHCC-CCA

3.4.1 Genetic landscape of cHCC-CCA

3.4.1.1 Molecular alterations

Whole genome and RNA sequencing of PLCs with a biliary phenotype, including cHCC-CCA, reported a median number of 60-70 mutations, including a higher frequency of TERT promoter mutations in cHCC-CCA (up to 53%) compared to iCCA (8%)(Fujimoto et al. 2015). *TERT, TP53, ARID1A and ARID2* promoter alterations were more frequent in cHCC-CCA, whereas *PBRM1, BAP1, KRAS, IDH1* and *FGFR2* were more often altered in iCCA. Finally, *CTNNB1* was most often mutated in HCC. However, it should be noted that the results summarized here are derived from patient cohorts with a high degree of variability in terms of the techniques used and the cHCC-CCA classification, which limits the generalization of this information. A summary table of techniques used and results is available below (Tab. 3). (Z.-H. Liu et al. 2018)(Joseph et al. 2019)(Motoko Sasaki, Sato, et Nakanuma 2017)(Moeini et al. 2017). Genomic analysis suggests an impact of viral hepatitis (HCV and HBV) on the genetic landscape of cHCC-CCA, that seems closer to HCC in term of genomic profiles and incidence of *TERT* promoter mutations (Coulouarn et al. 2012)(Fujimoto et al. 2015)(Le Faouder et al. 2019). The largest genomic study on cHCC-CCA was performed on 133 patients in Asia. It confirmed that *TP53, TERT promoter*, *AXIN1, KMT2D, ARID1A* are the major mutations in cHCC-CCA, close to those in HCC, with a lower frequency of *TERT* promoter mutations than found in HCC. Analysis of mutational signatures suggested exposure to aflatoxin B1 and hepatitis B. The authors applied one of the old classifications (Allen et Lisa 1949) identifying two distinct entities: 'combined' and 'mixed' HCC-CCA. In the first type, 'combined', the components of HCC and iCCA show colocalization while maintaining a visible separation between the areas. In the second type, 'mixed', the two neoplasms show close contact without clear identifiable borders. Genes of epithelial-mesenchymal transition, *EPCAM* and *KRT19*

were overexpressed in 'combined' type cHCC-CCA with KRAS mutation, whereas genes associated with xenobiotic and bile acid metabolism and overexpression of AFP, GPC3 and *SALL4* were more represented in 'mixed' type cHCC-CCA. The authors suggest that the 'mixed' type cHCC-CCA might be more similar to HCC and the 'combined' type cHCC-CCA more similar to iCCA (Xue et al. 2019).

3.4.2 Intratumoral heterogeneity

In term of spatial heterogeneity, comparison of iCCA and HCC components of cHCC-CCA confirmed the monoclonal origin of combined tumors, but also showed a significant intratumor heterogeneity overlapping with the morphological heterogeneity (A. Wang et al. 2018)(Xue et al. 2019). One study identified *TERT* promoter mutations in both HCC and iCCA components suggestive of an early event in carcinogenesis whereas mutations in other driver genes such as *TP53* harbored intratumoral heterogeneity (Joseph et al. 2019).

Concerning the pathogenesis of cHCC-CCA, a mouse model suggested that dysregulation of p53 in mice promotes the dedifferentiation of mature hepatocytes into nestin-positive progenitor cells that then differentiate into HCC or iCCA under the influence of *Wnt* and Notch(Katz et al. 2012). A cell line derived from cHCC-CCA could differentiate into either HCC or iCCA under different growth conditions, suggesting that cHCC-CCA may rise from a common precursor (Yano et al. 1996)(Fujii et al. 2000). Nestin is also an active factor involved in tumor differentiation, necessary but not sufficient to the development of the tumor (Tschaharganeh et al. 2016). Overexpression of nestin was identified in 81.3% of human cHCC-CCAs and were also associated with a poor clinical outcome (Xue et al. 2019). All these studies brought to the hypothesis that cHCC-CCA could derive from hepatic progenitor cells that express markers of both lineages (hepatocytes and biliary cells) (Roskams, Libbrecht, et Desmet 2003)(Yeh 2010).

Analysis of genetic landscape showed that CLC has a different genetic profile with more *ARID1A* mutations and less *TERT* promoter mutation compared to cHCC-CCA (Motoko Sasaki, Sato, et Nakanuma 2019). A recent study conducted in North America, which was inspired by the study of Xue et Al. (Xue et al. 2019), set out to describe the genomic profile of mixed tumors. This study was conducted on 73 mixed tumors that were compared to 4975 CCAs and 1470 HCCs. When CCA was compared with HCC, the genes that were most frequently altered in CCA were *ARID1A, BAP1, CDKN2A/B, FGFR2, IDH1, KRAS*, and *PBRM1*. By contrast, the genes most altered in HCC were *CTNNB1, MYC*, and *TERT*. The presence of Genomic HBV was most associated with HCC. The most frequent genetic alterations found in cHCC-CCA patients were *TP53, TERT, PTEN*. About 24.6% of cHCC-CCA harbored potentially targetable genomic alterations as *BRCA2* (8.2%), *ERBB2* (5.5%), *IDH1* (4.1%), *BRAF* (4.1%), *FGFR2 (*4.1%), and *MET* (2.7%). Interestingly, in line with the literature available to date, mixed tumors in which the genetic heritage was rather European were classified as CCA-like, whereas mixed tumors in which the lineage was rather Asian were classified as HCC-like (Murugesan et al. 2021). Main genetic characteristics of cHCC-CCA, and the relations with the other PLC subtypes are schematized in Fig 11.

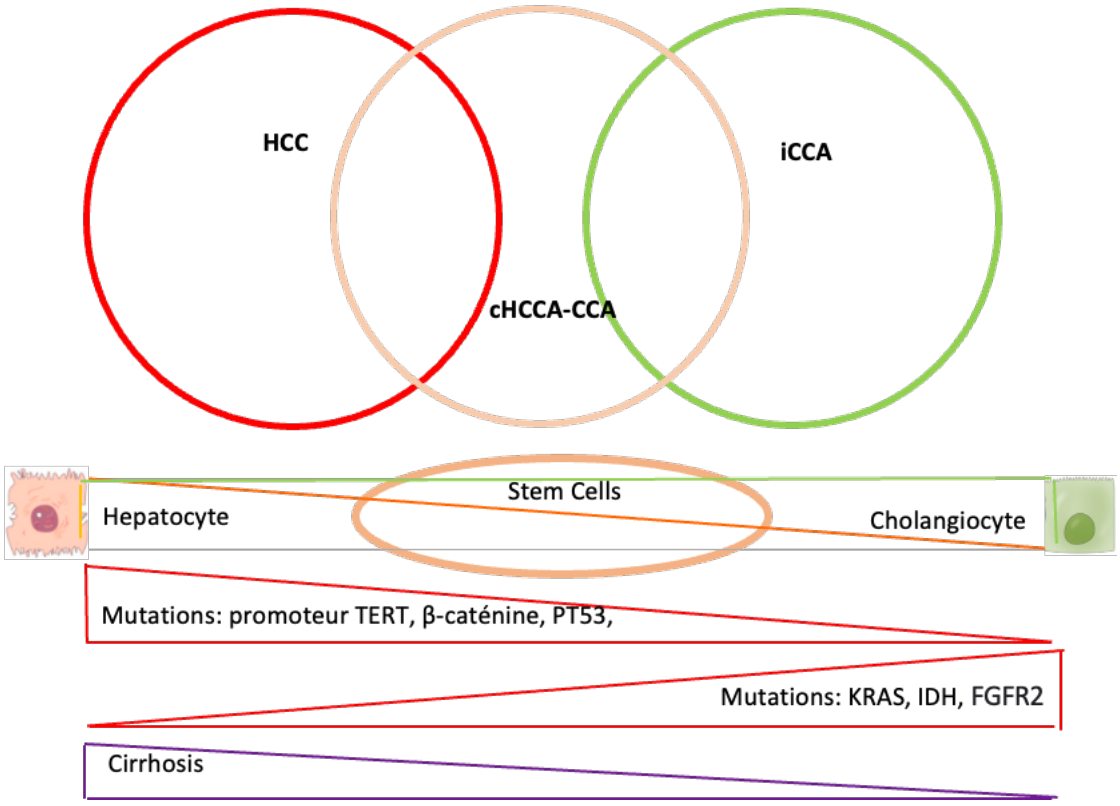
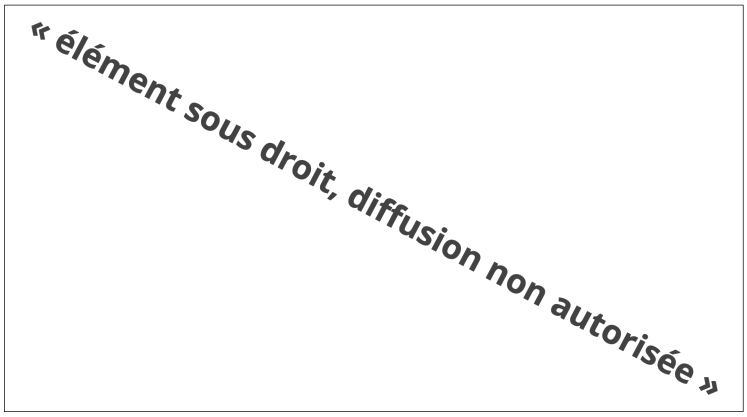


Figure 11: Mutational spectrum of cHCC-CCA, courtesy of Pr. Paradis

3.4.3 Heterogeneity and cancer

To the already complex molecular heterogeneity present in mixed tumors, we must add the fundamental concept of heterogeneity in solid tumors, especially in the case of advanced metastatic/tumors. We should take in to account that solid tumors are often polyclonal, and that following the selection pressure related to metabolic conditions, especially hypoxia, environmental (proximity to vessels, immune reaction, stroma) or treatment (especially chemotherapy), an event could confer a survival advantage that may favor the emergence of new tumor clones. These emerging clonal populations can co-exist or replace pre-existing clones, resulting in tumor heterogeneity (Hu et al. 2020; De mestier du bourg s. d.)

Figure 12: Mechanisms of tumor heterogeneity, from Hu et al.



Nowell's hypothesis on the development of tumor heterogeneity is particularly interesting and fits perfectly with mixed tumors. This theory is based on the fact that despite the presence of a possible common precursor cell, genetic instability allows the development of later clonal generations that have unique biological characteristics related to alterations of oncogenes and tumor suppressors genes (Nowell 1986).

3.4.4 New insights in cHCC-CCAs pathological mechanisms

A recent study was devoted to the characterization of the immune profile of cHCC-CCAs. This multicenter study aimed to analyze gene expression and characterize by immunohistochemistry the different immunological sub-populations. Among 96 cases, 57% of them were identified as high immunity while the remaining 43 were identified as low immunity. The cluster identified as high immunity included the overexpression of genes related to auto-immune cells recruitment, adaptive and innate response, antigen presentation, cytotoxicity and inflammation (Nguyen et al. 2022).

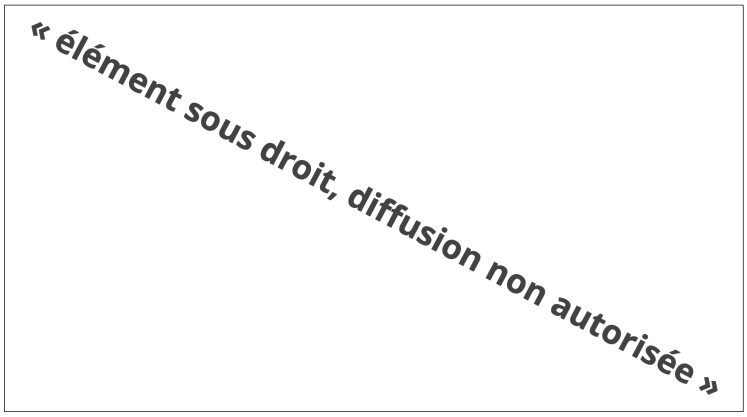


Figure 13: Prognostic impact of cHCC-CCA immune subtype.

From Nguyen et al. (Nguyen et al. 2022).

These same genes have recently been identified as predictors of response to immunotherapy in patients with HCC (Sangro et al. 2020). The authors found no association between genetic alterations and the types of cells infiltrating the tumor. The cluster identified with high immunity appeared to be associated with worse survival in patients undergoing surgery. Theoretically, patients identified as being in the high immunity cluster could benefit more from the new immune-modulating therapies (Nguyen et al. 2022). To palliate the absence to date of relevant mouse models of cHCC-CCA, and to fully explore the hypothesis that mixed tumors arise from stem cells, a team of researchers developed a mouse model in which liver stem cells could be traced in the context of constant liver inflammation (*Mdr2* KO mice). These mice developed both HCC and cHCC-CCA, but only cHCC-CCA had stem cell-related tracer expression. Later, by removing the progenitors, the cHCC-CCAs were slowed down while the HCCs remained active. Analysis by RNA-seq found an up-regulation of IL6-related pathways. Logically, administration of an anti-IL6 antibody arrested the development of cHCC-CCAs. In conclusion, the study suggested that stem cells give rise to cHCC-CCAs and that inhibition of IL6 pattern could be a possible therapeutic target (Rosenberg et al. 2022).

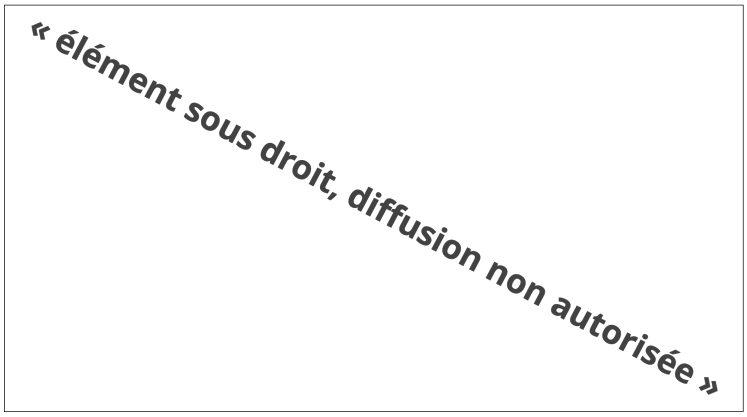


Figure 14: cHCC-CCA derives from liver progenitor cells

Adapted from Rosenberg et al (Rosenberg et al. 2022)

3.5 General conclusions (genetics)

In conclusion, these data suggest that:

1) cHCC-CCA is monoclonal, deriving from a common cell of origin.

2) cHCC-CCA genomic features may be closer to HCC than iCCA, even if some cHCC-CCA harbored genomic features considered more similar to iCCA.

3) Hepatic risk factors such as viral infection could be associated with specific genetic features in cHCC-CCA, especially in HBV positive patients.

4) Almost 24% of genetic alterations of cHCC-CCA are therapeutically targetable.

5) IL6 pattern could be an interesting therapeutical target to explore.

Table 3: Genomic alterations in hepatocholangiocarcinomas

Adapted from Gigante et al(Gigante et al. 2021)

Study and year	*Classification*	*Type of analysis*	*N patients Subtypes*	*Fibrosis (F3-F4)*	*Altered Pathways*
Calzas-Hatem 2004	*Lisa et Allen 1949*	*Target sanger sequencing*	*14 mixed, 1 fibrolamellar HCC 3 collision tumors*	*3/15*	*TP53*
Coulouarn 2012	*WHO 2010*	*Microarray*	*20 mixed tumors (mainly CLC)*	*10/20*	*Liver progenitor and EMT marker Activation of WNt and TGB signalling*
Sasaki 2017	*WHO 2010*	*Target sanger sequencing + IHC*	*53 mixed tumors 4 CT, 4 TS, 20 INT, 25 CLC*	*38/53*	*cHCC-CCA: TERT 50%, TP53 25%, KRAS 50% ARID1A 0% Intermediate: TERT 42%, TP53 58%, , KRAS 5%, ARID1A 11%*
Moeini 2017	*WHO 2010*	*Microarray, DNA copy number, WES*	*18 mixed tumors 6 CLC / 8SC / 4CT*	*10/18*	*Stem cell HCC-CCA: IGF, and MYC signature, SALL4 positivity Classic HCC-CCA: poor prognosis signatures CLC: TP53 and IDH1 mutations cHCC-CCA: TP53, TERT promoter ,BRAF, FGFR2-BICC1*
Liu 2017	*WHO 2010*	*WGS, WES and RNA-seq*	*4 cHCC-CCA not specified*	*NA*	*TP53, CTNNB1 and ARID1A mutations in cHCC-CCA.*
Fujimoto 2015	*WHO 2010*	*WGS and RNA-seq*	*30 Liver cancer displaying biliary phenotype 7cHCC-CCA not specified +2CLC*	*4/9*	*TERT promoter mutation 53%, PBMR1 20%, ARID2 27%*
Wang 2018	*WHO 2010*	*WES*	*7 cHCC-CCA*	*NA*	*TP53 and ARID2 mutations*
Xue 2019	*Lisa et Allen 1949*	*WES, WGS, RNA-seq, and single nucleus sequencing*	*121 6 separate type, 56 combined type, 59 mixed type.*	*54/115*	*TP53 49% , TERT promoter 23%, AXIN 10%, KMT2D 9%, KEAP1 8%, ARID1A 8%, RB1 8%, CTNNB1 6%, IDH1 5% Combined type: EMT Mixed type: xenobiotic and bile acid metabolism*
Joseph 2019	*Consensus 2019*	*Target next-generation sequencing*	*20CT*	*15/18*	*TP53 (80%), TERT (80%), ARID1A (15%), ,CTNNB1 (10%), AXIN1 (10%), KRAS (5%)*
Sasaki 2019	*Consensus 2019*	*Target sequencing + IHC*	*9 CT*	*6/9*	*TP53 (66%), TERT promoter (33%), KRAS (22%)*
Murugesan 2021	*NA*	*Comprehensive genomic profiling (CGP)*	*74*	*NA*	*TP53 (65.8%), TERT (49.3%), and PTEN (9.6%) BRCA2 (8.2%) ERBB2 (5.5%), IDH1 (4.1%), BRAF (4.1%), FGFR2 (4.1%), and MET (2.7%)*

CLC = cholangiolocarcinoma, WES = whole exome sequencing, WGS = whole genome sequencing, IHC = immunohistochemistry, CT = classical type, TS = typical subtype, INT = intermediate subtype, CLC = cholangiocellular subtype, SC= stem cell subtype, EMT= epithio-mesenchymal transition

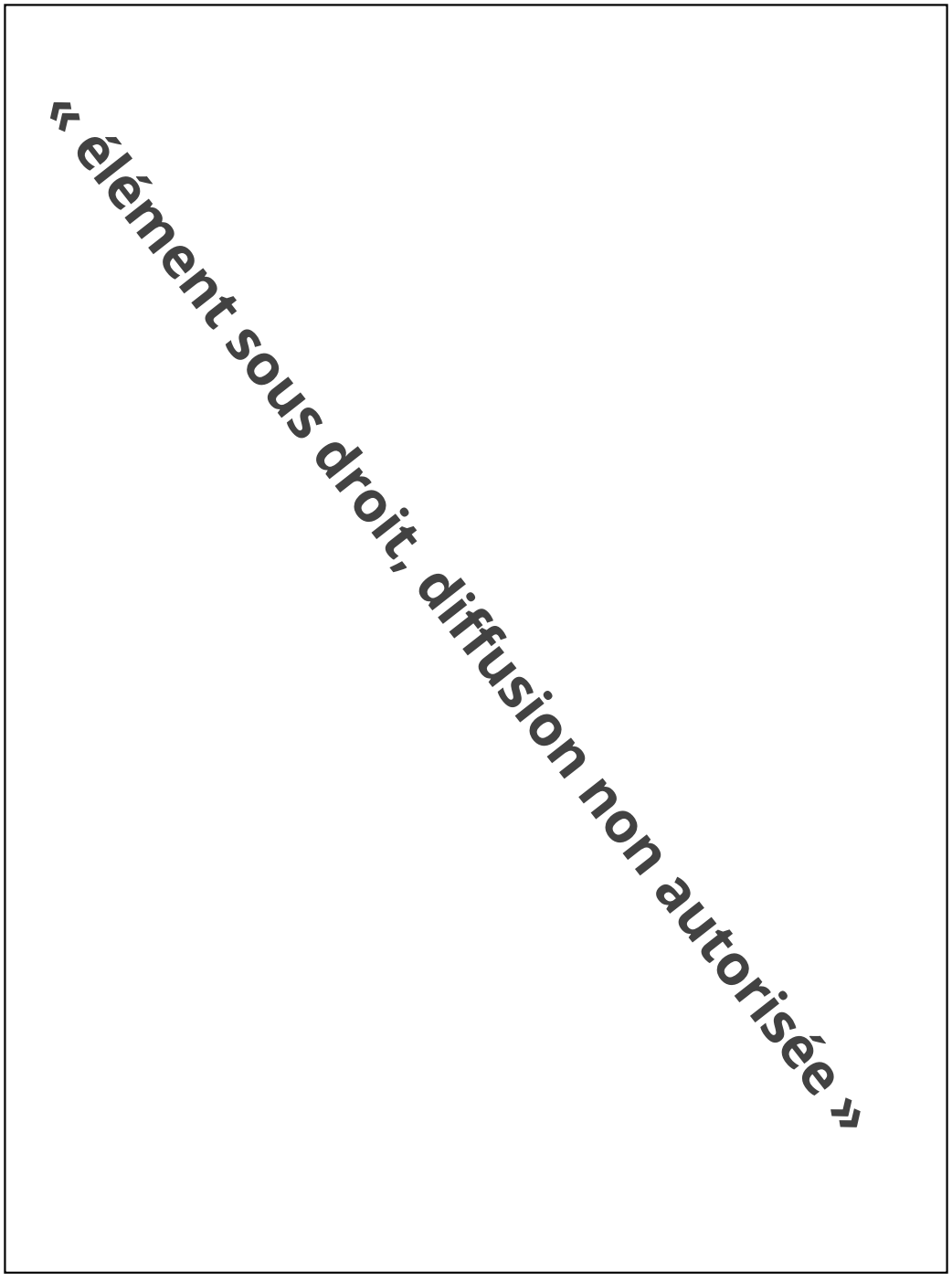


Figure 15: Combined Hepato-Cholangiocarcinoma in a glimpse

Adapted from Gigante et al.(Gigante et al. 2021)

3.6 Mass spectrometry

3.6.1 Technological aspects

Mass spectrometry is a technique for determining the mass of multiple types of molecules based on mass-to-charge (m/z) ratio analysis. The composition of a mass spectrometer can be schematized into four elements: the source, the analyzer, the detector, and finally a separate module that enables data transformation and analysis. The molecules under analysis are first ionized, then accelerated, and passed through the analyzer where they are separated according to their m/z ratio, to be finally measured by the detector. The signal perceived by the detector is transferred to the computer for data processing (Cazier 2019; de Hoffmann 2005; De Hoffman et Stroobant, s. d.). Over the years, different technologies have been developed for each of the phases and mechanical components required to acquire the spectrometry information. As far as the ionization step is concerned, it can be performed under vacuum or atmospheric pressure conditions. Under vacuum conditions, one of the most popular techniques, ionization can be performed by electron impact, chemical ionization or laser ionization. On the other hand, ionization under atmospheric pressure conditions can be carried out by chemical ionization, electrospray, photoionization or laser ionization. The choice of different combinations of ionizing sources depends on the type of molecules to be analyzed (De Hoffman et Stroobant, s. d.). The rapid developments in computer techniques over the years have made possible to apply the concept of mass spectrometry to many scientific fields, allowing precise analysis of various molecules of biological and non-biological derivation (Cornett et al. 2007). The application of these techniques allowed the development of detailed analysis of different classes of molecules currently indicated with the suffix -omic: lipids (lipidomics) (Kleinfeld, Kampf, et Lechene 2004; X. Wang et al. 2014; Hunter et al. 2018); proteins (proteomics) (Delcourt et al. 2018; Xin Liu et al. 2018; Garza et al. 2018) or more generally metabolic (metabolic) components (Fujimura et Miura 2014; Stopka et al. 2019;

Fenaille et al. 2017). In the last decade of the 20th century, the coupling of imaging techniques to spectrometric techniques allowed the development of *in situ* molecular analysis, allowing morphological and molecular analyses to be coupled with extreme precision. This particular technical application is called Mass Specrometry Imaging (MSI) (Amstalden van Hove, Smith, et Heeren 2010). The objective of this technique is to specifically locate molecules within the samples, and once the information is acquired, provides the molecular distribution (molecular mapping) graphically with respect to spatial distribution. Once the region of interest within the tissue samples of interest has been selected, the analysis will allow visualizing the distribution of molecules in the same area with different resolutions depending on the technique used. The concept of spatial resolution is identified as the distance present between two acquisition zones. For example, in the case of laser ionization, the resolution will be considered the distance between two laser shots (Cazier 2019; Amstalden van Hove, Smith, et Heeren 2010).

One of the first techniques developed in the 1960s is Secondary-Ion Mass Spectrometry (SIMS) (Castaing et Slodzian 2021), due to technological advances over the years, this technique has come to have spatial limits of detection resolution equal to 1 µm. The SIMS technique allows very high resolution, thanks to ion beam-induced ionization. The main drawback, however, is related to the induction due to the strength of the ion beam, the fragmentation of the samples, which makes it especially suitable for small molecules (Bich, Touboul, et Brunelle 2014). On the other hand, other more recently developed techniques such as Desorption Electrospray Ionization (DESI) use as sample ionization source an electro-aerosol containing a gas (N2). It is believed that this technique is softer for samples. The advantages of this technique actually lie in the fact that few pre-analytical steps are required; the drawbacks are mainly linked to the coarse resolution (approximatively 200 µm). In general, this technique is particularly used for the analysis of lipids and metabolites (Chughtai et Heeren 2010; Takáts, Wiseman, et Cooks 2005; Porcari et al. 2018).

Developed in parallel by two teams in the 1980s, the matrix-assisted laser desorption (MALDI) source uses a pulsed laser, mainly ultraviolet (UV) laser to desorb and ionize molecules crystallized on a conductive surface (Tanaka et al. 1988; Karas et al. 1987). This technique could be considered in a way as a good compromise between the two techniques mentioned above, as it allows a good resolution without being too aggressive towards the tissue. MALDI also allows a wider range of molecules to be examined. The techniques introduced here are schematized in Fig. 16.

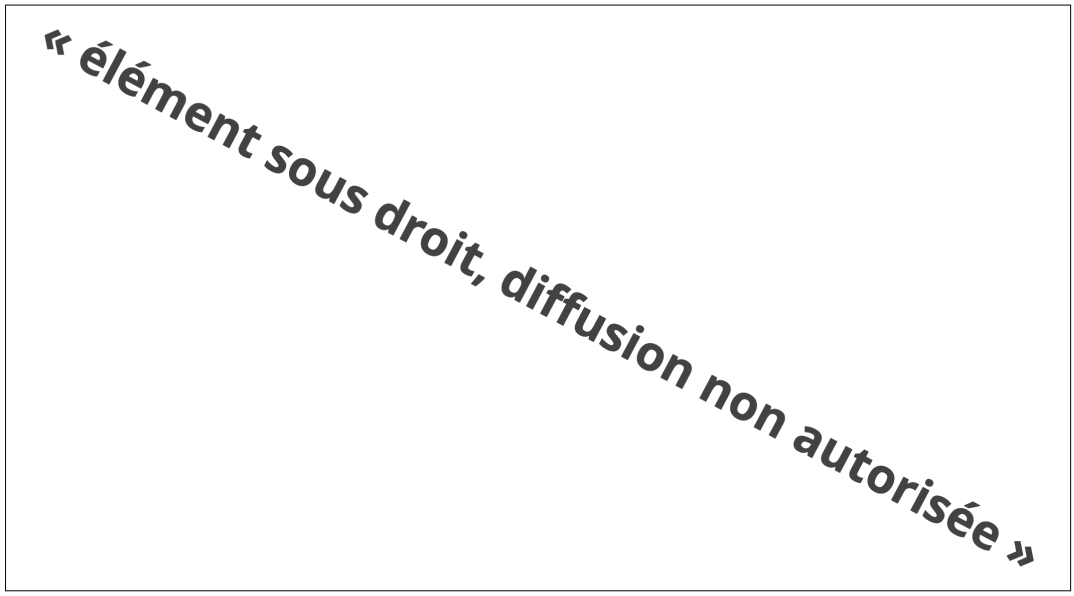


Figure 16: Different Ionization Techniques

Adapted from Cazier (Cazier 2019)

3.6.2 Treatment of biological samples

Depending on the type of study conducted, different protocols are available (Mulder et al. 2016; Oetjen et al. 2016). Indeed, tissue conditioning will greatly affect MSI analysis by potentially modifying the analytes by disrupting their integrity and thus the ability to examine them. In order to preserve biological tissues and thus block enzymatic and metabolic processes that contribute to the degradation of tissues, the two most widely used techniques in pathology are fixation and nitrogen freezing (used rather with research purposes). Fixation is mainly done by

formaldehyde and then subsequent inclusion in paraffin. This procedure represents the standard of tissue preservation in pathological department for diagnostic purposes. These tissues, called FFPE (Formalin-Fixed Paraffin-Embedded) tissues, are archived for many years (up to 20 for some samples), and thus can be used as an important biological resources for clinical research (Groseclose et al. 2008). The aforementioned fixation strategies have ensured the stability of compounds such as peptides and proteins for many years, but represent an obstacle for MSI analysis due to the formation of covalent bonds. In fact, the creation of molecular bridges can lead to decreased ionization of molecules and thus require pretreatment through paraffin removal methods and tissue rehydration. Oetjen et al. and Ly et al., by generating molecular images obtained with MALDI from FFPE tissues, recovered precise localization of metabolites, with satisfactory morphological integrity using an optimized deparaffinization protocol (Oetjen et al. 2016; Ly et al. 2019). Even more in the case of FFPE tissues, the preparation steps are of great importance, depending on the type of sample chosen. Different devices can be used for cutting tissues, such as microtomes, mainly used for room temperature cutting of FFPE samples, or a refrigerated chamber, such as cryotomes for cutting frozen tissues. For MSI analysis, the average section thickness ranges from 5 to 20 μm, depending on the type of sample studied. Tissues are then deposited on conductive slides such as those made of ITO (indium tin oxide) covered with a 130 Å film (Chughtai et Heeren 2010) to allow ion acceleration. This transparent conductive film does not prevent visualization of the specimen with an optical microscope, thus allowing the MSI image to be compared with images obtained after histological staining. The auxiliary staining can be performed on an adjacent section or on the same section after MSI analysis, after removal of the MALDI matrix.

Taking into account that peptides are easier to analyze than proteins and that, on the other hand, the extraction of whole proteins from FFPE tissues is not entirely possible, trypsin digestion of tissues has become a very common preparation step (Boskamp et al. 2017).

3.6.3 Matrix

In addition to sample preparation, the choice of matrix is essential to achieve optimal detection, as it is involved in desorption/ionization step. In fact, matrices must include a chromophore group, which is generally an aromatic core and which allows absorption at the wavelength of the laser beam. The release of the stored energy will allow the detachment of aggregates composed of matrix molecules and analytes. Therefore, the matrices must have essential criteria for desorption and ionization of the target molecules, such as the absorption coefficient calibrated to the laser wavelength of the instrument used. Matrices must form homogeneous crystals with the analytes while remaining chemically inert (excluding reactive matrices) and be a proton donor or acceptor or a source of cations, anions or radicals. In addition, MALDI matrices are often specific for a type of molecule and allow for greater sensitivity for a particular compound. For example, the DHB matrix is most suitable for lipids or oligonucleotides, while the HCCA matrix is most often used for ionization of peptides. The quality of the ionization also depends on the matrix/analyte ratio present in the sample. The quality of MALDI analysis is particularly dependent on the method of matrix deposition. Over time, there have been several techniques involving spray deposition (Aerni, Cornett, et Caprioli 2006), droplet deposition (Delvolve et Woods 2011; Meier et al. 2003) or sublimation (Fernández et al. 2019). Sublimation is the technique that provides the highest resolution, on the order of 2 μm, while vaporization deposition represents a better compromise between deposited volume control and spatial resolution (20 μm).

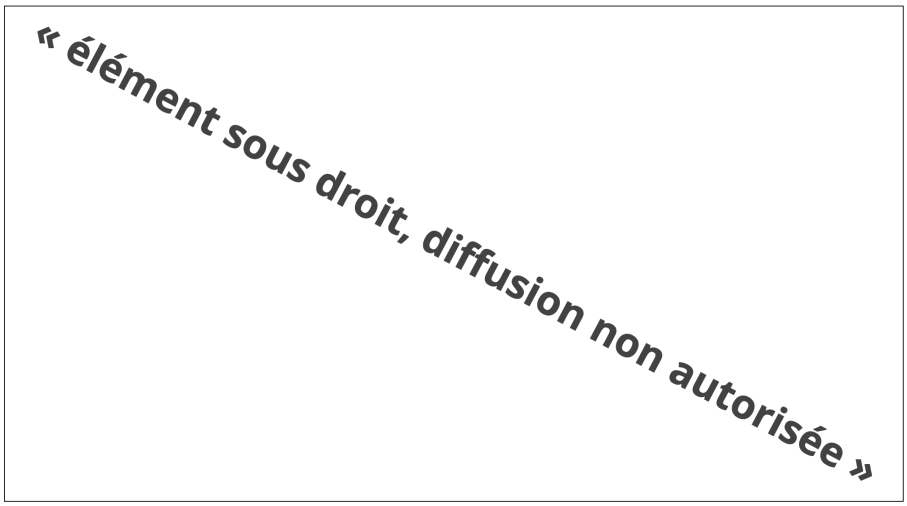


Figure 17: Ionization process in MALDI acquisitions

Adapted from Knochenmuss (Knochenmuss 2006)

~~*Schematic diagram of the main processes occurring in clustered MALDI ionization models. m = matrix, A = analyte, R2 = generic counterion. Preformed ions, separated in the preparation solution, are contained in clusters extracted from the initial solid material. Some clusters contain excess positive charge, others negative charge. If the analyte is already charged, evaporation of the cluster can directly release the ion. In other clusters, the charge may move from the initial position on the matrix to the most favorable position on the analyte (according to a secondary reaction). For analytes with multiple charges, hard and soft desolvation processes can lead to the release of different types of ions. Neutralization by electrons or counterions occurs, but it is usually not complete.*~~

3.6.4 The analyzers

The ions formed are separated according to their *m/z* ratio. There are therefore analyzers that differ according to the principle of measuring this *m/z* ratio. Among the various types, we can mention scanning analyzers that detect ions at consecutive times, such as quadrupoles and ion traps. On the other hand, there are detectors that allow simultaneous detection of ions such as time-of-flight analyzers (Fenaille et al. 2017).

3.6.5 Time-of-flight principle

The principle of the time-of-flight spectrometer is to measure the relationship between the ion's velocity and its mass. The analyzer measures the time taken by an ion, created by a pulsed source and accelerated by an electric field, to travel a distance corresponding to the time-of-flight tube (Fig 18). The ions are ejected from the source and accelerated by an electric potential

difference applied between the carrier and extraction grids placed at a given distance. Therefore, the ion in the source is accelerated by this field. The potential energy of the ion in the source depends on its mass and charge. The potential energy is thus converted into kinetic energy, and its velocity can be calculated according to an equation. By knowing the velocity of the ion, we can know how long it takes to the ion to travel the distance of the flight tube and through analysis of these variables determine the *m/z* ratio of the ion of interest (Cazier 2019; de Hoffmann 2005).

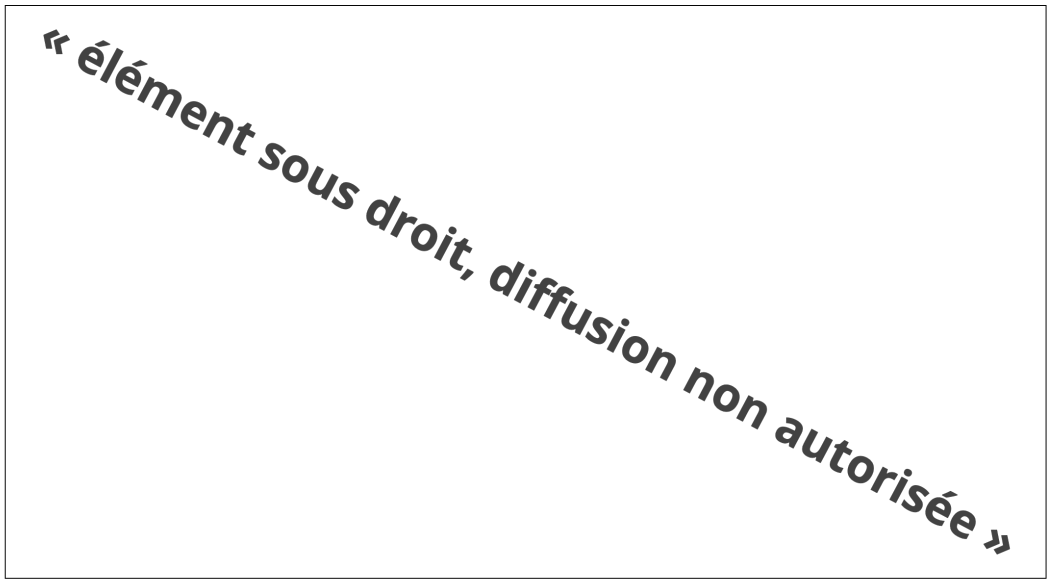


Figure 18: Time-of-flight principle

Adapted from Cazier (Cazier 2019)

3.6.6 Detectors in mass spectrometry

After the ions are separated in the analyzer, the resulting ion beam must be amplified to obtain a measurable signal. The generated ion current will then be transformed into an electronic current. For this purpose, there are several types of detectors that differ in the mode of current detected (ionic current for photographic plates and Faraday cylinders and electronic current for

electron-multiplier detectors). The latter system is currently the most widely used (De Hoffman et Stroobant, s. d.).

3.6.7 Data processing

In MSI, a sample is scanned to recreate an image in pixels corresponding to the signal obtained for a given ion in a specific area of the sample. The raw data generated by this analytical technique provide an intensity profile for each zone in the image as a function of the location of the acquisition point coordinates. Instruments are now capable of generating very high spectral resolution data, thus generating very rich datasets. These large datasets therefore require powerful instruments able to process and synthesize all these information. In general, material-producing industries also provide downstream analysis programs (i.e. FlexImaging for image acquisition, reconstruction and statistical analysis; SciLs Lab for image reconstruction and statistics analysis from Bruker). However, the growing interest of the scientific community in MSI has also led to the development of numerous open source software (Cazier 2019).

3.6.8 Normalization of raw data.

To perform MSI studies, normalization of the obtained signal plays an important role. This transformation of the intensities of each pixel to a common scale is a step that eliminates some of the variability due to the principles of mass spectrometry. Various mathematical approaches have been developed to achieve this, such as normalization for Total Ion Current (TIC), Signal-to-Noise Ratio (S/N), Root Mean Square (RMS) or median of the signals (Jones et al. 2012; Fonville et al. 2012). Normalization by TIC applies equal variation over the entire tissue analyzed and can eliminate the effect of variations induced by inhomogeneous matrix deposition. For the same reason, this method should be applied only to homogeneous tissues so as not to flatten and make uninformative the signal that might be due to area heterogeneity. Another kind of normalization, such as S/N ratio, can also be applied on homogeneous tissue and consists of replacing peak intensity with S/N ratio, which implies that analyte concentration

should be proportional to peak intensity. Normalization of intensity thus plays an important role in signal visualization in MSI, and can also affect the accuracy of quantification (Nimptsch et al. 2009).

3.6.9 Mathematical approaches in data analysis

Unsupervised analyses use the data set without having pre-existing information about its composition. The most commonly used techniques to analyze data in MALDI-MSI in an unsupervised manner are: hierarchical clustering analysis (HCA), principal component analysis (PCA) and stochastic t-distributed neighbor embedding (t-SNE). The (HCA) evaluates the distance between two observations of the data and generates a dendrogram. Based on this hierarchically organized dendrogram, detections (i.e., groups of spectra) are grouped under the same branches based on their mutual similarity. In mass spectrometry imaging, the acquired data correspond to individual spectra that are then represented graphically by pixels; the pixels are thus associated with the spectra. Therefore, the pixels corresponding to each individual spectrum at a given point can be represented with the same color generating an image superimposed on the initial scanner with a so-called "segmentation image". This technique comes to highlight areas of interest based on molecular specificity. This process is by definition carried out without having prior information on the molecular tissue composition. HCA is therefore particularly interesting because it can identify for histological analysis areas of molecular diversity not raised by routine morphologic analysis. (Murtagh et Contreras 2012; Alexandrov et al. 2010).

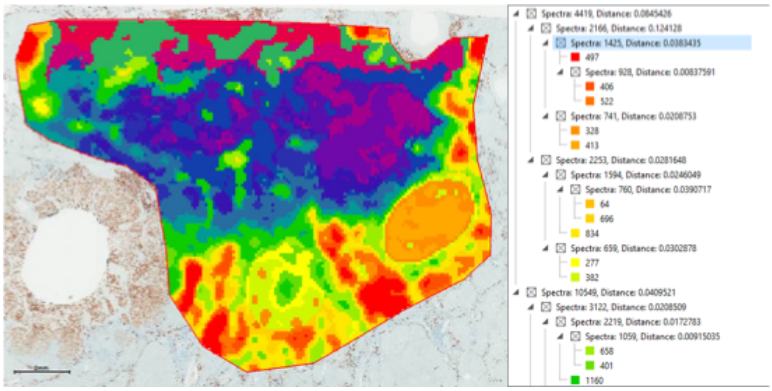


Figure 19: Hierarchical clustering analysis (Segmentation)

The figure shows how the technique was able to generate a series of clusters indicated by each individual color. The groups of ions are placed in a single arborescence according to their similarity. As indicated in the highlighted line, the distance between different groups of clusters indicated by different colors is noted. As the arborescence become more open, clusters become smaller and smaller and more colors are generated, losing the ability to associate a morphological meaning.

Principal component analysis (PCA), on the other hand, is a mathematical analysis technique that aims to reduce the size of the data; it is aimed at simplifying a large data set into a smaller one while preserving most of the information about variation. PCA generates new variables (called principal components, PCs) from the linear combination of the various peaks. To avoid redundancy, the PCs are orthogonal to each other and ordered by the amount of variability in the initial dataset summarized by the single component (Fig. 20). This is done in such a way that an overview of almost all the information in the data can be obtained by looking at the first main components. The result of a PCA provides a chart with the schematic consists of a score chart and a loadings plot. The views of the score plot (Fig. 20 B) allows to assess the degree of similarity between the spectra based on their distribution in the graph; the loadings graph is derived from the score graph and allows one to assess in detail which component (peak) contributes most significantly to determining the distribution. In conclusion, this analysis serves as an initial test to assess whether the data can identify subclasses and thus guide further analysis. PCA is often used to see if the experiment is successful or if preparation artifacts are present (Jolliffe et Cadima 2016; Smith et al. 2017).

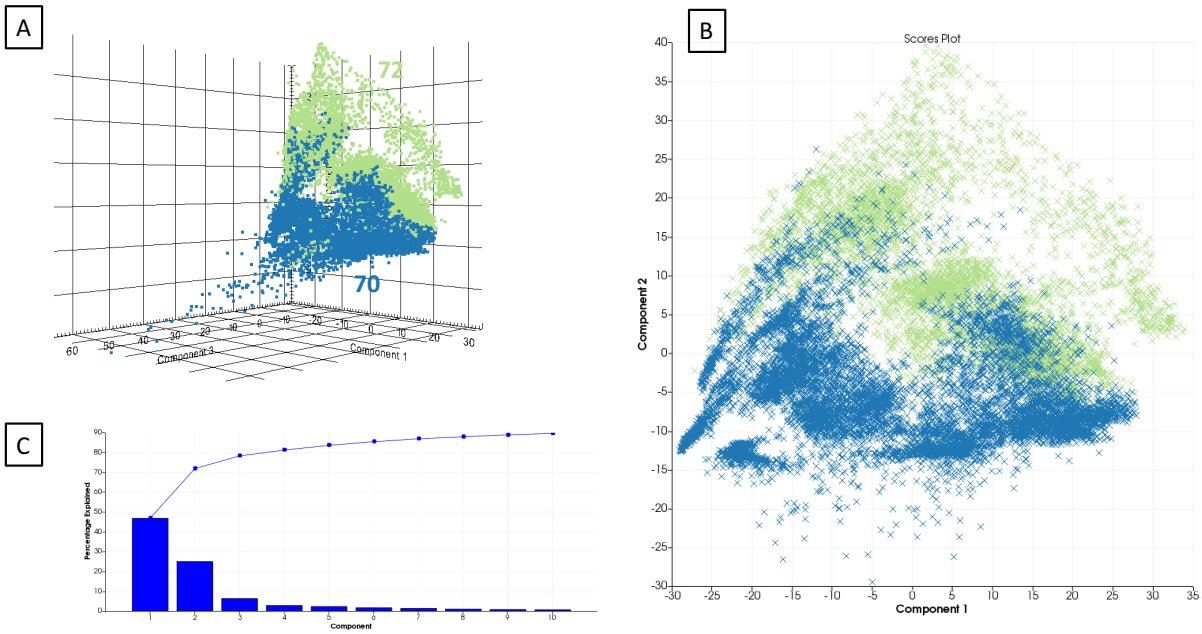


Figure 20: Principal component analysis (PCA)

A: 3D visualization of the components; B: Scores plot; C: Impact of each component on the variance.

Another unsupervised technique is t-distributed stochastic neighbor embedding (t-SNE), which is based on a non-linear dimension reduction that aims to reduce the number of dimensions to two or three dimensions to allow for 2D or 3D visualization, so that components with a high degree of similarity correspond to neighboring points in the graphical representation. While PCA creates new variables the t-SNE preserves all the features of the data to perform the calculations by simplifying them(Smith et al. 2017; Abdelmoula et al. 2016).

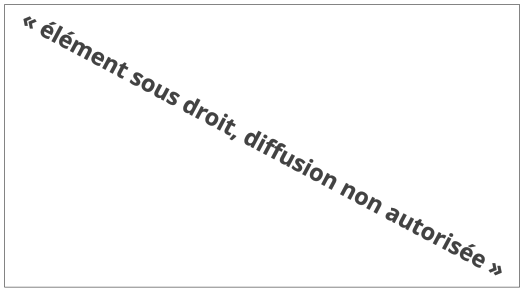


Figure 21: t-SNE.

Adapted from Abdemoula et al (Abdelmoula et al. 2016)

~~*Nonlinear clustering of tumor cell-specific MSI data from 63 patients with gastric cancer. The t-SNE scatterplot reveals clear structural separations based on molecular heterogeneity.*~~

The other strategy that can be used to analyze the data generated by MALDI is supervised analysis. The latter employs algorithms, called classifiers, which learn to categorize on the basis of data labelled by pathologists. These data then correspond to areas identified by their morphology that contain a certain set of peaks used as a reference for the analysis of the rest of the sample. Usually, this type of analysis is divided into a learning phase and a subsequent validation phase. In both phases, different methodological approaches and thresholds are applied to obtain the best combination of sensitivity and specificity suitable for the analyzed sample (Smith et al. 2017).

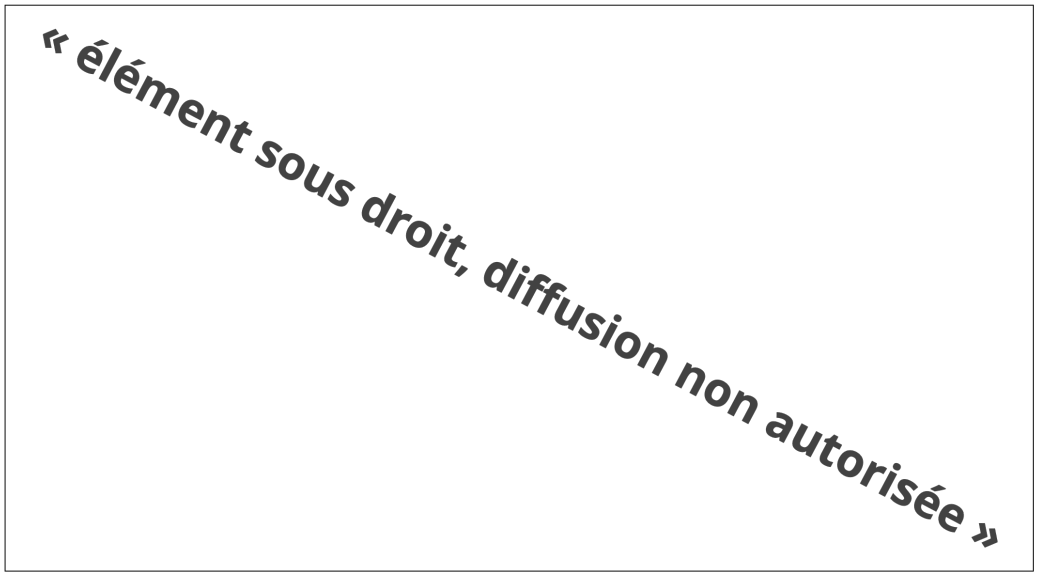


Figure 22: Mass spectrometry imaging (MSI) data elaboration workflow.

Adapted from Smith et al (Smith et al. 2017).

~~(A) Data cube; (B) Pre-processing step performed on spectra; (C) unsupervised (PCA, principal component analysis; HCA, hierarchical clustering) and (D) supervised statistical analysis.~~

3.7 MALDI imaging and tumors

The extent to which morphological heterogeneity may reflect molecular heterogeneity in complex tumors such as cHCC-CCA has not yet been defined in details. Indeed, molecular studies addressing such tumors should ideally include a preliminary microdissection step in order to obtain gene expression profiles according to the different morphological patterns of the tumor. In a small series of 11 cHCC-CCA, the authors used tissue microdissection aimed at analyzing clonal status of HCC and CCA areas (Fujii et al. 2000). This technique in practice is difficult to perform on a large scale, and requires an additional tissue processing. An alternative approach is to use imaging *in situ* techniques that provide molecular profiles associated with specific histologic features, without preliminary steps of molecular extraction, dissection, or labeling. Among them, MALDI imaging emerged as a powerful technique for analyzing the spatial arrangement of various molecules (proteins, peptides, lipids, metabolites) in complex tissues. This technology has enabled the identification of new diagnostic and prognostic markers in several types of human malignancies, including HCC and iCCA (Le Faouder et al. 2014; Laouirem et al. 2014). Once identified and sequenced, these markers can be further assessed by immunohistochemical methods (Poté et al. 2013). Although it was initially developed on frozen tumor sections, MALDI imaging is now applied on FFPE tissue sections, which provide the best morphologic analysis and represent the main source of routine tumor specimens archived in pathology departments (Groseclose et al. 2008).

MALDI technology has established itself as a reliable tool for mapping the molecular composition of tissue samples due to its very high spatial resolution, while maintaining good sensitivity of analysis. With the use of tissue micro-arrays (TMA), it is possible to obtain information on a large number of samples in a single acquisition, limiting experimental bias. (Caprioli 2016; Caprioli, Farmer, et Gile 1997).

3.7.1 MALDI imaging applications in oncology

Oncology is probably the field of study in which MSI has been most widely used. Thanks to frozen tissue banks in pathology departments and, lately, protocols adapted to FFPE tissues, studies have been conducted on a wide variety of tumors, including lung, breast, genitourinary, gynecological, renal, cerebral and gastrointestinal cancers (Basu et Agar 2021). The applications of MSI in the field of oncology have focused on multiple research axes. On one hand, the most fervent area is that of diagnostics, as MSI can be a powerful tool to help the pathologist establishing a diagnosis, as it can function as an enhancement of immunohistochemistry. Nowadays, diagnosis of cancer is based on various useful tools in addition to the routine Hematoxylin and Eosin staining. Technical and cultural advances have also made it possible to identify specific therapeutic targets that can be identified with the help of antibodies or molecular tests. It is therefore increasingly common to use ancillary techniques to achieve a diagnosis of cancer and introduce prognostic elements. Techniques routinely used are immunohistochemistry, *in situ* hybridization, and molecular extraction techniques for gene sequencing. As explained in the section on tumor heterogeneity, the location and distribution of target molecules may be heterogeneous per se in the initial tumor or acquired in the course of treatments, adding a further degree of spatial complexity (Porta Siegel et al. 2018). The schematic comparison between routine histology, immunohistochemistry and MSI are shown in Table 4.

Table 4: Comparison of histology, immunohistochemistry, and MALDI imaging.

Adapted from Lee et al (P. Y. Lee et al. 2021)

	Histology	**Immunohistochemistry**	**MALDI Imaging**
Application	Examination of tissue morphology	Detection of the presence and expression pattern of specific antigens	Analysis of the abundance and spatial distribution of biomolecules
Principle	Requires chemical/chromogenic stains to provide contrast and differentiate different structures Observation under light microscope	Requires antibodies that target the antigens of interest Observation under light microscopy	It is a label-free measurement of molecular profiles using mass spectrometry
Multiplexing	Not applicable	Restricted to a few target antigens	Global analysis of thousands of biomolecules
Resolution	Subcellular (<1 mcm)	Subcellular (<1 mcm)	5–200 mcm
Quantification	Enables quantification of stained cells and tissue structures	Enables semi-quantitative assessment of selected antigens	Enables relative and absolute quantification of biomolecules
Identification	Not possible	Not possible (requires prior knowledge of target antigens)	Capable to identify unknown analytes
Advantages	Well-established method Easy to perform Widespread	Well-established method Highly specific Widespread	Does not require any labeling Simultaneous analysis of hundreds to thousands of a wide range of biomolecules High specificity and sensitivity
Disadvantages	Non-specific Subjective interpretation Needs medical training	Depends on the availability and quality of antibodies Interpretation	Requires specialized instrument Limited resolution Costs

3.7.2 MALDI imaging in heterogenous tissues

The pathologist can use MSI to better explore tissues with a high content of heterogeneity, identifying cell subpopulations not visible by conventional means with high resolution (up to 50 mcm). MALDI imaging can classify tumors at the molecular level without relying on their morphology. It can also be used to derive prognostic or therapeutic biomarkers (Caprioli 2016; Basu et Agar 2021; Berghmans et al. 2020).

In order to obtain accurate information about the composition of the tissues analyzed, it is first necessary to construct robust classification models. Some authors have focused on the impact of histological annotations on classification accuracy, especially in oncology. Intra-tissue heterogeneity has an important influence on annotation efficiency, with a more pronounced effect on more heterogeneous tissues, such as ductal adenocarcinoma of the pancreas, where the accuracy of annotation-derived systems in semi-supervised systems is strongly improved by labelling. On the other hand, when they are used in more homogeneous samples, histologic annotations have less impact on classification accuracy (e.g. renal tumors) (Juliana Pereira Lopes Gonçalves et al. 2021). The presence of multiple tumor clones within the same lesion or patient and thus phenotypic heterogeneity has been explored in the literature with growing interest and awareness (Marusyk, Almendro, et Polyak 2012; Gerlinger et al. 2012). One of the most original approaches is probably that based on the MALDI technique. A study conducted on samples obtained from gastric and breast carcinomas allowed the identification, by clustering data, of tumor subpopulations within lesions not identified by histological analysis. The presence of these populations was then associated with worse prognosis; while in the case of gastric cancer, their presence was associated with a worse overall survival; in breast cancer, they correlate with the development of metastases. The minimum amount of tumor subpopulation required to have a clinical impact on patients was estimated to be between 10-14%. However, it must be considered that each individual sample analyzed did not represent

the overall proportion of subpopulations in the complete tumor. The proposed thresholds must therefore be considered specific to this experiment. What can be taken as a message is the notion that heterogeneity has a strong impact on prognosis (Balluff et al. 2015). Since the first decade of the 2000s, MALDI imaging applied to tumor samples has been shown to be able to detect, after a single acquisition, the presence of cell subtypes identified on the basis of hierarchical clustering techniques. One of the earliest studies in this regard showed that MALDI imaging was able to identify healthy and cancerous tissue in gastric cancer specimens despite the coarse resolution (Deininger et al. 2008). The basic concept of unsupervised analysis is to take the raw data without labeling from outside, and then aggregate the data in clusters based on intrinsic information, to highlight unseen patterns. This type of analysis can also be done with partial labeling (Smith et al. 2017). In gastric cancer, MALDI has been applied in its various possibilities: lipidomic, allowing detailed analysis of the lipid composition of cancerous and healthy tissue; proteomic by identifying proteins associated with poor outcome; and finally metabolomic by identifying the different distribution of a metabolite resulting from experimental chemotherapy (Smith et al. 2017; Balluff et al. 2011). MSI was used to decipher tumor heterogeneity in triple-negative breast cancers, the analysis on pathologic and healthy tissues discovered some proteins associated with poor prognosis. The authors first created a peptide list through a technique of liquid chromatography coupled to matrix-assisted laser desorption/ionization mass spectrometry (LC-MALDI-MS/MS) and then searched for matches with tissue MALDI imaging. Among these proteins, some had never been associated with breast cancer(Phillips, Gill, et Baxter 2019).

3.7.3 MALDI imaging in less heterogenous tissues, TMA approach.

A very effective application of MALDI imaging is the analysis of TMAs. Small tissue cores of interest from several FFPE tissue blocks derived from individual cases can be harvested and

subsequently included in a few tissue blocks, called tissue microarrays (TMAs). The cylindrical tissue cores that are assembled into TMAs can be of different sizes, and the construction can be manual or automatic. Constructing this type of sample can reduce the errors associated with multiple acquisitions and also reduces the testing time. This approach was applied to lung cancers and identified two main subgroups of non-small cell lung cancers, squamous cell carcinomas and adenocarcinomas. Tissue annotations made by the pathologists on the TMA were overlaid on the MALDI imaging data and regions of interest were manually marked. All mass spectra obtained from the annotated areas were used for data analysis. The spectra were normalized and then, a classification system was generated using the Linear Discriminant Analysis Algorithm (LDA) analysis model. The algorithm generated a list of peaks that were selected to create a classification model in the two cancer classes. This system was generated in a training cohort and subsequently confirmed in a validation cohort (Fig. 23). The sensitivity and specificity of the model for adenocarcinomas were 100 and 98% and 98 and 100% for squamous cell carcinoma, respectively. At least four peptides showing an area under the ROC greater than 0.7 were found between the two groups. The four peptides, through database analysis, were identified as fragments derived from the digestion of cytokeratins (Kriegsmann et al. 2016).

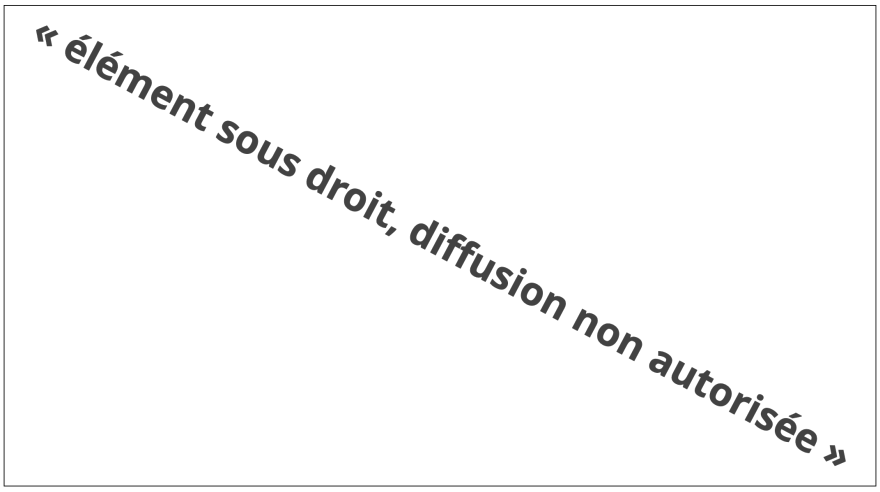


Figure 23: MALDI workflow.

Adapted from Kriegsmann et al.(Kriegsmann et al. 2020)

~~*1-TMA construction and preparation of the tissue samples, 2-test set was analyzed by MALDI imaging in order to find subgroup with specific MALDI profile differences. 3- The MALDI algorithm was subsequently validated on a separate cohort.*~~

A few years later, the same group of authors, implementing the number of samples, reproduced the same type of results in about 1000 lung cancer samples. To improve their MALDI imaging classification, they used three algorithms Random Forest (RF), support vector machine (SVM), and linear discriminant analysis (LDA). The Random Forest seemed to be better than the other algorithms. The sensitivity and specificity achieved were 92.9% and 89.3%, respectively (Kriegsmann et al. 2020). Interestingly, in a recent study, the discrimination between squamous cell carcinomas and adenocarcinomas was again upgraded using an approach based on neural network and LDA with a validation on whole section resulting in 100% test accuracy (Janßen et al. 2022). The effectiveness in lung cancer classification derives probably in part from the homogeneity of these tissues. Both supervised and unsupervised analytical approaches were used to predict the development of metastasis in a large cohort of colon cancer patients combined in TMA samples. The comparison of the two approaches is difficult but, in a sense, complementary. Although supervised classification is more accurate due to the direction given by labelling, it has a tendency to rely on the most intense peaks present in the annotated tissue

and can sometimes ignore less intense peaks. Furthermore, the supervised approach uses a combination of preponderant elements for classification, making it difficult to identify a single m/z value of interest. The unsupervised approach, can be used to better detect the smaller differences in a larger data set by better reflecting the heterogeneity of the sample. Thanks to their combined analytical strategy, the authors were able to identify a classification system capable of predicting with 90% accuracy the development of metastases and, on the other hand, identified peptides of interest associated with the development of metastases and reduced survival (Kriegsmann et al. 2020). Again, to empower the MALDI analysis on TMAs, 302 colorectal cancers and 257 endometrial cancers were analyzed combining supervised machine learning and mass spectrometry. It was possible by this approach to distinguish colorectal cancer tumor tissues from healthy tissue of the same patients with 98% accuracy (98.2% sensitivity and 98.6% specificity). In endometrial cancers, the algorithm could predict the presence of lymph node metastasis with an accuracy of 80% (90% sensitivity and 69% specificity) (Mittal et al. 2021).

3.7.4 MALDI imaging approach in digestive cancers

In the field of digestive neoplasms, and in particular in pancreatic biliary neoplasms, MALDI imaging has been used to discriminate extrahepatic CCA from pancreatic ductal carcinoma (PDAC), both characterized by a glandular appearance with a stromal desmoplasia. However, clinical management and thus therapy are different and require accurate differentiation prior to treatment. The classification systems formed through the S.V.M. technique for me allowed discrimination between both tumors with 91% accuracy (Bollwein et al. 2022). In pancreatic precancerous lesions “pancreatic intraductal mucinous neoplasms” (IPMNs), MALDI imaging was also able to identify biomarkers associated with the degree of dysplasia. The identified protein peaks were validated in an independent series of IPMNs derived from surgical

specimens and endoscopic fine-needle aspiration (EUS FNA) specimens. Through this analysis, differential spectra of proteins in two groups according to the degree of dysplasia, were found to show significant intensities. Validation on external samples confirmed that ubiquitin and thymosin-b4 were overexpressed in IPMNs with high-grade dysplasia (Rebours et al. 2014).

In order to better understand the pathological mechanisms involved in the progression of pancreatic cancer, which still remains one of the neoplasms with the worst prognosis, some authors have recently characterized the protein composition of pancreatic adenocarcinoma and related metastases. The generated AI-based classification models were over 90% accurate in discriminating between the two tissues (pancreatic adenocarcinoma and metastases). The following collagen fragments (COL1A1, COL1A2 and COL3A1) were later identified as associated with tumor progression (J. P. Gonçalves et al. 2022). Using MALDI imaging, discriminatory peptide signatures associated with pancreatic carcinoma tumor invasiveness characteristics were recently identified. These peptides were subsequently correlated with nine proteins in a cohort of patients using a nanoliquid chromatography (nLC)-MS/MS technique on adjacent tissue. Associated prognostic features were lymphatic vessel invasion, lymph node metastasis and angioinvasion (Loch et al. 2021). Although CCA arises from biliary epithelial cells, its molecular expression varies considerably depending on the localization of the neoplasm. According to their localization, CCAs can be divided macroscopically into intra-hepatic or extra-hepatic. In the group of iCCA, spectrometric analysis allowed the differentiation of tumors developed either on healthy or cirrhotic liver. In fact, iCCA developed on cirrhotic liver had a tendency to have angiogenesis-related protein overexpression in a manner similar to HCCs while extra-hepatic CCAs had a strong upregulation of mucins and molecules involved in the secretory pathways (Le Faouder et al. 2019). In addition, hilar (h) and peripheral (p) CCA were further compared with MALDI technology generating 19 differential protein peaks, of which 14 were overexpressed in h-CCA and five in p-CCA.

Among the markers expressed in h-CCAs, the most discriminating were neutrophil peptides 1-3 and S100 proteins (A6 and A11), while thymosin 4 was overexpressed in p-CCA (Le Faouder et al. 2014). In the field of liver cancer, the MALDI-based approach has enabled the identification of some factors implicated in liver carcinogenesis. Showing how this technique can not only identify biomarkers but also mechanisms of pathogenesis. Under the assumption that end-stage cirrhosis with or without HCC appears identical in H&E sections, Laouirem et al. were able to classify the two types of cirrhosis differently. Among the set of markers used to establish the classification model, a truncated form of ubiquitin differentially expressed between low-risk and high-risk cirrhosis, and between high-risk cirrhosis and HCC (Laouirem et al. 2014). As mentioned earlier, the MALDI approach has also provided innovative prognostic tissue markers in liver malignancies. One of the factors negatively influencing the prognosis of HCC is certainly microvascular invasion (MVI), given its association with post-operative tumor recurrence and mortality. This histologic feature is commonly detected only after the extensive examination of the surgical specimen, and is therefore not assessable in tumor biopsy. Comparative analysis of mass spectra acquired from the two groups of samples derived from HCC with or without (MVI) yielded a set of 30 differential protein peaks. Among them, two peaks were identified as being modified forms of histone H4 (Poté et al. 2013). These results were then validated on “virtual” biopsies (derived from surgical samples) by immunohistochemistry based on three markers (H4K16ac; H4K20me2; Prothrombin induced by Vitamin K Absence-II (PIVKA-II) (Poté et al. 2018).

MALDI imaging is not the only technique based on an " unlabeled " approach. In a recent work, Raman spectroscopy was compared to MALDI in HCC samples. Raman spectroscopy alone showed an accuracy of 84% in identifying HCC from non-tumoral tissue. MALDI was able to classify HCC in the different degrees of differentiation with an accuracy of 90%. Combining Raman data with MALDI IMS did not improve these results (Kirchberger-Tolstik et al. 2021).

3.7.5 Unsolved issues

Before MSI can be integrated to routine diagnostic methods, several points need to be standardized. The main point to be addressed is the implementation of dedicated protocols for sample preparation, data analysis and transmission of results in a way that makes them comprehensible for all actors involved in patient management. These protocols must then be approved by the competent authorities. In the same direction of simplification, it is also important to think about creating more user-friendly interfaces. It remains clear that in order to standardize and democratize the use of this technique, it is necessary to create databases comprising a large quality and quantity of tissue samples (Juliana P. L. Gonçalves, Bollwein, et Schwamborn 2022). One of the main limitations that has so far curtailed the large-scale use of MALDI is certainly the doubt about the reproducibility of the experiments. Each analytical center generally uses a specific protocol, and each operator adjusts the spectrometer according to his or her analytical needs. The question has often been raised about the presence of a possible batch effect. Several studies have proven the validity of results from FFPE samples from various centers but often with a centralized IMS analysis (Lazova et al. 2016). A collaboration among several German spectrometry analysis laboratories tried to answer this question. The authors tried to show that classification based on different MALDI spectrometers performed at different centers on the same samples was possible. For this purpose, a TMA composed of various tumor types was analyzed by different centers with different protocols. Using standard data preprocessing, a classification accuracy of 91.4% per pixel was achieved. The limitation of the study was the fact that the samples included in the TMA had a high degree of homogeneity in the various subtypes, which were particularly different from each other in terms of histological type. The potential for differentiation was therefore high. Moreover the effectiveness of the classifier also derived from the correct histological labelling (supervised analysis) (Deininger et al. 2022) .

3.8 Conclusion about MALDI and cancers

It can be proposed from the above discussion that MALDI imaging is a particularly promising tool in the field of oncology. The different applications of MALDI can be dichotomized according to the degree of tissue and cell heterogeneity present in the neoplasm being studied. On one hand, particularly homogeneous tumors can be easily sampled and studied by constructing TMAs, as this methodological approach will allow a large number of samples to be collected and grouped into smaller samples. These will then be analyzed in a short period with only a few experiments, minimizing the bias related to the experimental procedures. In this type of samples, supervised classification systems are highly effective, as are artificial intelligence analyses, and make it possible to accurately identify different tumor types and find relevant diagnostic and prognostic markers.

On the other hand, there are tumors with a high degree of intralesional heterogeneity. For this type of tumors, the strategy based on the construction of TMAs, especially if small cores (0.5-1mm) are included, carries the risk of insufficient sampling of the variety of cell populations within the lesion. Moreover, supervised classification systems struggle to create effective models given the variety of inputs. Unsupervised techniques will therefore allow the appreciation of intra-tumor variability and the identification of features not visible to the pathologist's eye. For this type of tumor, however, considerable post-acquisition data processing is required to synthesize the results. Another fundamental application of MALDI is the direct identification of proteins or the identification via databases search.

4 RESULTS FIRST AXIS: Improving the diagnosis of cHCC-CCA

Article 1: Combining imaging and tumor biopsy improves the diagnosis of combined hepatocellular-cholangiocarcinoma (Published)

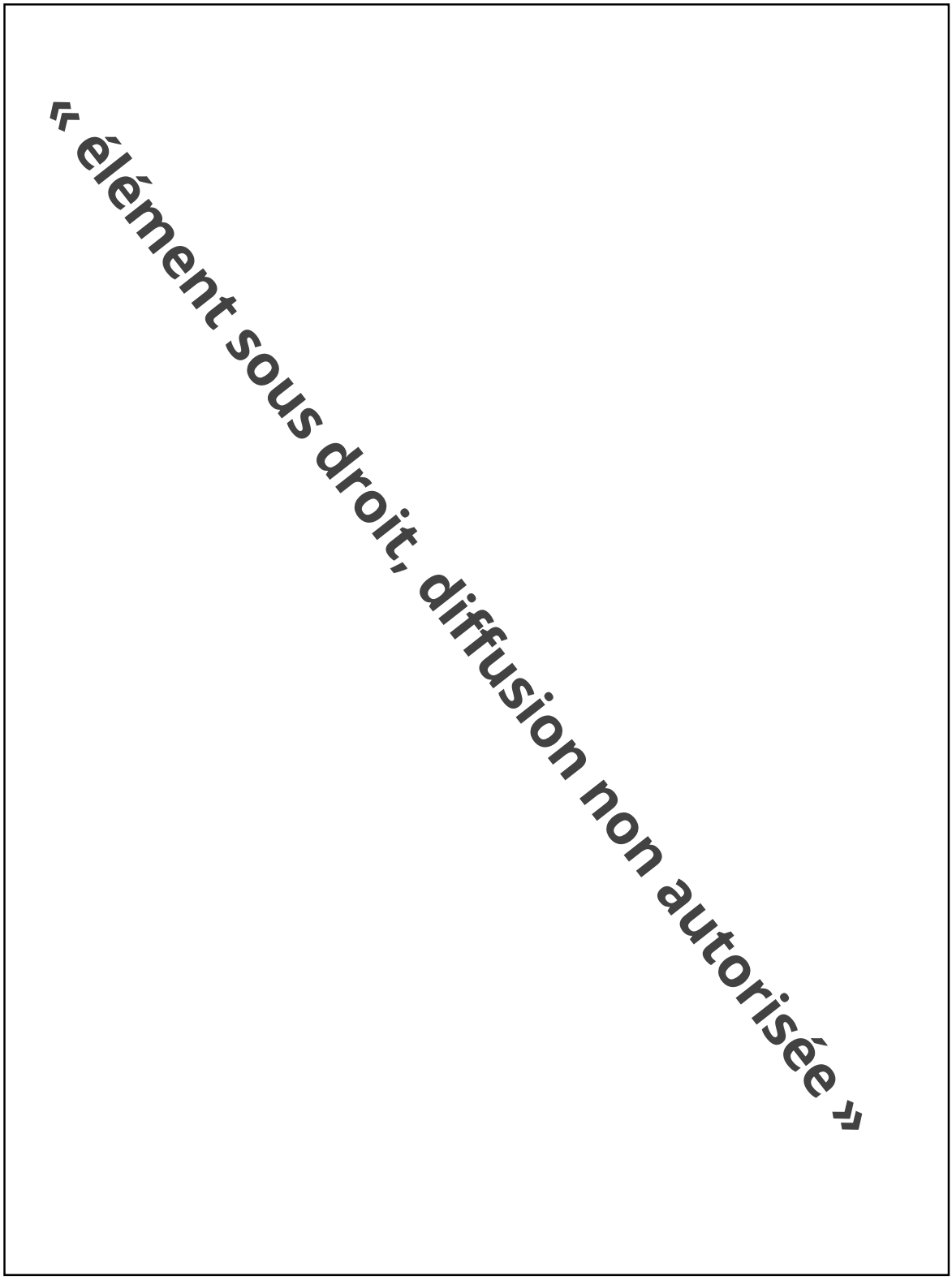
Elia Gigante, Maxime Ronot, Caroline Bertin, Maria Ciolina, Mohamed Bouattour, Federica Dondero, François Cauchy, Olivier Soubrane, Valérie Vilgrain, Valérie Paradis. Liver International. December 2019.

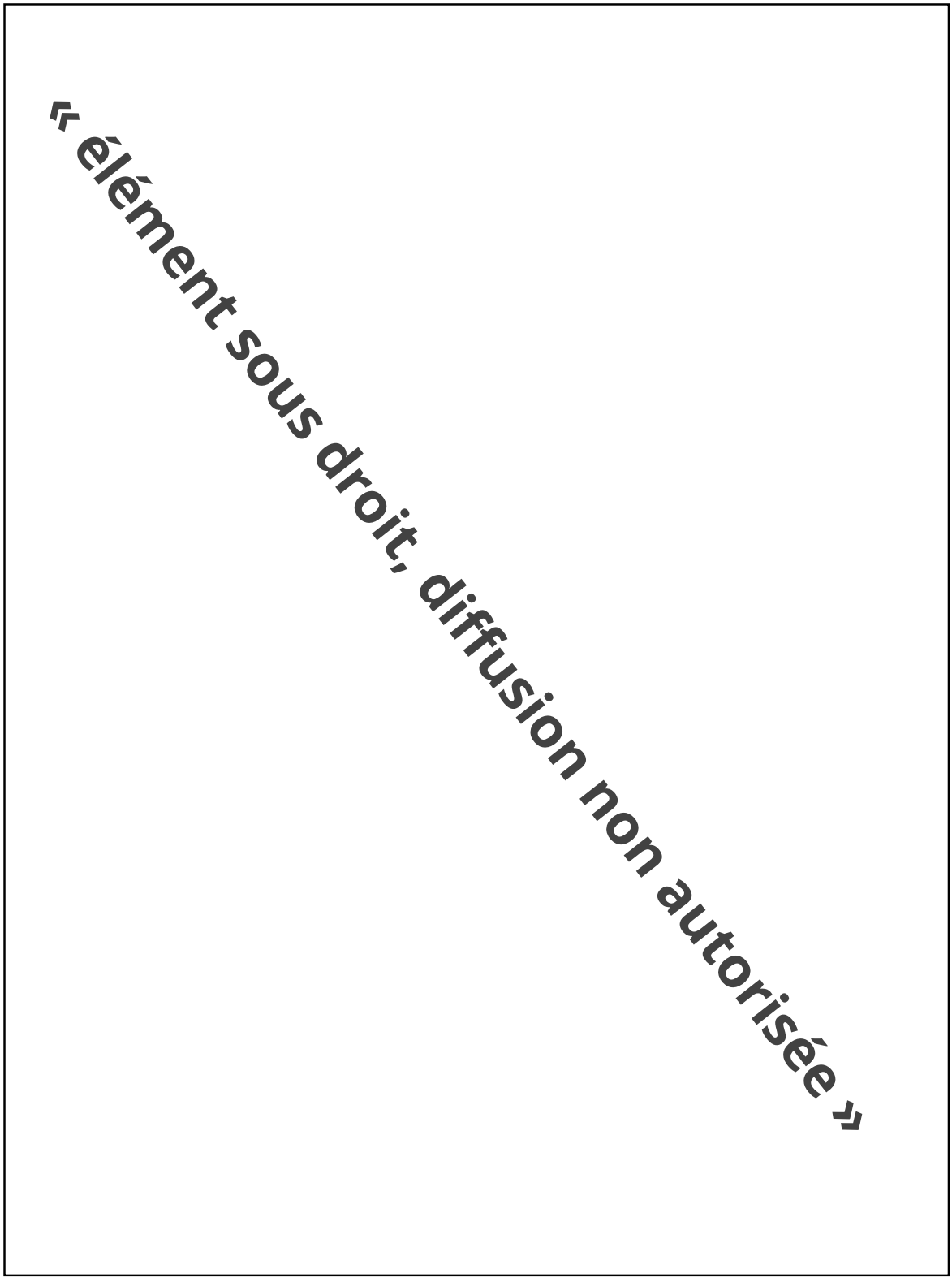
cHCC-CCA is a highly heterogeneous tumor, considering that the performance of conventional diagnostic means has never been accurately assessed, we decided to evaluate the efficacy of imaging (CT and MRI) and liver biopsy on the lesion to confirm the diagnosis of cHCC-CCA compared to intrahepatic cholangiocarcinoma (iCCA). To address this issue, we retrospectively included a set of cHCC-CCA with available biopsy and imaging performed prior to resection.

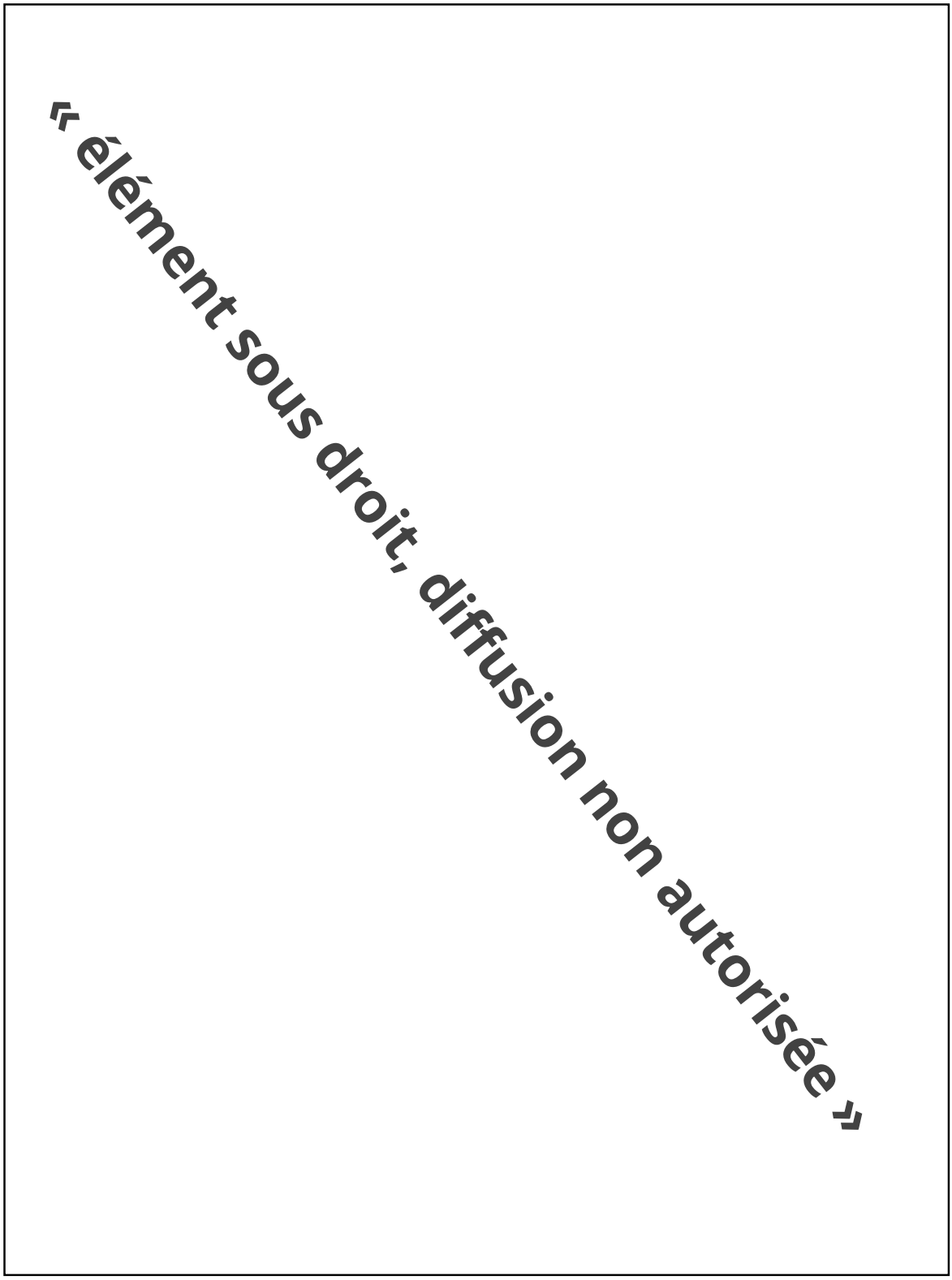
Main results demonstrated the relatively low performance of both imaging approaches (Radiology and histology) when used separately. However, and with the support of immunohistochemistry, a 2-step strategy (radiology then biopsy) is much more performant.

Such approach may be improved through a more extensive tumor sampling based on radiological features. Although not easy to propose in clinical practice, increasing the number of image-guided biopsy passages in tumors seems to us a recommended practice to probe all components.

« élément sous droit, diffusion non autorisée »


« élément sous droit, diffusion non autorisée »


« élément sous droit, diffusion non autorisée »


« élément sous droit, diffusion non autorisée »

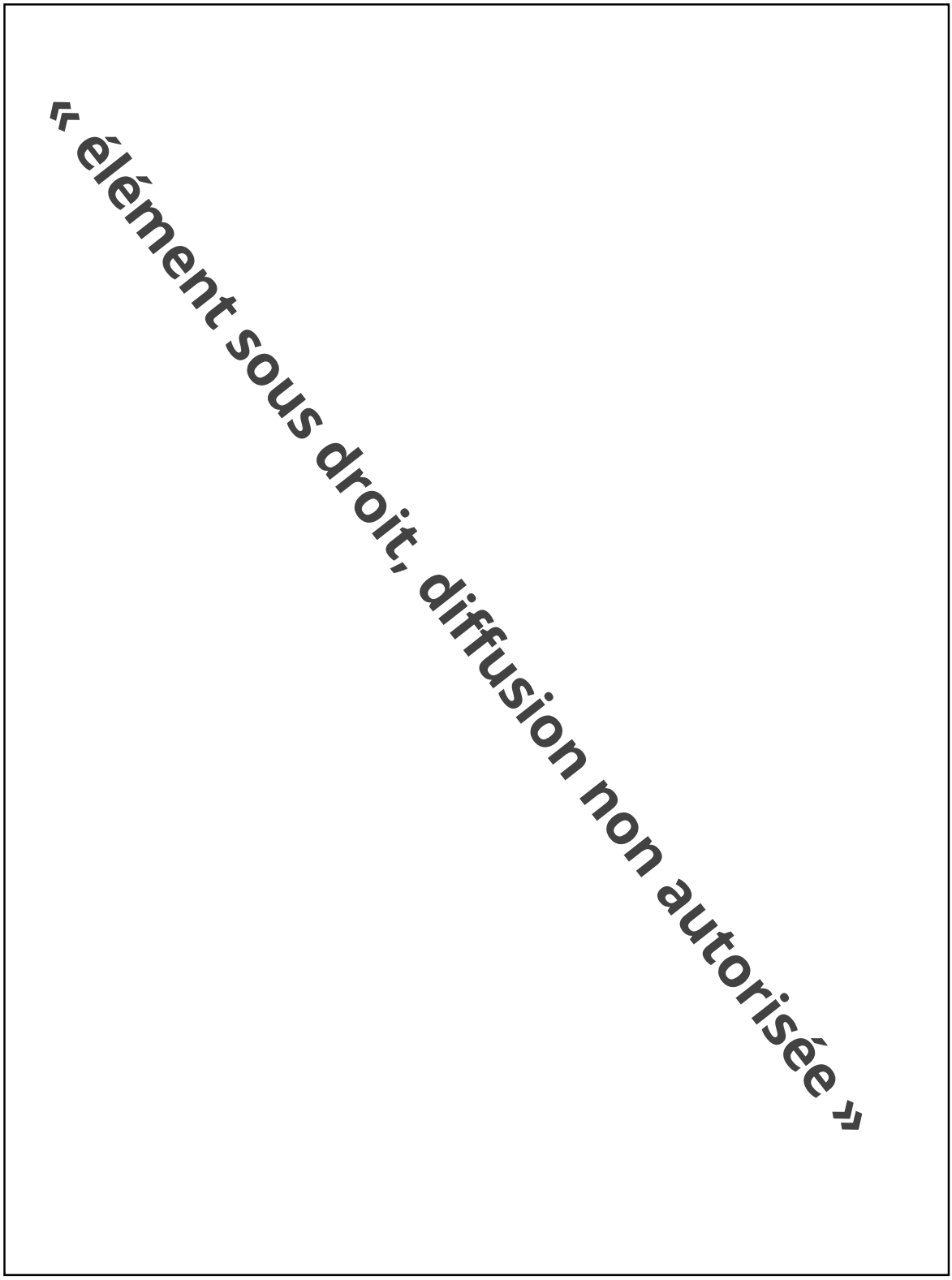
5 RESULTS SECOND AXIS: Improving the management of systemic therapy of unresectable or metastatic cHCC-CCAs.

Article 2: Systemic treatments with tyrosine kinase inhibitor and platinum-based chemotherapy in patients with unresectable or metastatic hepatocholangiocarcinoma (Published)

Elia Gigante, Christian Hobeika, Brigitte Le Bail, Valérie Paradis, David Tougeron, Marie Lequoy, Mohamed Bouattour, Jean-Frederic Blanc, Nathalie Ganne-Carrié, Henri Tran, Clémence Hollande, Manon Allaire, Giuliana Amaddeo, Hélène Regnault, Paul Vigneron, Maxime Ronot, Laure Elkrief, Gontran Verset, Eric Trepo, Aziz Zaanan, Marianne Ziol, Massih Ningarhari, Julien Calderaro, Julien Edeline, Jean-Charles Nault. Liver Cancer. June 2022.

The therapies used in advanced stages of cHCC-CCA in clinical practice are based on the strategies used for the either HCC and iCCA. To date, there are no studies with substantial patient numbers aimed at evaluating systemic therapies in cHCC-CCA. With our study, we initially aimed to describe the survival of patients with cHCC-CCA undergoing chemotherapy and to compare them with other PLCs. Furthermore, to address the lack of scientific evidence regarding systemic treatments for metastatic/unresectable cHCC-CCA, we wanted to compare the different treatments used. To achieve this, we collected data from 11 French centers creating a retrospective multicenter cohort of unresectable or metastatic cHCC-CCA who received systemic treatment with sorafenib or platinum-based chemotherapies and compared them with two cohorts of advanced HCC and iCCA patients treated with systemic therapies.

Main results: Patients with cHCC-CCA had the same survival as HCC and iCCA when treated with systemic therapies. ALBI score, ascites and tobacco use were independently associated with OS in patients with cHCC-CCA. Treatment with TKIs or platinum-based chemotherapy in patients with cHCC-CCA is equivalent in terms of survival. The ALBI score was helpful to predict the survival. Our study provided a reliable basis in the literature to justify the clinical attitudes used empirically to date. Given the recent introduction of systemic immunotherapy-based treatments for advanced PLCs, it is our intention to update our study to include cHCC-CCA patients treated with the new immunotherapies.


« élément sous droit, diffusion non autorisée »

« élément sous droit, diffusion non autorisée »

« élément sous droit, diffusion non autorisée »

« élément sous droit, diffusion non autorisée »

« élément sous droit, diffusion non autorisée »

« élément sous droit, diffusion non autorisée »

6 RESULTS THIRD AXIS: Exhaustive molecular characterization of cHCC-CCA by MALDI imaging

6.1 Article: MALDI imaging, a multiplex approach without a priori, is a powerful tool for deciphering intra-tumoral heterogeneity: combined hepato-cholangiocarcinomas as proof of concept (In preparation)

MALDI imaging, a multiplex approach without a priori, is a powerful tool for deciphering intra-tumoral heterogeneity: combined hepato-cholangiocarcinomas as proof of concept.

Gigante E.[1*], Cazier H.[1,3*] Beaufrère A.[1,2], Albuquerque M.[2], Laouirem S.[1], and Paradis V.[1,2]

1) Centre de recherche sur l'inflammation, Inserm, Université de Paris, INSERM UMR 1149 « De l'inflammation au cancer », Paris, France.
2) Service d'Anatomo-Pathologie, Hôpital Beaujon, AP-HP, Clichy, France et Centre de recherche sur l'inflammation, Inserm, Université de Paris, INSERM UMR 1149 « De l'inflammation au cancer », Paris, France.
3) Plateforme iMAP, Centre de recherche sur l'inflammation, Inserm, Université de Paris, INSERM UMR 1149 « De l'inflammation au cancer », Paris, France.
*The authors shared the first authorship

Abstract

Combined hepato-cholangiocarcinomas (cHCC-CCA) belong to the spectrum of primary liver carcinomas, which include hepatocellular carcinomas (HCC) and intrahepatic cholangiocarcinomas (iCCA) at both ends. Mainly due to the high intratumor heterogeneity, diagnosis and pathological description are still challenging. Taking advantage of *in situ* non-targeted molecular mapping provided by MALDI, we sought to develop a multiscale morphological approach, integrating molecular and conventional pathological analysis. MALDI imaging was applied to 5 resected cHCC-CCA cases. Principal component analysis and segmentations were performed. A list of peptide peaks derived from *'in silico'* digestion was obtained from the Mascot database for each immunohistochemical (IHC) marker used in the routine and was matched with MALDI peak list. Segmentation clearly identified iCCA and

HCC related areas and recognized several sub-tumour populations of interest. Comparison of IHC images with the ions from in silico digestion revealed a more accurate identification of iCCA and HCC areas by the latest. Furthermore, the overlap between segmentation and IHC images provided a more comprehensive description of HCC-CCA tumor heterogeneity by identifying transitional and micro-metastatic areas. In conclusion, our study suggests that MALDI imaging is a powerful tool to provide molecular information from samples of cHCC-CCA. This approach provides a large amount of informative data with a single acquisition, improving the conventional pathological approach based on HE and IHC.

Graphical Abstract

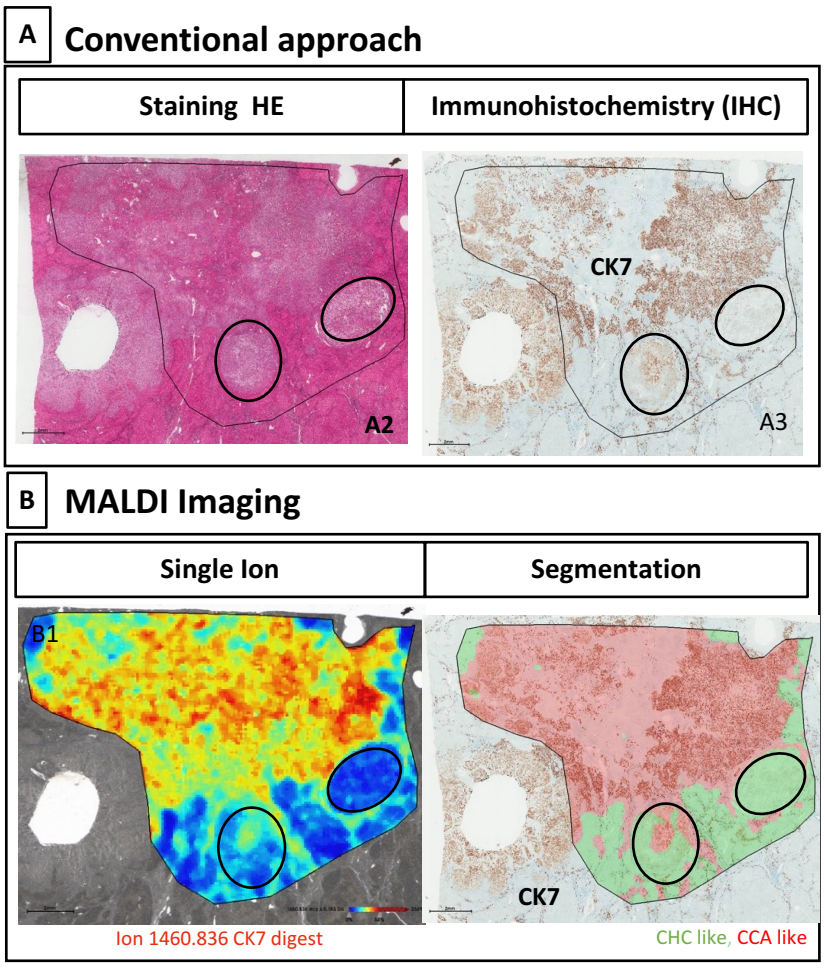


Figure 24: Graphical abstract.

In the upper part of the figure (A) are shown:
On the left part the staining hematoxylin and eosin (A2), in the right partis shown the immunohistochemistry (CK7) (A3).
In the lower part of the figure (B) are shown:
Visualization of the single ion 1460,836 derived from in silico digestion of CK7 protein, in the right part of figure B is shown an analysis by segmentation overlapping CK7 immunohistochemistry.
In red the iCCA-like tissues and in green the HCC-like tissues.

Introduction

Combined hepatocellular cholangiocarcinoma (cHCC-CCA) is a rare primary liver carcinoma (PLC). Its diagnosis is based on the histological analysis by identifying hepatocellular carcinoma (HCC) and intrahepatic CCA (iCCA) components within the same tumor (Allen et Lisa 1949)(Koster et Kasman 1932). In the most recent 2019 WHO classification, the frequency of cHCC-CCA is estimated to be between 2%-5% of all PLCs (E. Brunt et al. 2018; Sempoux, s. d.). Several morphological classifications have been proposed and used in the literature, leading to a certain degree of confusion and misunderstanding. The latest classification has been simplified to include only tumors showing typical areas of hepatocytic and cholangiocytic differentiation within the same tumor. IHC markers targeting hepatocyte, cholangiocyte and stem cell phenotypes, support the morphological diagnosis They are useful to better characterize PLC and to guide differential diagnoses (E. Brunt et al. 2018; Sempoux, s. d.). (Beaufrère, Calderaro, et Paradis 2021). Recently, a study reported the reliable diagnostic and prognostic value of Nestin in cHCC-CCA (Calderaro et al. 2022).

cHCC-CCA may illustrate the best example of morphological intratumor heterogeneity. Whether morphological heterogeneity mirrors underlying molecular heterogeneity has not yet been clearly explored. To provide a comprehensive molecular overview of such heterogeneous tumors, ideally, a preliminary tumor microdissection step should be included to obtain specific profiles related to the different constituent tumor areas of the lesion. To circumvent the limiting step of tumor microdissection, *in situ* approaches represent an attractive alternative. Among them, MALDI imaging (MSI) has emerged as a powerful technique for analyzing the spatial arrangement of various molecules (proteins, peptides, lipids and metabolites) directly from tissue sections without preliminary microdissection and labelling steps. MSI has already enabled the identification of new diagnostic and prognostic markers in several types of human malignancies, including HCC and iCCA (Le Faouder et al. 2014; Laouirem et al. 2014). Once

sequenced, the candidate markers can be routinely assessed by immunohistochemistry (Poté et al. 2013)(Caprioli 2016; Basu et Agar 2021; Berghmans et al. 2020). In addition, MSI applied on gastric carcinoma samples allowed to show the impact of tumor heterogeneity on prognosis (Balluff et al. 2015). The aim of this study was to explore various features of MSI to decipher intratumoral heterogeneity of cHCC-CCA. Our main interests were to evaluate the potential of MSI to diagnose cHCC-CCA and identify any additional tumor areas not identified by conventional pathological analysis.

Materials and methods

cHCC-CCA patients

Five cHCC-CCA cases were retrieved from our pathology department among archival cases collected in the last 6 years. The cases were selected according to their typical morphological features with well-defined areas of HCC and CCA as defined by the 2019 WHO classification. Cases were examined by two pathologists specialized in liver disease (AB, VP) using hematin and eosin (H&E) staining. The most representative tumor sample section for each case was selected for immunohistochemical analysis and MSI.

Immunohistochemistry

The tumor was phenotypically characterized by immunohistochemistry using a panel of antibodies mentioned below (Supplementary Material). An automated immunohistochemical stainer was used according to the manufacturer's guidelines (streptavidin-peroxidase protocol; Benchmark, Ventana, Tucson, AZ). Immunostained slides were digitalized (ScanScope AT turbo®, Leica) at ×20 magnification.

MSI

For all cases, analysis was performed on one 3 µm thick serial section mounted on ITO-coated conductive slides for MALDI Mass Spectrometry analysis. Slides were dried at 37°C overnight before analysis. For MSI analysis, slides were pre-heated at 85°C for 15 minutes and dewaxing was done with xylene (2x5 min). Slices were rehydrated with successive bath of isopropanol (100%) and ethanol (100, 96%, 70% and 50%) for 5min each. Antigen retrieval was performed using a decloaking chamber (BioCare Medical, Concord CA) by heating the section in H2O at 110°C for 20 min. Trypsin solution (25µg/mL, 20 mM ammonium bicarbonate and 0.01 % glycerol) was deposited onto tissue sections using an automatic sprayer (15 µL/min, 16 cycles, TM Sprayer, HTX Technologies). The incubation time for digestion was 3 h in at 50°C in a wet chamber with a saturated solution of K_2SO_4. HCCA MALDI matrix (10 mg/mL in ACN/H_2O, 70/30 v/v, 1% TFA) application step was also done with TM sprayer (120µL/min, 4 cycles). The MALDI measurement was performed using an Autoflex III MALDI-TOF/TOF mass spectrometer with a Smartbeam laser using FlexControl 3.4 and FlexImaging 4.1 software packages (Bruker Daltonics) in the range of m/z 600–3200 at spatial resolution of 100 µm. A peptide calibration standard mix including angiotensin II, angiotensin I, substance P, bombesin, ACTH clip 1-17, ACTH clip 18-39, and somatostatin 28 (Bruker Daltonik GmbH) was used for external calibration. After MSI analysis, matrix was removed from each slide by washing in 100% ethanol for 5 min. Tissue sections were then stained with H&E and examined by a pathologist to correlate MALDI data with histological features of the same section. Statistical analysis of MALDI imaging data was performed with SCiLS Lab Pro 2022 from regions of interest corresponding to the different morphological patterns of cHCC-CCA in order to assess biomarkers of each region. The raw images were loaded in the software SCiLS Lab (Bremen, Germany). Baseline subtraction was performed using the convolution algorithm as well as a weak denoising. The spectra were normalized by total ion current (TIC). The peaks were then aligned using special software provided by Bruker.

Results

cHCC-CCA patients

cHCC-CCA were obtained from surgical specimens performed in 5 patients (3 men, 2 women). Non tumoral liver displayed advanced liver fibrosis bridging (F3) or cirrhosis (F4) in 3 patients (60%). Clinicopathological features are detailed in Table 5.

Table 5: Clinical and pathological features of patients

Sex	Age (Y)	Advanced fibrosis (≥F3)	Risk factors	BMI	Tobacco smoke	Satellite nodules	Tumoral emboli	Perineural invasion	Tumoral thrombosis	Tumor size mm
F	65	Yes	Alcohol,MS	40	Yes	Yes	Yes	Yes	No	42
M	57	Yes	Alcohol,MS	27	Yes	No	Yes	Yes	No	25
F	29	Yes	Genetic	44	Yes	No	No	No	No	35
M	40	No	HBV	31	Yes	No	Yes	Yes	No	40
M	77	No	MS	24	Yes	Yes	Yes	Yes	Yes	70

MS: Metabolic syndrome

Analysis by segmentation

MSI analysis of the overall set of samples identified 413 peptides of interest. The segmentation analysis allowed to identify separated clusters of ions (Figures 25 and 26). The two main clusters corresponded, when overlapped on the HE slides, to the HCC (and pre-neoplastic areas) and CCA areas. In addition, tiny HCC foci were observed within CCA component and vice versa. Furthermore, the segmentation allowed the identification of mixed HCC and CCA areas within a microvascular invasion (MVI) (Figures 25-B2 arrow)

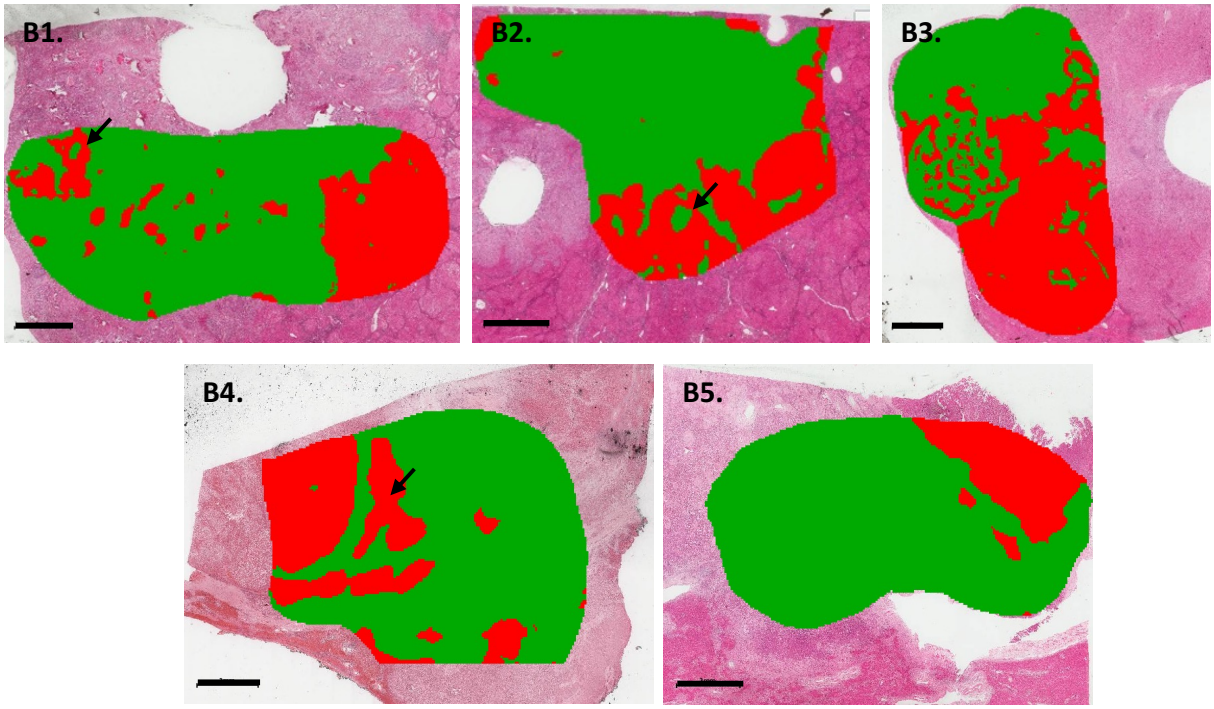


Figure 25: Segmentation analysis.

In the picture, the first arborescence of the segmentation analysis is shown. Identification of 2 main groups of spectra. Tissues with hepatocyte component (HCC and non-tumor liver) (in red). Tissues with iCCA component (in green). Some islands of tumor tissue of different nature included in majority areas of tumor (e.g., a limited area of HCC in areas of iCCA or conversely areas of minority iCCA surrounded by areas of majority HCC) are indicated with arrows.

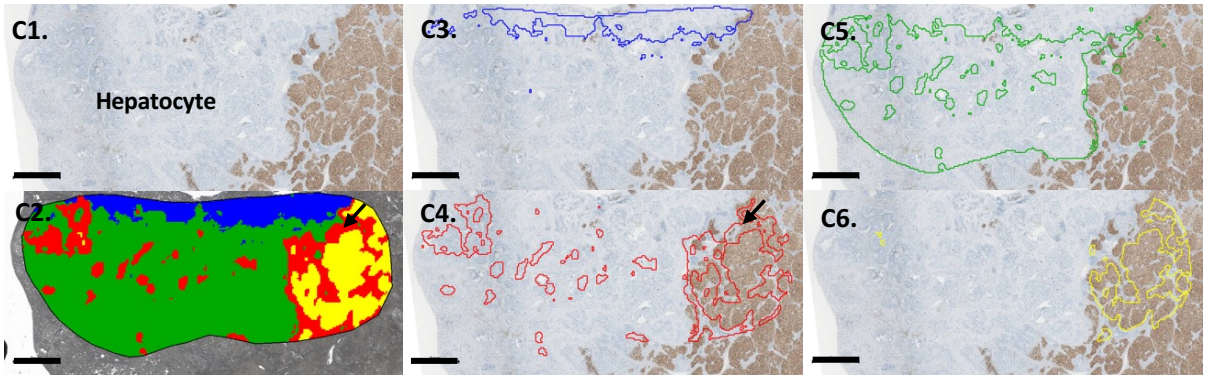


Figure 26: Segmentation, division in four clusters.

The division of the second segmentation arborescence allows distribution into four main clusters, the four main clusters are highlighted in four colors: Blue: cholangiocarcinoma-related fibrosis, red: HCC, green: iCCA and yellow: cirrhosis. MALDI images are overlapped to Hepatocyte IHC. Each of the figures a single cluster is shown superimposed on an immunohistochemistry for Hepatocyte (C3-C6). A tumor area responding to HCC is identified by the arrowhead.

A further division of the segmentation arms into four clusters allowed more accurate identification of tissue zones (mainly fibrotic areas in iCCA and preneoplastic cirrhotic nodules in HCC). Furthermore, the segmentation provided a more complete description of the tumor heterogeneity of cHCC-CCA, identifying the transition areas and micro-metastases of the

constituent CCA and HCC components of the tumor. Further segmentation analyses are shown in Supplementary Figure 30. The molecular analysis permitted the description of the histological heterogeneity that was not initially evident.

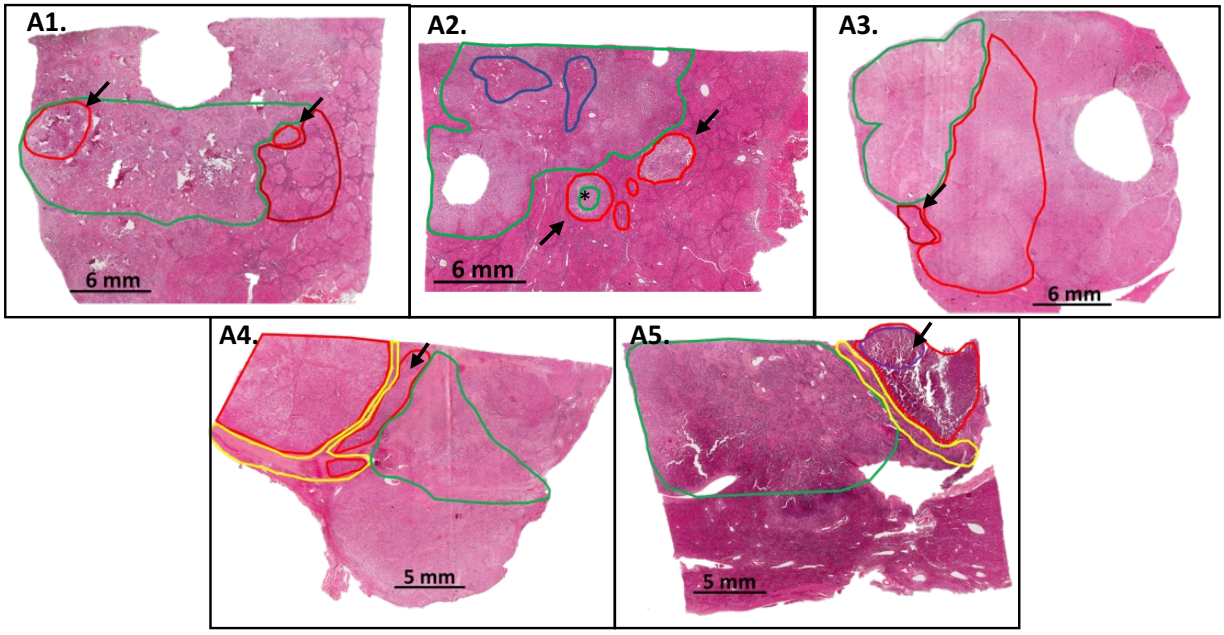


Figure 27: Pathological labelling of 5 cHCC-CCA

The picture shows the labelling obtained by two experienced anatomic pathologists following re-reading. The different colors indicate the areas of interest. Color legend. Green: areas of cholangiocarcinoma, bright red: areas of hepatocarcinoma, blue: fibrosis derived from cholangiocarcinoma, yellow fibrosis from tumor capsule, purple: macrotrabecular hepatocarcinoma of massive type. A1 right and left arrows: HCC; A2 arrow and asterisk: MVI; A3 arrow: non tumoral zone. A4 arrow HCC; A5 arrow: macrotrabecular area.

Analysis by principal component analysis

The principal component analysis (Figure 28) identified two defined groups of ions (Component 1, X-axis, Fig.28) corresponded to HCC and iCCA.

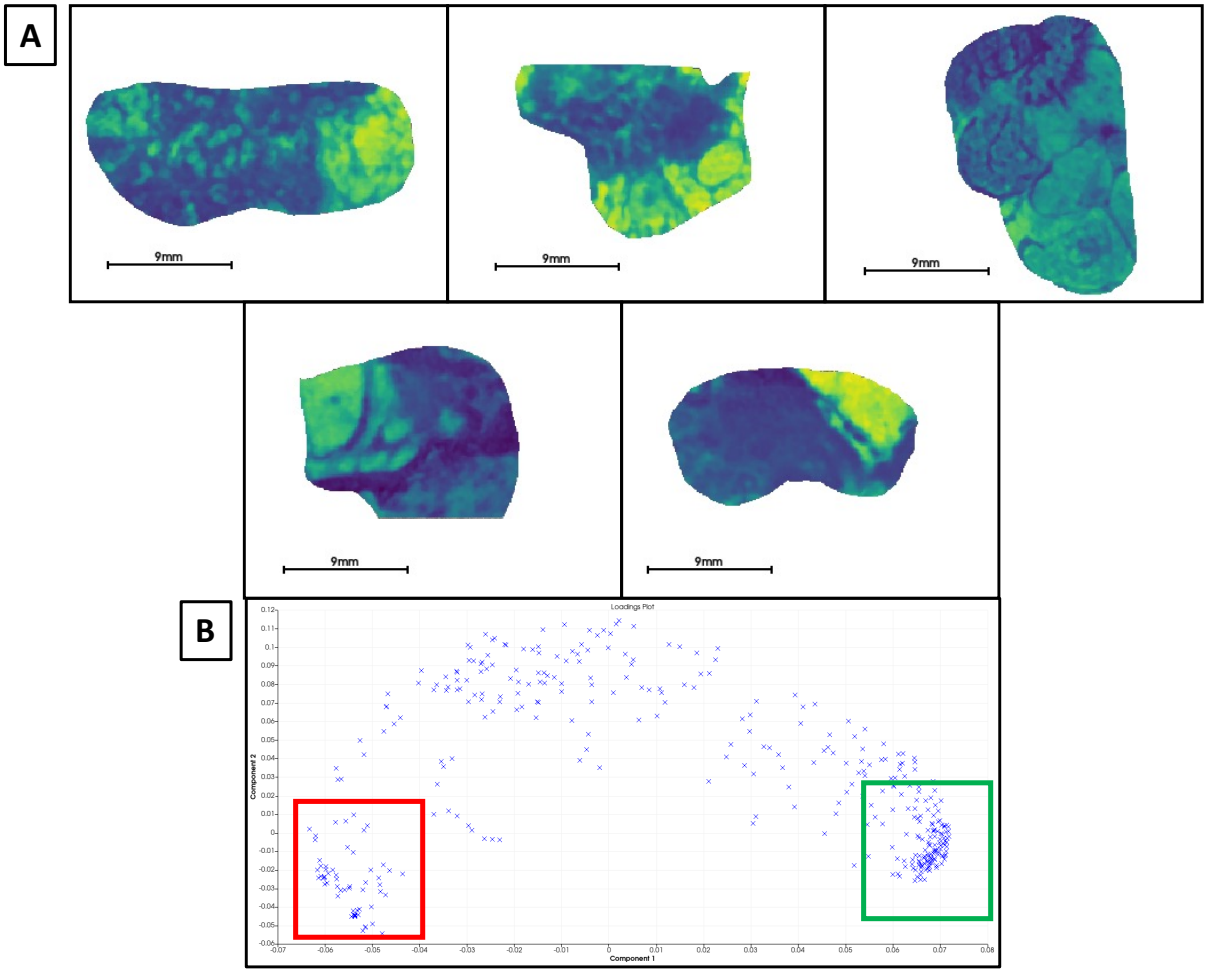


Figure 28: Principal component analysis. Component 1 and 2.

A: Component 1 and 2 representations on cases. In yellow-green are identified HCC like tissues while in shades of blue are shown the most iCCA like tissues. B: Loading plot PCA. In red square (left)peptides corresponding to HCC-like tissues, in green square (right) peptides corresponding to iCCA-like tissues

Comparison with IHC analysis

In order to generate a list of peptides comparable to those obtained following the trypsin treatment process of the samples in MALDI experiment, each immunohistochemical marker of cHCC-CCA (HepPar1, glypican-3, CK7, EpCAM, CK19, Nestin) was digested in silico with trypsin generating a virtual peak list. Each peaklist derived from the individual markers was then manually filtered by overlaying the ion images on the histological scan. Ions were retained when they matched with the underlying morphological structures. Then the ions of interest were

used for image construction which were compared with conventional IHC. This analysis amplified the positive signal from all peptide ions compared to their respective IHC marker, revealing a more accurate identification of tumoral areas (Fig; 29). The ion image also allowed a more quantitative description (higher presence in red, low presence in blue). Images of all cases are shown in Supplementary Figure 31.

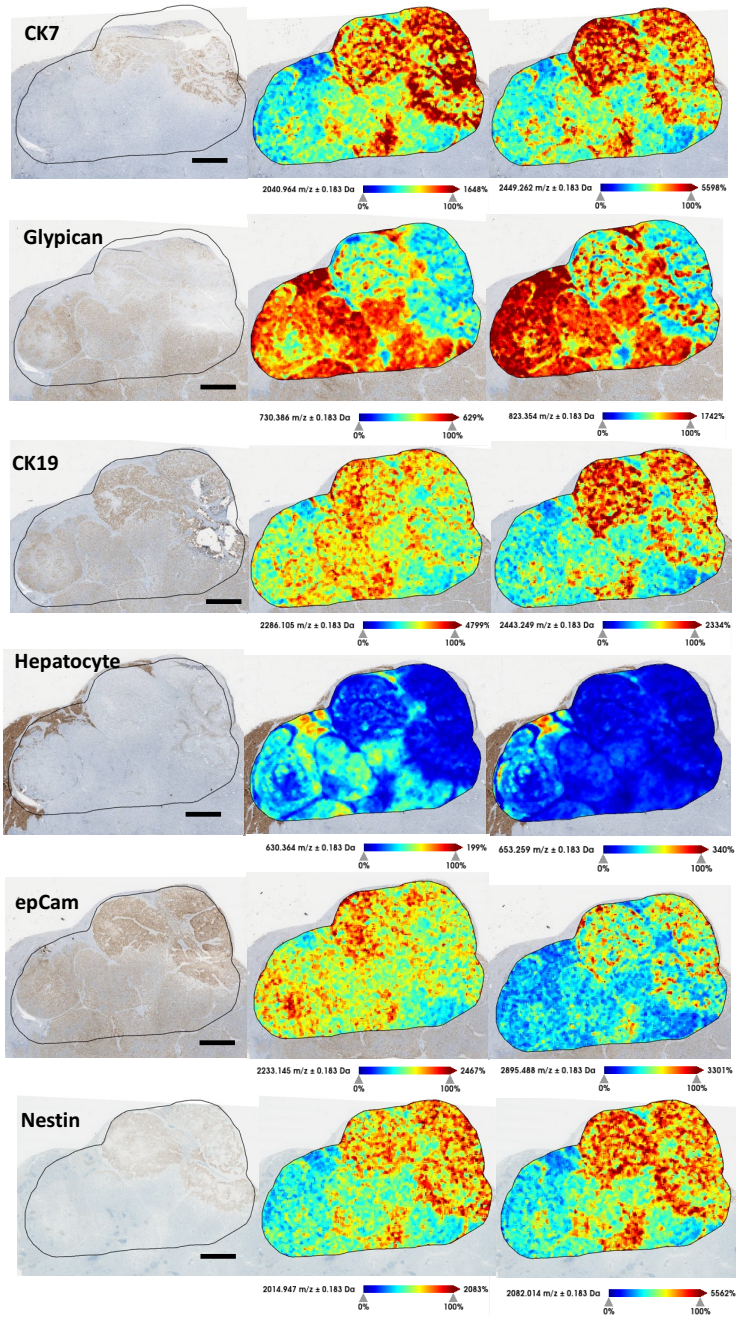


Figure 29: Comparison of tryptic peptides derived from current IHC markers

Individual ions derived from tryptic digestion of each marker are shown alongside immunohistochemistry of the same marker. Scale bar = 3mm

In silico identification of proteins of interest.

A MASCOT search using the Peak list obtained identified a list of proteins with a positive score (>56) (Supplementary Figure 32, Supplementary table 7). The proteins identified with a higher interest were Ladinin-1 (LAD1), 5-aminolevulinate synthase, nonspecific (ALAS1), mitochondria-eating protein (MIEAP), Protein FAM76B, Inactive phospholipase C-like protein 2 (PLCL2), Zinc finger protein 185 (ZN185), Zinc finger protein 783 (ZN783).

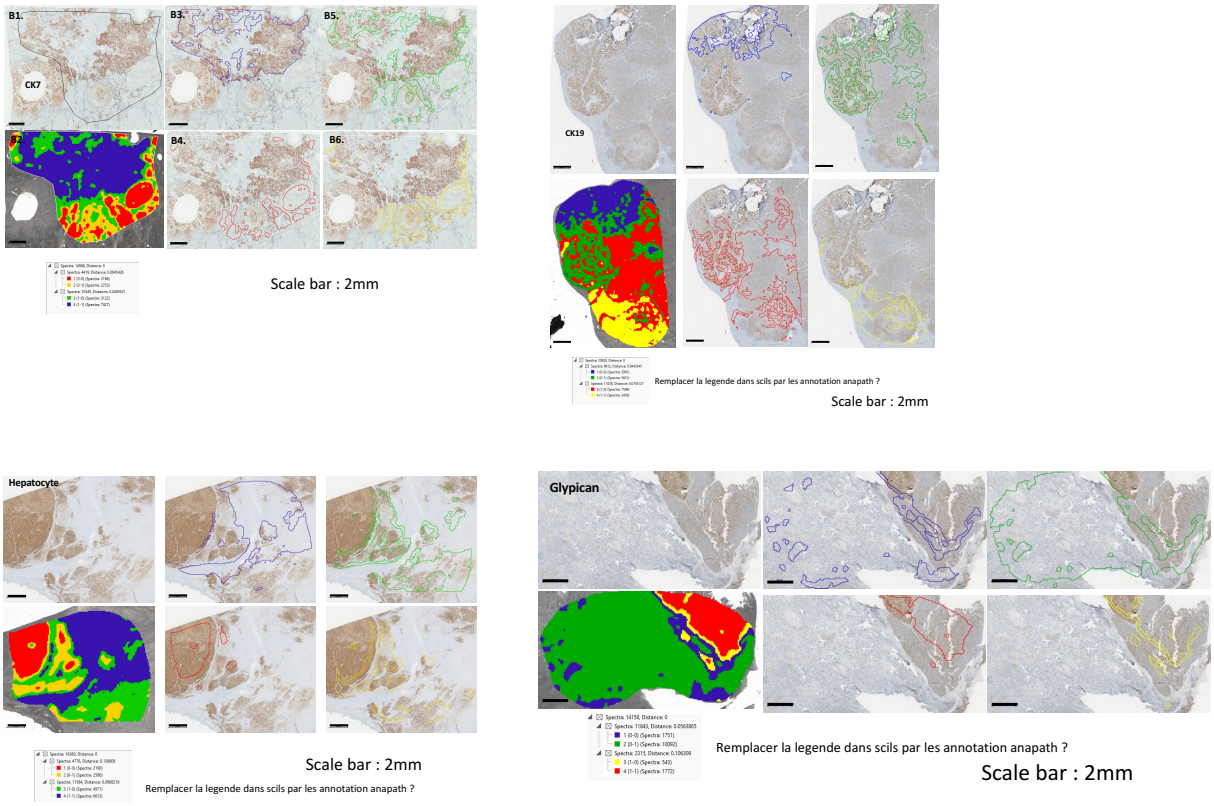
Discussion

This study aimed to explore intratumor heterogeneity in cHCC-CCA using MSI, a non-targeted imaging molecular approach. Our segmentation analysis based on peptide profiles allowed the identification of two main clusters corresponding to HCC and iCCA components, respectively. In addition, using MSI, small tumor foci, initially not identified by routine histological analysis, were highlighted, suggesting the high potential of imaging compared to conventional histology. Accordingly, MALDI molecular analysis appears as a powerful approach, especially in heterogeneous tumors. By definition, diagnosis of cHCC-CCA is based on the histological identification of both HCC and CCA components, whatever their respective extent. However, the percentage of each component (HCC and iCCA) could be of paramount importance for predicting prognosis and gauging therapy response (E. Brunt et al. 2018; Gigante et al. 2021). Interestingly, unsupervised analysis (segmentation) from MSI using a representative sample could allow the quantitative identification of the different tumor contingents quickly and accurately. Moreover, using MALDI analysis, by exploring the different clusters in a more granular way, we have shown how intratumoral heterogeneity can be comprehensively studied. The impact of heterogeneity is not merely descriptive, as recently shown in breast cancers where the presence of high tumor heterogeneity has been associated with reduced survival (Balluff et al. 2015).

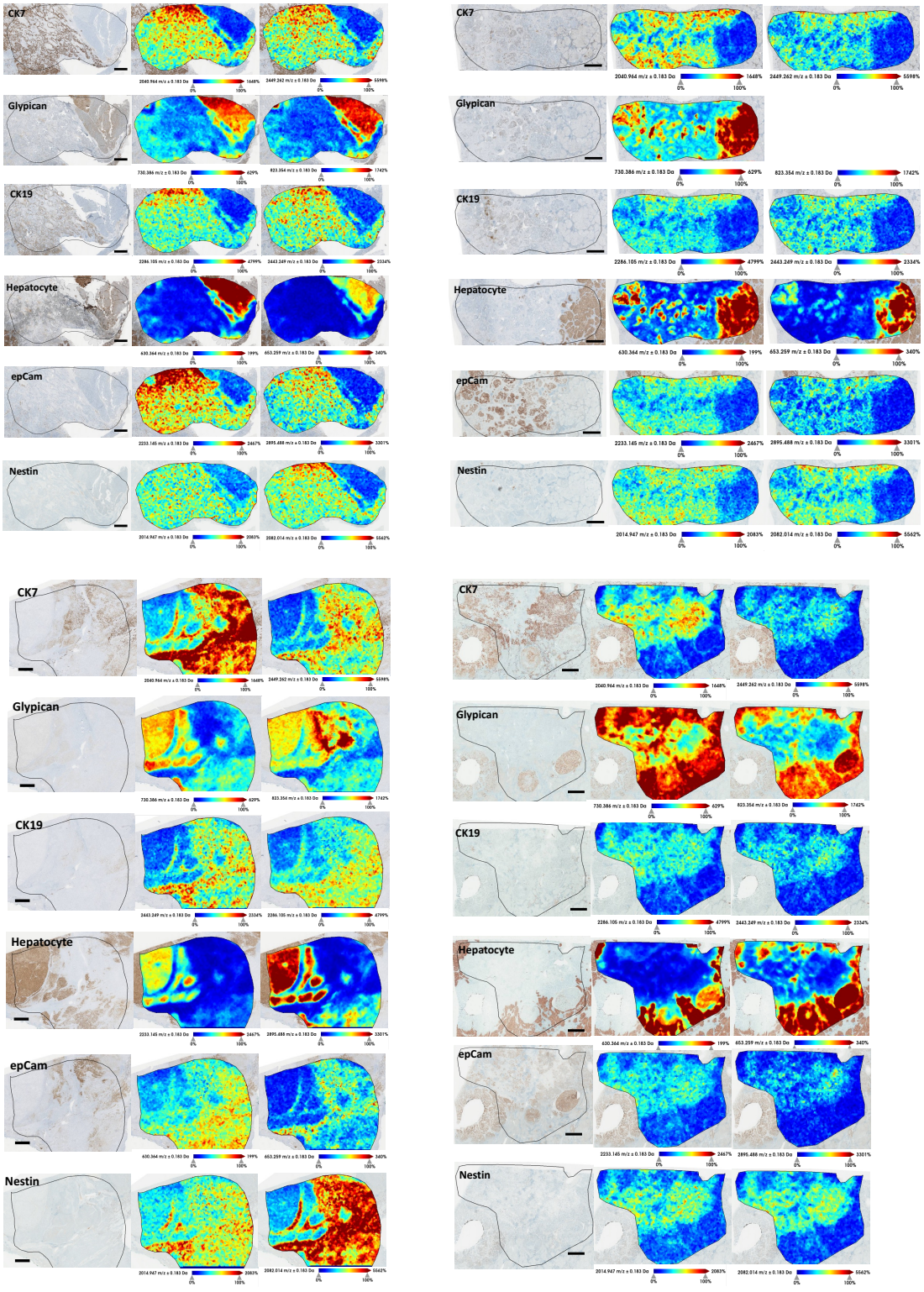
Immunohistochemistry is not formally required for the diagnosis of cHCC-CCA but is always performed as an accessory analysis to better phenotype tumor sample. Using the list of peptides derived by *in silico* digestion, we could reproduce and improve on unlabeled slides the information provided by IHC staining. This analysis also provided a more quantitative approach through a colorimetric scale. This quantitative appreciation is not available by immunohistochemistry which provides only semi-quantitative analysis. To the best of our knowledge, our study is the first to use *in silico* digestion to derive markers from already known IHC. Although widely applied, inexpensive and easy to interpret, immunohistochemical analyses have the inherent limitation of recognizing a single protein. Our approach would theoretically allow unlimited evaluation of large panel of markers from one single unstained slide. Indeed, markers for which routine IHC does not yet exist, could be sought by knowing the structure of the protein. Finally, we used the list of peaks generated by the MALDI analysis to identify proteins of interest *via* the Mascot site. Interestingly, we were able to identify proteins with a high identification score, which could be the subject of further studies. Among these, at least three proteins were part of predisposing factors for various types of cancer, such as lung, breast and gastrointestinal cancers. Ladinin-1 (LAD1), a known 59-kDa protein is one of the cytoskeletal phosphorylation targets of the EGFR pathway. Particularly in breast cancer, LAD1 depletion inhibits tumorigenesis in an animal model, and LAD1 overexpression is typical of high-grade breast tumors and predicts a poor prognosis (Roth et al. 2018). Another interesting protein is non-specific 5-aminolevulinate synthase (ALAS1), which limits heme biosynthesis and is retro-regulated by heme itself (Kubota et al. 2016). ALAS1 overexpression has been associated with the development of various cancers such as non-small cell lung cancer and colorectal neoplasms (Sohoni et al. 2019; Zhao et al. 2020). The mitochondria-eating protein (MIEAP) regulates the quality of mitochondria and also plays the role of tumors suppressor and

can be stimulated by p53; its role as tumor suppressor was found in gastrointestinal, breast cancers and thyroid cancers models (Sano et al. 2020; Hamada et al. 2022; Gaowa et al. 2018). The limitations of our methodological approach lie mainly in the fact that we did not include the analysis of controls and that we included a small number of patients. This limits our possibility of being able to draw general conclusions on cHCC-CCA. On the other hand, it must be pointed out that the aim of our study was not to obtain generalizable molecular information for the management of cHCC-CCA, but rather to explore the usefulness and potential of MALDI in this particular type of tumor. The MALDI MSI approach could be fundamental in increasing the diagnostic power of histological analysis, ensuring better management of patients. The limits still to be overcome for the possible application of MALDI in routine are essentially related to a necessary standardization between the various analysis centers, a limited spread of technical platforms and a reduction in costs for individual acquisitions, which still remain high.

Supplementary material



Supplementary Figure 30: Segmentation, division in four clusters. All cases



Supplementary Figure 31: Comparison of a selection of tryptic peptides

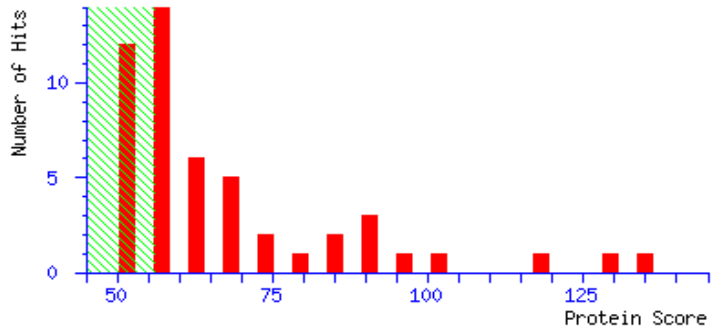
Peptides are derived from current IHC markers, all cases are shown

Supplementary Table 6: Immunoistochemistry list

Anticorps anti-	Dilution	Clonality	Supplier	Reference
CD56 +	1/50	CD564	Novocastra	NCL-L-CD56-504
CD133	1/20	AC133	Miltenyi Biotec	130-090-422
CK7	1/500	50V-TL 12/30	DAKO	M7018
CK19	1/200	RCK108	DAKO	M0888
Glypican	1/100	1G12	Zytomed	MSK067-05
Ep Cam Ber-EP4	1/50	Ber-EP4	DAKO	M0804
a-Hepato	1/250	OCH1E5	DAKO	M7158
Nestin	1/500	10c2	Santa Cruz	sc-23927

Mascot Score Histogram

Protein score is -10*Log(P), where P is the probability that the observed match is a random event.
Protein scores greater than 56 are significant (p<0.05).



Supplementary Figure 32: Mascot Score Histogram

Supplementary Table 7: List of proteins with a protein score > 56

FA76B_HUMAN Mass: 38683 Score: 68 Expect: 0.0031 Matches: 23
Protein FAM76B OS=Homo sapiens OX=9606 GN=FAM76B PE=1 SV=3
LAD1_HUMAN Mass: 57097 Score: 58 Expect: 0.03 Matches: 41
Ladinin-1 OS=Homo sapiens OX=9606 GN=LAD1 PE=1 SV=2
SH2D3_HUMAN Mass: 94352 Score: 56 Expect: 0.057 Matches: 30
SH2 domain-containing protein 3C OS=Homo sapiens OX=9606 GN=SH2D3C PE=1 SV=1
PLCL2_HUMAN Mass: 125785 Score: 64 Expect: 0.0091 Matches: 43

Inactive phospholipase C-like protein 2 OS=Homo sapiens OX=9606 GN=PLCL2 PE=1 SV=2
HEM1_HUMAN Mass: 70536 Score: 63 Expect: 0.01 Matches: 27
5-aminolevulinate synthase, nonspecific, mitochondrial OS=Homo sapiens OX=9606 GN=ALAS1 PE=1 SV=2
ADA19_HUMAN Mass: 104928 Score: 60 Expect: 0.019 Matches: 32
Disintegrin and metalloproteinase domain-containing protein 19 OS=Homo sapiens OX=9606 GN=ADAM19 PE=1 SV=3
RMXL1_HUMAN Mass: 42116 Score: 59 Expect: 0.026 Matches: 28
RNA binding motif protein, X-linked-like-1 OS=Homo sapiens OX=9606 GN=RBMXL1 PE=1 SV=1
ZN185_HUMAN Mass: 73480 Score: 62 Expect: 0.013 Matches: 25
Zinc finger protein 185 OS=Homo sapiens OX=9606 GN=ZNF185 PE=1 SV=3
MBP_HUMAN Mass: 33097 Score: 61 Expect: 0.016 Matches: 21
Myelin basic protein OS=Homo sapiens OX=9606 GN=MBP PE=1 SV=3
MIEAP_HUMAN Mass: 61071 Score: 60 Expect: 0.02 Matches: 30
Mitochondria-eating protein OS=Homo sapiens OX=9606 GN=SPATA18 PE=1 SV=1
C2D1B_HUMAN Mass: 94166 Score: 60 Expect: 0.022 Matches: 33
Coiled-coil and C2 domain-containing protein 1B OS=Homo sapiens OX=9606 GN=CC2D1B PE=1 SV=1
F184B_HUMAN Mass: 120969 Score: 60 Expect: 0.023 Matches: 48
Protein FAM184B OS=Homo sapiens OX=9606 GN=FAM184B PE=2 SV=3
CC152_HUMAN Mass: 29960 Score: 59 Expect: 0.026 Matches: 22
Coiled-coil domain-containing protein 152 OS=Homo sapiens OX=9606 GN=CCDC152 PE=1 SV=3

TNNI1_HUMAN Mass: 21679 Score: 57 Expect: 0.045 Matches: 23
Troponin I, slow skeletal muscle OS=Homo sapiens OX=9606 GN=TNNI1 PE=1 SV=3
ZN783_HUMAN Mass: 60976 Score: 57 Expect: 0.045 Matches: 25
Zinc finger protein 783 OS=Homo sapiens OX=9606 GN=ZNF783 PE=1 SV=2
CC168_HUMAN Mass: 801411 Score: 56 Expect: 0.048 Matches: 163
Leucine-rich repeat transmembrane protein CCDC168 OS=Homo sapiens OX=9606 GN=CCDC168 PE=2 SV=3
Zinc finger protein 883 OS=Homo sapiens OX=9606 GN=ZNF883 PE=1 SV=1

6.2 MSI on TMAs of cHCC-CCA

6.2.1 Objectives

As explained several times in the various sections of this manuscript, cHCC-CCA is composed of HCC and iCCA. The first question we tried to answer in this experimental part was whether cHCC-CCA was more similar to HCC, iCCA or whether it was a completely different entity. To address this question, we compared the molecular protein signatures of cHCC-CCA with those of HCC and iCCA by MSI. To obtain relevant results, a large number of cases is required, so we decided to use an experimental approach based on TMAs. Secondly, we sought to describe the complexity of cHCC-CCA on a large series of patients and to identify new diagnostic and prognostic markers.

6.2.2 Materials and methods

6.2.2.1 Patients and Tumors

The study was performed on a surgical set of cHCC-CCAs obtained from resections or liver transplantations collected and archived in the Pathology Department of Beaujon hospital. The cases which have been selected were carefully classified according to the 2010 WHO

classification and then revised with the 2019 WHO classification. The study was performed on 60 cHCC-CCA cases. For each case, paraffin blocks representative of the different morphological tumor patterns were retrieved and used for the MALDI imaging. 52 cases of conventional HCC, iCCA and normal liver samples already used for research purposes in other projects were used as controls (23 and 29, respectively). At a later stage, due to the need to add new controls, an additional TMA consisting of 10 cases of HCC and 10 cases of iCCA was constructed.

6.2.2.2 Case selection and pathological analysis

Local database was searched for suitable cases from 1989 to 2017. Main pathological data (size, number of nodules, vascular invasion, perineural invasion, status of underlying liver) were collected from pathological reports. Epidemiological and main clinical features including follow-up data were collected from clinical charts when available. According to the World Health Organization criteria (2010 edition), cHCC-CCA were classified into classical type or type with stem-cell features including typical, intermediate and cholangiolocellular (CLC) subtypes; the presence of other associated minority cell contingents was also recorded. A second pathological review according to the new 2019 classification was performed. The constructed TMAs were finally labelled as cHCC-CCA, HCC, iCCA and not classifiable (NC) tumors following the morphology of the selected core.

6.2.2.3 Immunohistochemistry

The tumor was phenotypically characterized by immunohistochemistry on whole sections of tumor included in paraffin, using a panel of antibodies mentioned below. An automated immunohistochemical stainer was used according to the manufacturer's guidelines (streptavidin-peroxidase protocol; Benchmark, Ventana, Tucson, AZ). A panel of antibodies related to HCC, including hepatocyte paraffin 1 (HepPar1), and Glypican-3 (GPC-3), and iCCA including Cytokeratin 7 (CK7). Stem/progenitor cell phenotype was assessed using the most

commonly used in the literature such as cytokeratin 19 (CK19), CD133, CD56, EpCAM, Nestin (Beaufrère, Calderaro, et Paradis 2021; Calderaro et al. 2022b). Immunostaining was considered positive for any markers when at least 5% of tumoral cells were labeled. Comprehensive information about antibodies is mentioned above in Supplementary Table 6.

6.2.2.4 TMA construction

Small tissue cores from multiple FFPE tissue blocks can be transferred into receiving tissue blocks, called tissue microarrays (TMA), the procedure could be manual or assisted by an automated machine. This approach allows multiple tumors to be analyzed during a single experiment. The first step of the TMA construction was the identification of the zone of interest that was circled (Fig. 33). The cores were then removed from highlighted zones and assembled in the TMAs (Fig 34.). Cylindrical cores of tissue from multiple tumor blocks have been assembled in 12 TMAs. This procedure made it possible to reduce the analysis time and also reduced the number of experiments required and thus the experimental variability. It has to be considered that the size of the core may have an impact in the following analysis; thus small cores from tumors with great morphological heterogeneity might not be representative of the original tumor (R. Casadonte et al. 2017). Usually, the average size of cores is 0.5–1 mm and two to four cores are extracted per tumor, resulting in a TMA with around 50–200 patients. Given the high degree of heterogeneity assumed in cHCC-CCAs, tumoral cylindrical cores of larger size (2 mm) were taken from tumor FFPE blocks and arranged in TMAs structured as shown in Figure 34. Each row is constituted of tissues coming from one patient, resulting in blocks with 5 patients each and 40 cores.

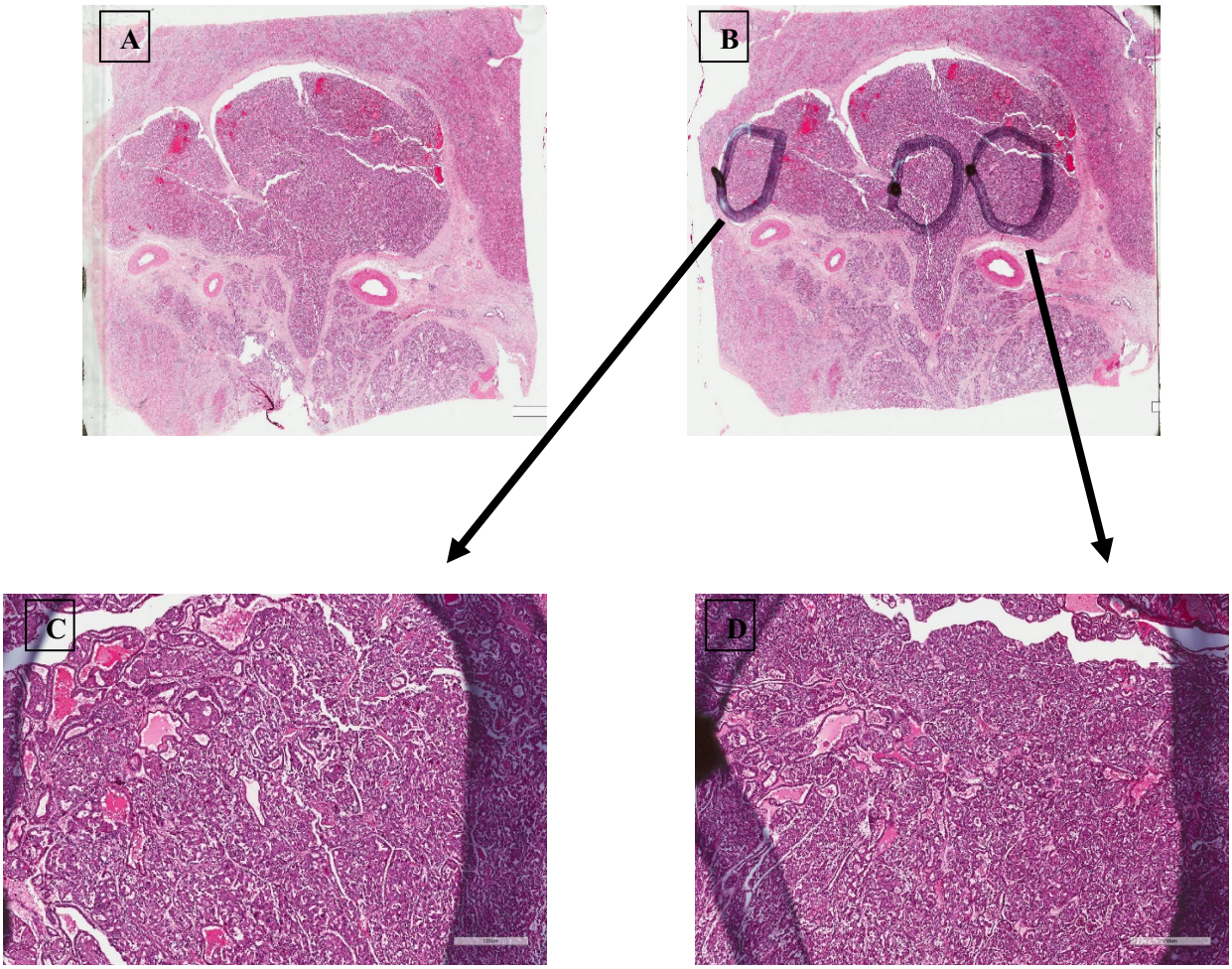


Figure 33: Tissue selection

A: The hematoxylin and eosin slides of cHCC-CCA were selected and reviewed, *B: The different contingents of interest were manually circled highlighting areas of interest*

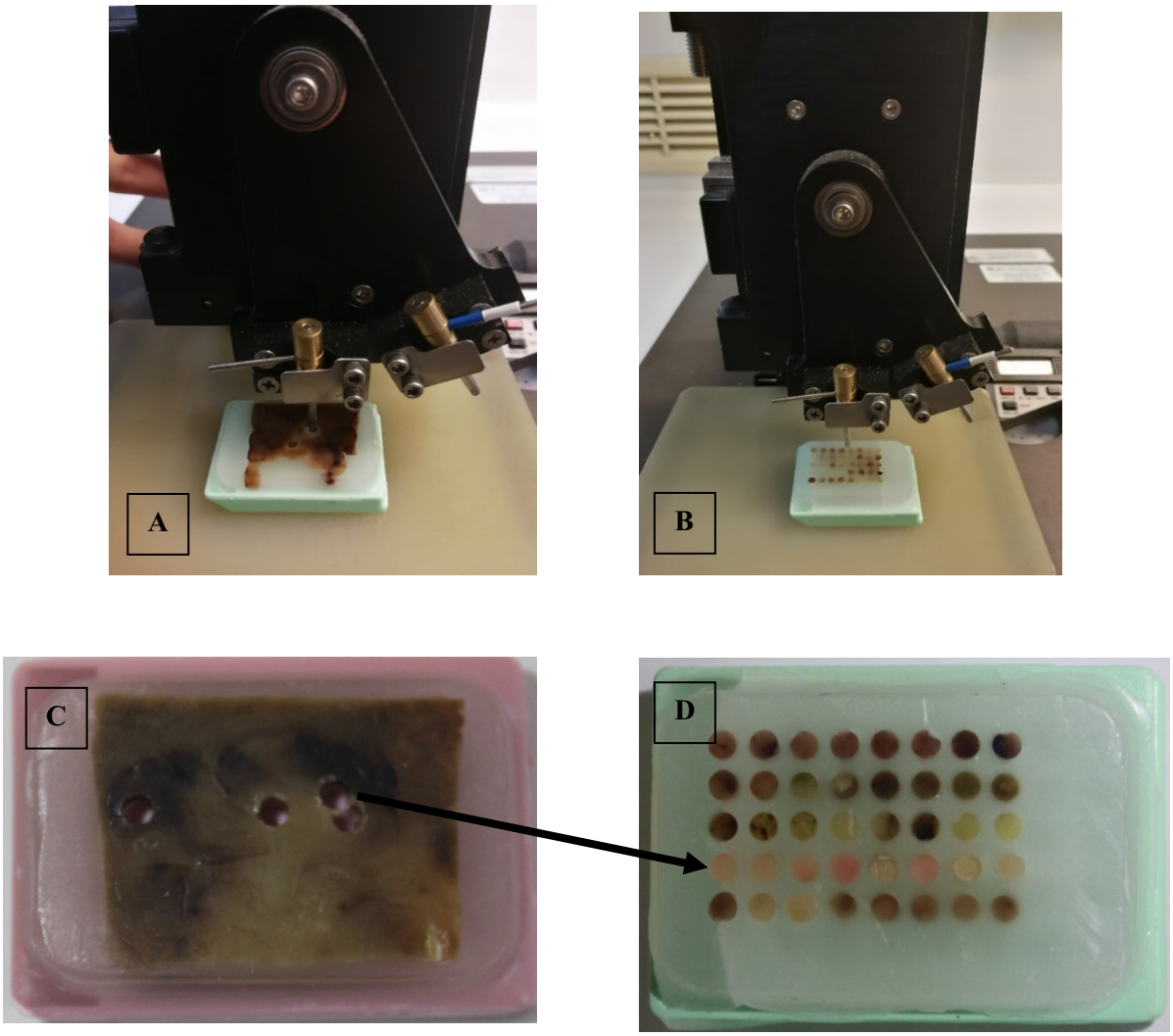


Figure 34: Tissue microarray construction

(A,C) cores are retrieved according with the pre-selected areas (Fig. 34) and transferred on the tissue microarrays (B,D).

6.2.2.5 TMA analysis by mass spectrometry imaging

6.2.2.5.1 MALDI (ProteoPath materials and methods)

Conductive indium tin oxide ITO-coated glass slides were purchased from Delta Technologies, Loveland, USA). Ammonium bicarbonate, alpha-cyano-4-hydroxycinnamic acid (CHCA) matrix and Tris base were bought from Sigma-Aldrich Chemie GmbH (Taufkirchen, Germany). Trifluoroacetic acid and all solvents including xylene, ethanol, acetonitrile, were obtained from Fischer Scientific GmbH (Schwerte, Germany). Trypsin Gold was purchased from Promega GmbH (Mannheim, Germany).

Five µm sections of each TMA FFPE block were cut on a microtome and mounted onto ITO-coated glass slides for MALDI MSI analysis. All slides were dried at 37 °C overnight and stored in a desiccator until used. Tissue sections were pre-heated at 60° for 60 minutes and processed for dewaxing with xylene, rehydrating through graded ethanol, and heat induced antigen retrieval in Tris buffer (10 mM, pH 9.0) at 95 °C for 20 min, as previously described (Rita Casadonte et al. 2014). Trypsin solution (composed by 200 µL of 20 mM ammonium bicarbonate, 800 µL of 0.01% Glycerol and 20 µg of trypsin) was deposited onto tissue sections using an automatic reagent sprayer (TM Sprayer, HTX Technologies). On-tissue digestion occurred in a humidity chamber at 37 °C for 2 hours. A water solution of 10 mg/ml of CHCA matrix in 70% acetonitrile, 1% Trifluoroacetic acid (TFA), was then deposited onto digested sections in four layers using the same sprayer devise. MALDI MSI was performed using a RapifleX MALDI Tissue-typer mass spectrometer (Bruker Daltonik GmbH) operated in reflectron mode with positive polarity (ProteoPath Laboratory Trier). Each mass spectrum was automatically generated using the auto-execute software in FlexControl 4.0 (Bruker Daltonik GmbH) in the range of m/z 600–3200 at spatial resolution of 50 µm. A peptide calibration standard mix including angiotensin II, angiotensin I, substance P, bombesin, ACTH clip 1-17, ACTH clip 18-39, and somatostatin 28 (Bruker Daltonik GmbH) was used for external calibration. FlexImaging 5.0 (Bruker Daltonik, GmbH, Bremen) was used to visualize ion images, all displayed intensities were total ion count (TIC) normalized. After MSI analysis, matrix was removed from each slide by washing twice in 100% methanol for 5 min. Tissue sections were then stained with hematoxylin & eosin (HE) and examined by a pathologist to correlate MALDI data with histological features in the same section. (Data were acquired at ProteoPath laboratory, Dr. Casadonte).



Figure 35: RapifleX MALDI Proteopath Laboratory, Trier, Germany

6.2.2.5.2 MALDI (iMAP materials and methods)

Conductive indium tin oxide ITO-coated glass slides were purchased from Bruker Daltonics (Bremen, Germany). Ammonium bicarbonate, alpha-cyano-4-hydroxycinnamic acid (CHCA) matrix, Tris base and all solvents including xylene, ethanol, acetonitrile, were acquired from Sigma-Aldrich (Saint-Quentin Fallavier, France). TFA was obtained from Fischer Scientific (Illkirch, France). Trypsin was purchased from Promega (Charbonnières les bains, France).

Analysis was performed on 3 µm thick sections mounted on ITO-coated conductive slides for MALDI Mass Spectrometry analysis or on regular slides for H&E staining for histological analysis. All slides were dried at 37 °C overnight before analysis. For MSI analysis, slides were pre-heated at 85°C for 15 minutes and dewaxing was done with xylene (2x5min). Slice were rehydrated with successive bath of isopropanol (100%) and ethanol (100, 96%, 70% and 50%) for 5 minutes each. Antigen retrieval was performed using a decloaking chamber (BioCare

Medical, Concord CA) by heating the section in H_2O at 110°C for 20 min. Trypsin solution (composed by 200 µL of 20 mM ammonium bicarbonate, 800 µL of 0.01% Glycerol and 20 µg of trypsin) was deposited on tissue sections using an automatic sprayer (16 cycles at 15µL/min, TM Sprayer, HTX Technologies). The incubation time for digestion was 3h in at 50°C in a wet chamber with a saturated solution of K_2SO_4. HCCA MALDI matrix (10 mg/mL in ACN/H_2O 70/30 v/v, 1% TFA) application step was also done with TM sprayer (4 cycles at 120 µL/min). The MALDI measurement was performed on an Autoflex III MALDI-TOF/TOF mass spectrometer with a Smartbeam laser using FlexControl 3.4 and FlexImaging 4.1 software packages (Bruker Daltonics) in the range of m/z 600–3200 at spatial resolution of 50 µm. A peptide calibration standard mix including angiotensin II, angiotensin I, substance P, bombesin, ACTH clip 1-17, ACTH clip 18-39, and somatostatin 28 (Bruker Daltonik GmbH) was used for external calibration. After MSI analysis, matrix was removed from each slide by washing in 100% ethanol for 5 min. Tissue sections were then stained with hematoxylin & eosin (HE) and examined by a pathologist to correlate MALDI data with histological features in the same section. Statistical analysis of MALDI imaging data were performed with SCiLS Lab Pro 2022 from regions of interest corresponding to the different morphological patterns of cHCC-CCAs in order to assess biomarkers of each region. The raw images were loaded in the software SCiLS Lab (Bremen, Germany). Baseline subtraction was performed using the convolution algorithm as well as a weak denoising.

The spectra were normalized by total ion current (TIC). The peaks were then aligned using special software provided by Bruker.



Figure 36: AutofleX III MALDI Inserm U1149, Clichy, France

6.2.2.6 Statistical analysis

6.2.2.6.1 Statistical and classification analysis of MALDI data (ProteoPath)

Statistical and classification analysis were carried out using SCiLS Lab 2016 software (SCiLS, Bremen). A completely unsupervised data analysis was first performed using Principal Component Analysis (PCA) to identify specific mass spectra profiles discriminating the different pathological entities. PCA was applied to the spectra from all entire tissue sections. Linear discriminant analysis (LDA) was used to generate discriminatory features among study groups. Reproducibility and variability issues between tissue cores were also evaluated in the dataset. The raw images were loaded separately in the software SCiLS Lab. Baseline subtraction was performed using the Top Hat algorithm as well as a weak denoising. The spectra were normalized by total ion current (TIC). The algorithm for peak peaking and spectra alignment was used from the skyline spectrum. The peaks were then aligned and a segmentation processing was realized. For the segmentation processing, the algorithm bisecting k-means and

the correlation distance metric were used, and all spectra were analyzed. ±0.009 Da was set as the interval width value.

6.2.2.6.2 Statistical and classification analysis in MALDI (Imap)

The raw images were loaded together in the software SCiLS Lab Pro 2023a software. Baseline subtraction was performed using convolution algorithm as well as weak denoising. The spectra were then aligned using the SCiLS script and segmentation pipeline was used to generate peaks list and hierarchical clustering for the different groups compared in the data MSI set. Based on this created peak list, PCA or statistical analysis were achieved.

6.2.2.6.3 Processing of MALDI data

For all paired combinations of sample type, a non-parametric Mann-Whitney test was applied to each peak to evaluate their differential quantification. Multiple hypothesis correction was performed using Benjamini and Hochberg false discovery rate control. To create the correlation plots HCC and iCCA centroid was constructed by taking the average peak quantification of each tumor type for every peak with a significant differential quantity (FDR 5%). These centroids were then used as prototypes, e.g. average representative of each type of cancer HCC, iCCA, cHCC-CCA. The similarity of each sample with each centroid was then computed using Pearson's correlation. Barplot peaklist shows the number of differential peaks calculated with FDR of 5% for each pair of sample type. Barplot of correlations are built showing the distribution for each sample type of the correlation with the iCCA centroid or HCC centroid (Data were computed in association with Nicolle Team CRI, Inserm U1149).

6.2.2.6.4 Processing of MALDI and clinical data

Survival and treatment duration curves has been estimated using the Kaplan-Meier method, and differences in survival rates assessed by the log-rank test curves. Patients were initially considered at the date of the pre-treatment evaluation (time zero) from which the treatment decision was taken, until the date of death or last visit. Other prognostic factors for mortality

were analyzed by Univariable Cox proportional hazard regression model of survival with log-rank p-values and Multivariable analysis.

6.2.3 Results:

6.2.3.1 Clinical and histological data.

6.2.3.1.1 Patient's characteristics

60 cases of cHCC-CCAs were analyzed. Only patients undergoing surgery (resection or liver transplantation) between 1989 and 2017 were included in the study. In the final analysis, 50 patients were retained. The diagnosis of cHCC-CCA was based first on the 2010 WHO classification and then on the more recent 2019 classification. Patients were predominantly males (66%), with advanced liver fibrosis (F3 or F4 / cirrhosis) in 46% of them. 70% of the patients were smokers, 36.6% had dyslipidemia and 45% were affected by hypertension. The majority of patients underwent liver resection 84%, a minority underwent transplantation 16%. Details of the patients' characteristics are given in Table 8.

Table 8: Patients characteristics and relative percentage

		N. Patients	% Patients	Median (IQR)
Age		50		60 (48-65)
Male sex	no	17	34,0%	
	yes	33	66,0%	
HBV	no	44	88,0%	
	yes	6	12,0%	
HCV	no	42	84,0%	
	yes	8	16,0%	
Alcohol	no	28	65,1%	
	yes	15	34,9%	
Cirrhosis/F3	no	27	54,0%	
	yes	23	46,0%	
Steatohepatitis	no	39	78,0%	
	yes	11	22,0%	
Portal hypertension	no	36	85,7%	
	yes	6	14,3%	

Hypertension	no	22	55,0%	
	yes	18	45,0%	
Dyslipidemia	no	26	63,4%	
	yes	15	36,6%	
Tobacco smoke	no	12	29,3%	
	yes	29	70,7%	
Diabetes	no	30	73,2%	
	yes	11	26,8%	
Surgery	yes	42	84,0%	
Liver transplantation	yes	8	16,0%	
Biggest tumor size mm		50		50 (35-110)
Satellite nodules	no	22	44,0%	
	yes	28	56,0%	
Tumoral emboli	no	11	22,0%	
	yes	39	78,0%	
Perineural invasion	no	36	72,0%	
	yes	14	28,0%	
Tumoral portal thrombosis	no	43	86,0%	
	yes	7	14,0%	

6.2.3.1.2 Characteristics of the surgical samples.

The median size of the tumors was 50 mm, and the majority of patients had microvascular invasion. 56% of patients had satellite nodules and 28% perineural invasion. At first reading of cHCC-CCA with whole slide analysis used to buid the TMA, 76% of the patients had a diagnosis of a classical type, some of them having another minor component including cholangiolocarcinoma (CLC). Almost all tumors expressed CK7 (92%); in positive cases, the average positivity rate was 72%. EpCam was expressed in 86% of the patients with a mean positivity of 80%. Glypican3 was expressed in 58% of samples with a mean positivity rate of 41%, while HepPar was positive in 48% of patients with a positive rate of 42%. Details of the positivity of the samples and the relative percentage are expressed in tables 9 et 10.

Table 9: Immunohistochemistry staining and relative percentage of positivity

		N° of cases	(%)
CK7	neg	4	8,0%
	pos	46	92,0%
CK19	neg	11	22,0%
	pos	39	78,0%
EpCam	neg	6	12,0%
	pos	43	86,0%
Nestine	neg	19	38,0%
	pos	5	10,0%
Glypican	neg	21	42,0%
	pos	29	58,0%
HepPar	neg	26	52,0%
	pos	24	48,0%
CD133	neg	20	40,0%
	pos	30	60,0%
CD56	neg	28	56,0%
	pos	22	44,0%
Sall4 TMA	neg	46	92,0%
	pos	4	8,0%

Table 10: Immunohistochemistry staining, relative positivity

	N°	Min	Max	Mean%	Standard deviation
EpCam%	43	10	100	80,23	27,987
CK7%	46	5	100	72,07	32,721
CK19%	39	5	100	56,41	33,638
HepPar%	24	5	100	42,92	31,205
Glypican%	29	5	95	41,03	29,166
CD56%	22	5	100	28,86	30,077
CD133%	30	5	80	25,83	24,036
Sall 4 TMA %	4	10	45	22,50	15,546
Nestine%	5	5	5	5,00	,000

6.2.3.2 *MALDI dataset analysis*

Preliminary data were analyzed according to unsupervised and supervised approaches

6.2.3.2.1 Preliminary analysis of all dataset: unsupervised analysis

The initial samples included four historical TMAs including 2 representative of iCCA and 2 representative of HCC. cHCC-CCA cases were regrouped in 12 TMAs. Pre-analytical tissue scans of all the TMA are shown in Figure 37.

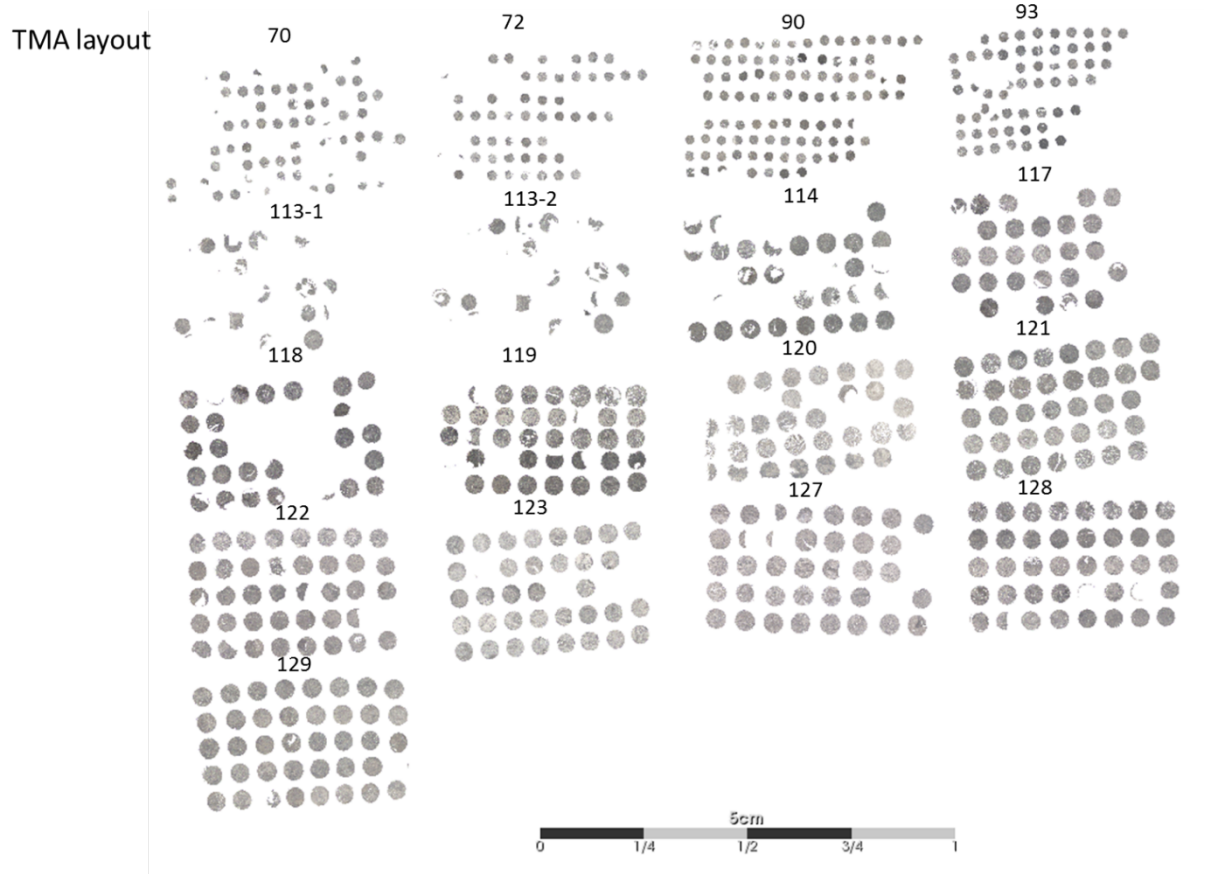


Figure 37: TMA analysis. Complete dataset. Optical scanner image.

Twelve TMA composed bof cases and four TMA composed of controls were analyzed

Controls: TMA 70 iCCA, TMA 72 iCCA, TMA 92 HCC, TMA 93 HCC.
Cases (cHCC-CCA) TMA 113,114, 117,118, 119,120, 121, 122, 123, 127, 128, 129

MSI segmentation analysis showed multiple peptide clusters distributed throughout the series, revealing significant heterogeneity between all TMAs, including the 4 controls. We also

observed a clusterization that was partially related to TMA construction (data acquisition of TMA performed in different times) (Fig. 38).

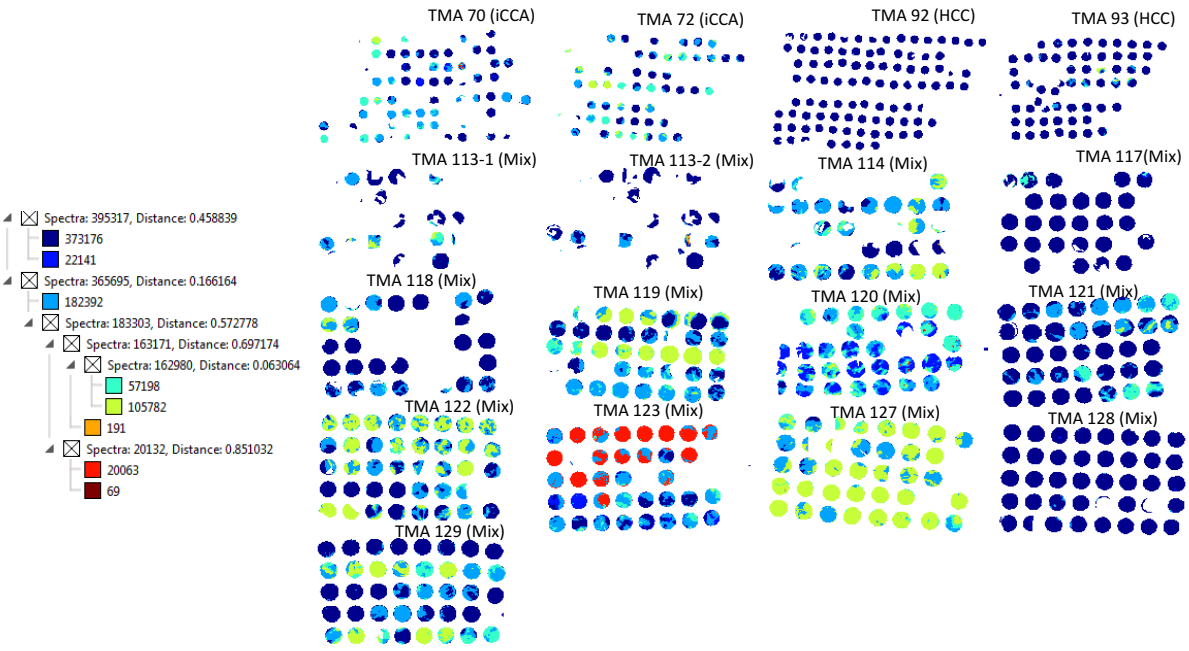


Figure 38: Clustering analysis, segmentation

Left side shows the dendrogram of segmentation. On the right side the graphical representation of the different clusters is shown. It can be seen that in some cases the clusters obtained are related to the individual TMA, each TMA was acquired in a separate experiment. For example, the TMA 123 are stained in red and the TMA 127 are stained in fluorescent green.

6.2.3.2.2 Preliminary analysis of all dataset: supervised analysis by classification

Cases were firstly classified according to the following sub-types: HCC, CCA, cHCC-CCA, CLC, Classical stem cells, Intermediate stem cells, Sarcomatoid. Linear Discriminant Analysis (LDA) Classification Model was created using a small number of spectra selected from the regions annotated by the pathologist. An example of the area used for the classification is shown in figure 39. The analysis by LDA showed a classification inconsistent with histological analysis (Fig.39). In some cases, such as in TMAs 117, 123, and 121, it can be seen that the TMA classification is particularly homogeneous, suggesting a potential effect related to the analysis of the sample rather than its molecular composition. This analysis also tended to

overestimate the presence of histological subtypes less represented in our set, such as CLC or the Stem cells subtypes.

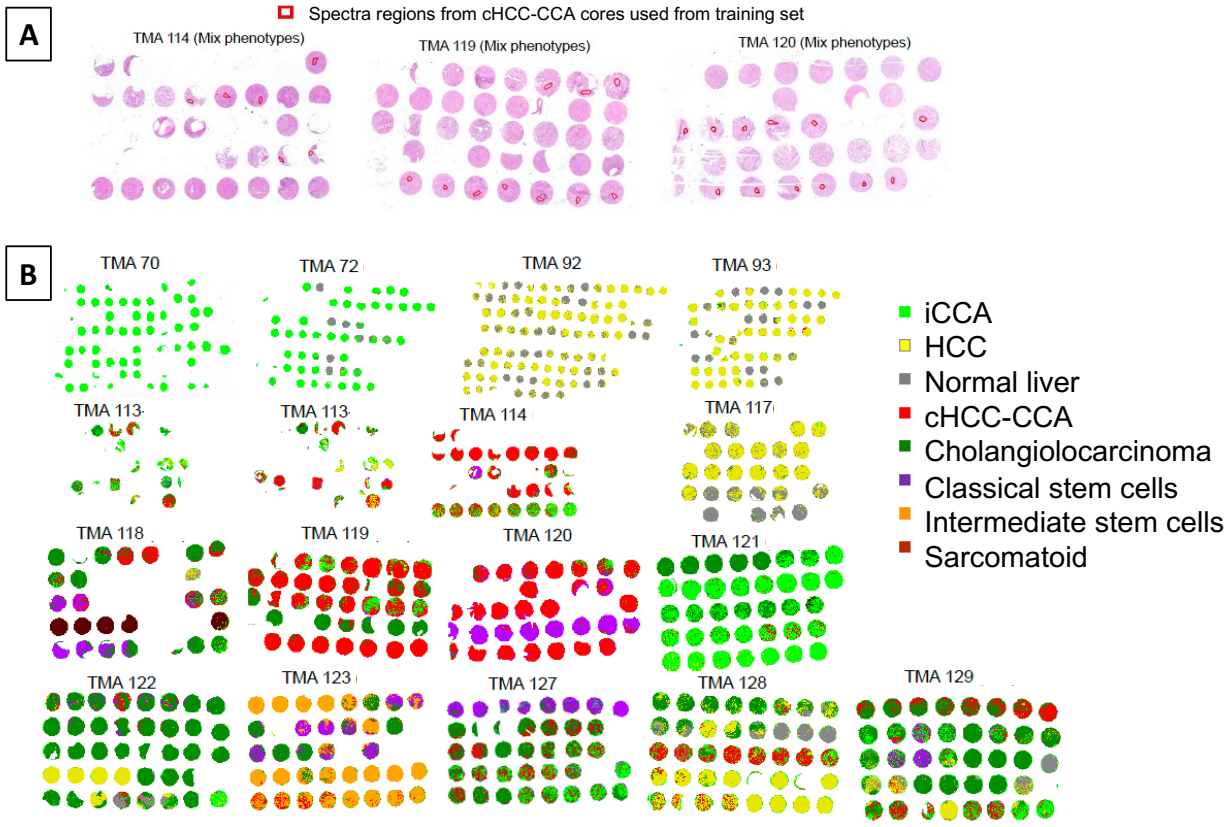


Figure 39: Linear Discriminant Analysis (LDA) Classification Model applied to data

A: The areas highlighted in red served as training samples for the algorithm.
B: Application of LDA to data. In a manner inconsistent with histological composition, TMA 92 TMA 93 are classified together with TMA 117. A strong effect related to the individual TMA can be seen. For example, TMA 121 is classified entirely as iCCA in fluorescent green, TMA 123 is classified almost entirely as intermediate in orange and TMA 119 is classified entirely as cHCC-CCA.

6.2.4 Conclusion-1

The unsupervised and supervised analyses did not allow a clear differentiation of histological subtypes of cHCC-CCA, also suggesting a possible analytical bias. These results support the need for data verification and inclusion of other methodological approaches.

6.2.4.1 *Quality control of MALDI dataset*

6.2.4.1.1 Elimination of biased data

Comparing the spectra of the different TMA controls, we found a similarity between TMAs 70 and 72 (CCA) with differences in intensity. Between TMAs 72, 70 and 93 (HCC), there were similarities with more marked differences in intensity values. On the other hand, TMA 92 was completely different from the other TMA typical of HCC (TMA 93). These data were confirmed by segmentation and PCA analysis (Fig. 40).

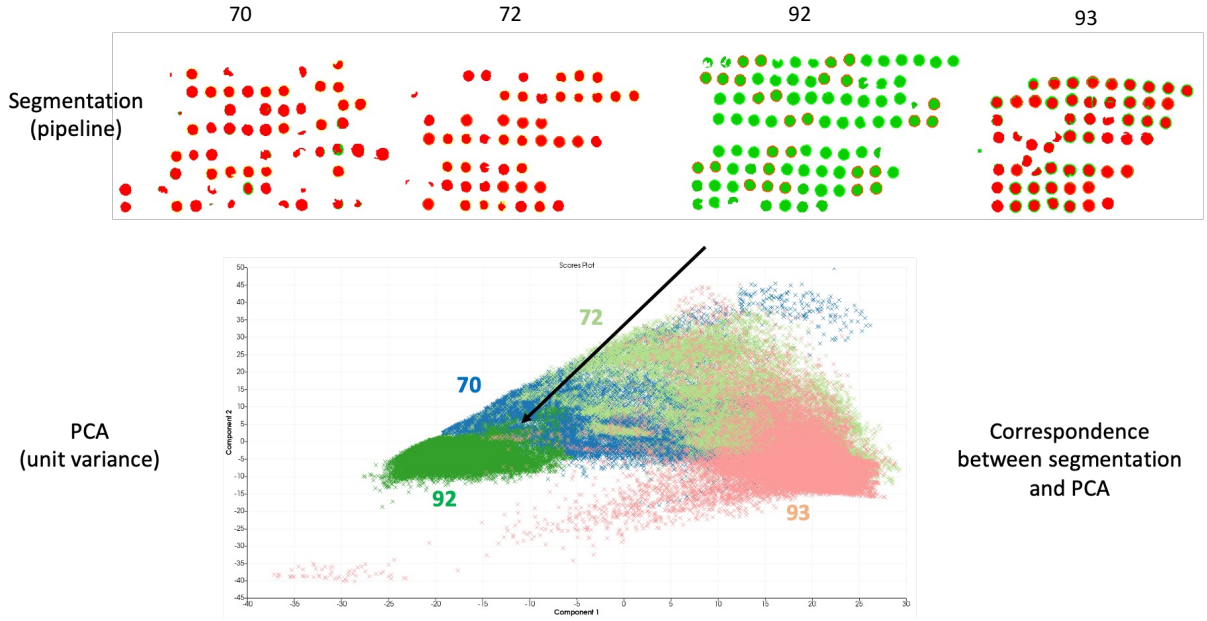


Figure 40: Correlation between PCA and segmentation in controls TMA

In the upper part of the figure, the segmentation of the four control TMAs is shown. The lower part of the figure shows the PCA distribution of the same controls. The X-axis shows component 1 while the Y-axis shows component 2.
It can be seen that TMA 92, despite being composed of HCC like TMA 93, clusters in isolation in both analyses: in green in the segmentation (top part) and in dark green in the PCA (bottom part of the figure).

PCA results performed on TMAs 92 and 93 showed a marked difference between them (Fig. 41).

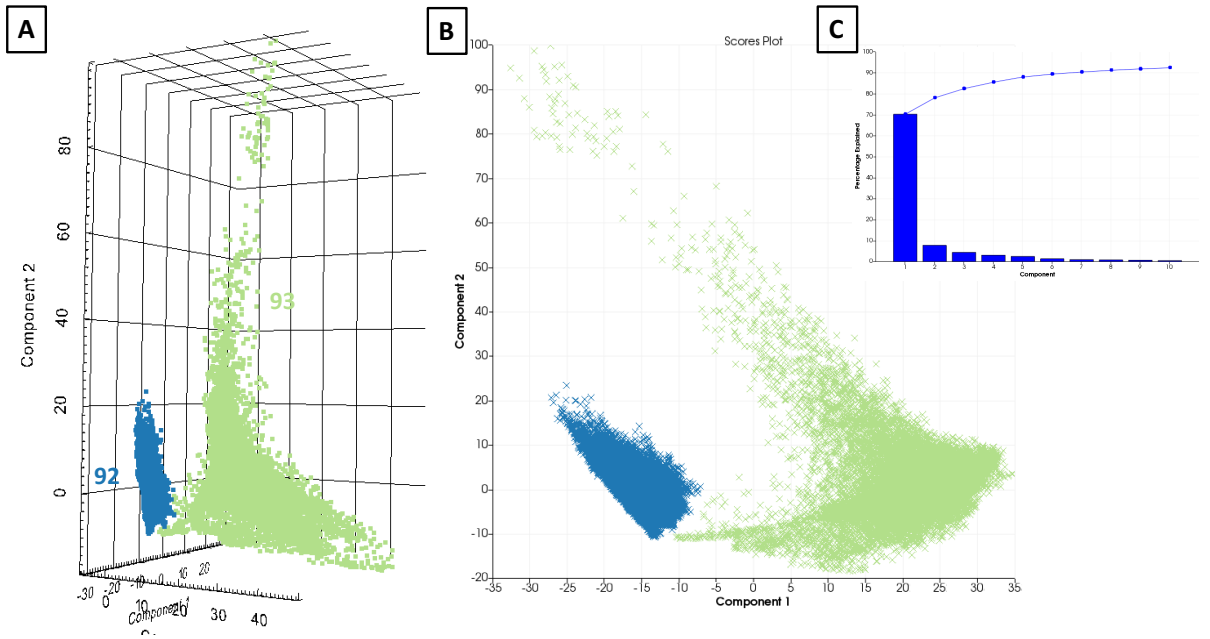


Figure 41: PCA of TMA 92 and 93

PCA of TMA 92 (green) and 93 (blue). A: 3D visualization; B:2D visualization score plot; C: Variance of components. In this figure, it is clearly seen that the two HCC-control TMAs composed of morphologically similar tissues are graphically represented by PCA as two different entities.

Considering that some of these results were not congruent with the morphology shown by histology, we made several hypotheses about possible factors perturbing the analysis. As a first hypothesis, we assumed a desynchronization of the spectra of samples acquired at different times. As second hypothesis, we thought of a possible analytical error for some samples. We tested the first hypothesis following advice from the productor's technicians of MALDI (Bruker) who had already described this phenomenon. By analyzing the overlap of some peptide peaks, we confirmed that some aspects were actually desynchronized. Thanks to synchronization software, the fusion of the various spectra was made homogeneous. Following synchronization, TMA 117 (cHCC-CCA) and 92 (HCC) showed the same clustering pattern in segmentation. Analyzing the laboratory records about the acquisitions we realized that TMAs 117 and 92 had been acquired on the same day following maintenance work on the spectrometer (Fig. 42).

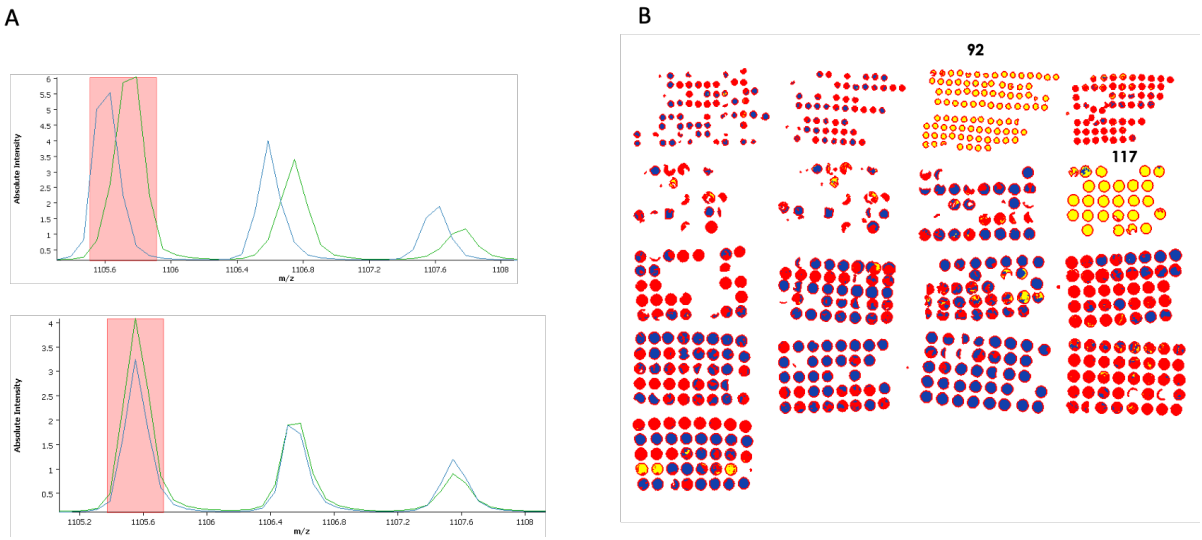


Figure 42: Peak alignment and segmentation

A: The peaks corresponding to the same peptides were misaligned between individual acquisitions (upper part of the figure). Following data processing with special program, the peaks were realigned between different spectra (lower part of the figure). B: It can be seen that even after the peaks were aligned, the TMA 92 composed of HCC controls, clustered abnormally with TMA 117 composed of cHCC-CCA (in yellow).

We concluded that differences between TMAs 92 and 117 and the other TMAs were probably due to an experimental bias. They were excluded for further analysis by the dataset. TMA 113 was also excluded for further analysis from the dataset due to the paucity of data.

Final layout of dataset is shown in Fig. 43.

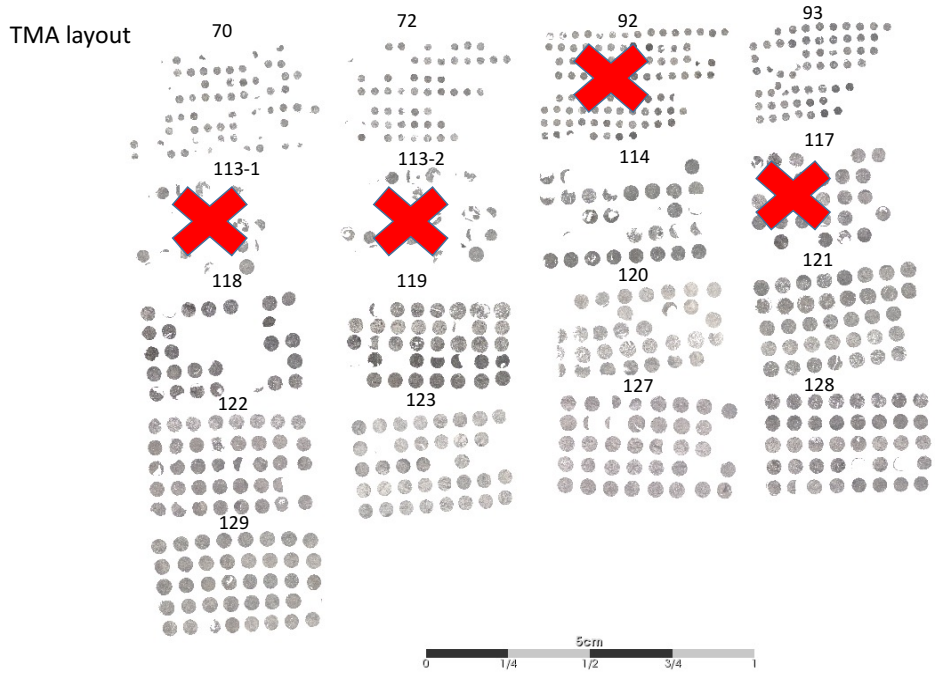


Figure 43: TMA layout after revisions..

TMAs 92, 113 and 117 were excluded from further analysis.

6.2.4.2 New tissue revision

Considering the first results showing heterogeneity in controls, we also decided to perform an extensive review of the controls by selecting only typical cases of HCC and iCCA and excluding areas of healthy liver. An exhaustive review of the controls led to the identification of 30 cores of typical iCCA (CT-CCA, from 12 patients) and 24 cores of typical HCC (CT-HCC, from 7 patients) (Fig. 44). Spectral analysis of controls showed a difference between HCC and iCCA, this difference was also identifiable in the PCA (Fig 45). We also subclassified HCC and iCCA into the main recognized morphological subtypes. Within the iCCA group, three subtypes were identified according to their degree of differentiation and presence of fibrous stroma (Fig. 44).

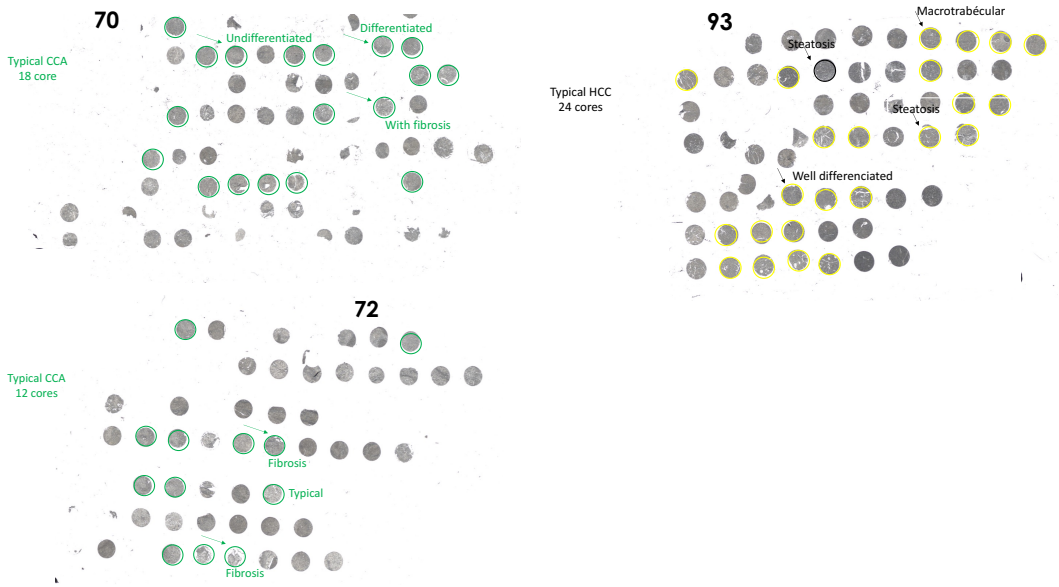


Figure 44: Exhaustive review of controls and identification of subtypes of interest

Performed on optical scan images.

Tissues from cholangiocarcinoma controls (TMA 70 and 72) are highlighted in green :reas considered for further analysis were classified into undifferentiated, differentiated, with fibrosis, and typical cholangiocarcinoma. Tissues of HCC controls derived from TMA 93 were highlighted in yellow with further subdivision into well-differentiated macro trabecular and steatosis-associated

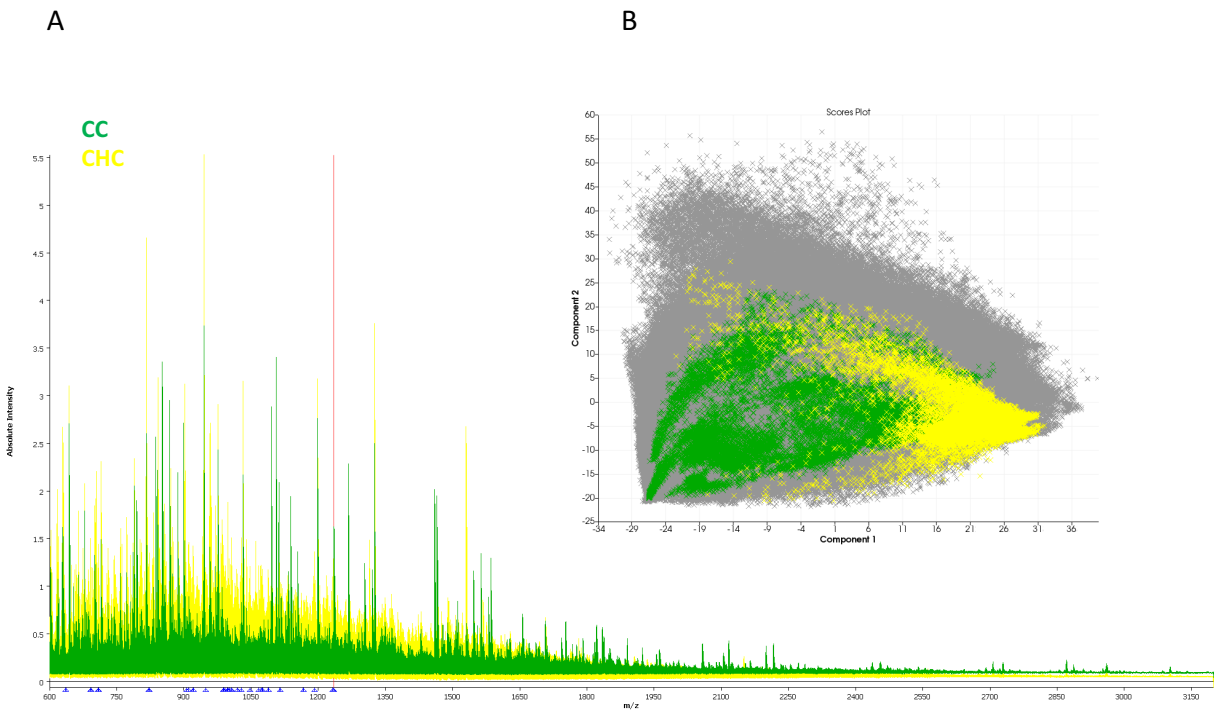


Figure 45: Analysis of controls spectra distribution after revision and 2D PCA

A: Spectra of HCC and iCCA included in the controls; B: PCA of iCCA and HCC showing a good separation between the two histotypes (HCC in yellow, iCCA in green, all TMA dataset in grey).

In iCCA controls, PCA showed a distribution of the spectra according to TMA (TMA 72 (top) TMA 70 (bottom). Also, PCA showed a distribution according to the morphological subtyping (differentiation according to component one, and fibrous stroma on component two) (Fig. 46). Such distribution may reflect a biological relevance. In conclusion, thanks to the PCA analysis, it could be seen that the typical iCCA controls were rather heterogeneously distributed. The main part of this heterogeneity could be explained by the molecular heterogeneity of the controls while the minor part of this heterogeneity could be explained as an effect related to the TMA acquisitions.

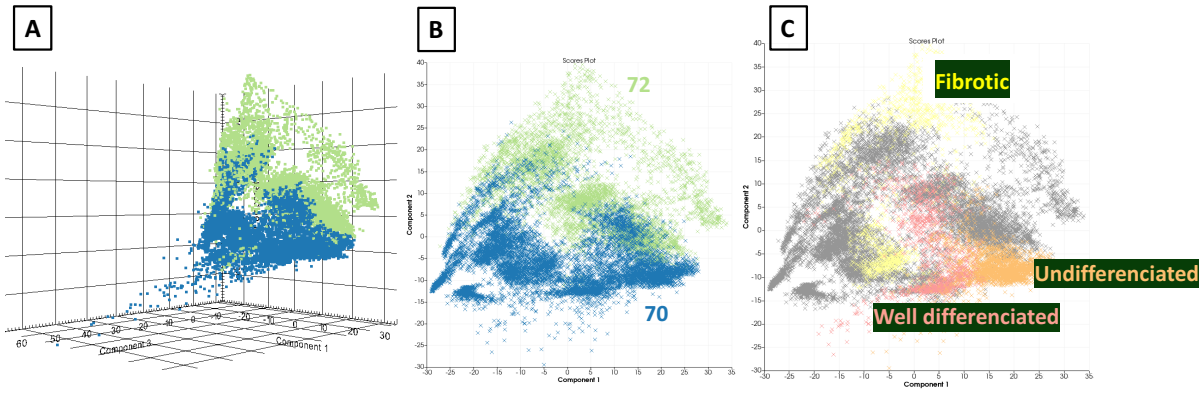


Figure 46: PCA of iCCA subtypes

A: 3D representation of PCA. B: 2D representation PCA, TMA 70 in blue; TMA 72 in green. iCCA undifferentiated in orange, iCCA differentiated in pink and with high fibrous component in yellow, all typical control in grey.

The control HCC TMAs were also analyzed by highlighting their subtyping (HCC typical and macrotrabecular). Among typical HCCs, HCC well differentiated, HCC with steatosis, HCC pseudoglandular, HCC fibrotic, HCC clear cells and other types were recorded. Following the exclusion of TMA 92, the HCC controls present in TMA 93 predominantly belonged to the well differentiated HCC, HCC with steatosis, and macrotrabecular HCC (Fig. 47).

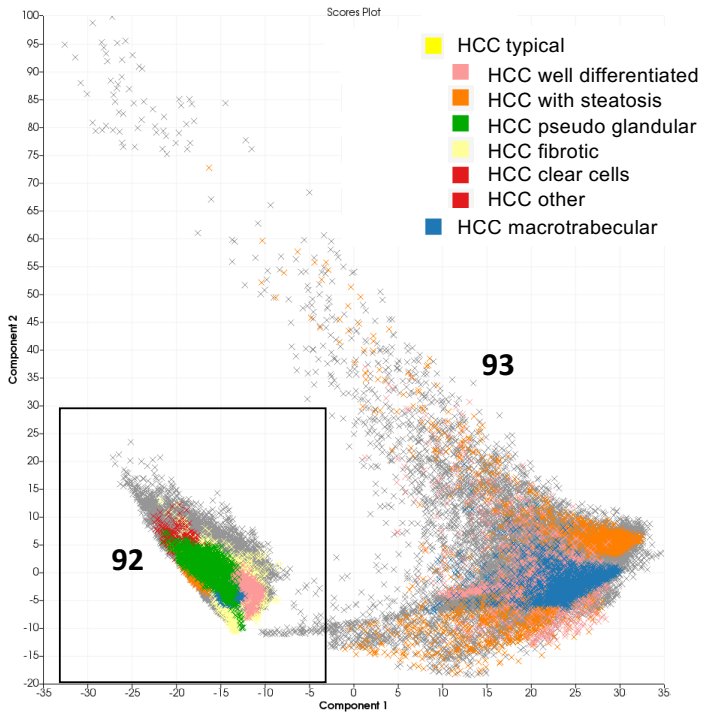


Figure 47: PCA in HCC controls

In PCA representation of the different HCC subtypes, it can be seen that TMA 93, the only one considered for further analysis, has a more heterogeneous distribution compared to TMA 92 (in black square). The majority constituents of TMA 93 were steatosis-associated HCC (orange), well-differentiated HCC (pink) and macro trabecular HCC (blue).

6.2.4.3 Differential peaks (cHCC-CCA, HCC and iCCA after quality control and new labelling)

Comparison of the peaks expressed in all the cases (TMAs cHCC-CCA) compared to those of the controls (CT-HCC and. CT-CCA) allowed the identification of a new list of peaks of interest.

Table 11: Discriminating ROC curve shown for cHCC-HCC TMA, ROC with AUC >0.75

Number of peaks with a ROC curve showing a AUC >0,75 ; >0,8 ; >0,9 respectively. Peaks derived from cHCC-CCA are compared to CT-HCC and CT-CCA.

	114		118		119		120		121		122		123		127		128		129	
AUC	iCCA	HCC	iCCA	HCC	iCCA	HCC	iCCA	HCC	iCCA	HCC	iCCA	HCC	iCCA	HCC	iCCA	HCC	iCCA	HCC	iCCA	HCC
> 0,75	1	13	81	0	64	94	61	43	0	0	28	81	63	46	116	122	188	0	118	69
> 0,8	0	0	16	0	3	59	37	26	0	0	4	41	43	36	87	114	110	0	39	34
> 0,9	0	0	0	0	0	0	17	15	0	0	0	0	13	11	15	69	5	0	0	1

Table 11 indicates the number of peaks having ROC curves with an area under the curve (AUC) greater than 0.75, 0.8, 0.9, respectively. The differential peaks were obtained by comparing peak intensity between cHCC-CCA and CT-HCC and CT-CCA, respectively.

Table 12: Discriminating ROC curve shown for cHCC-HCC TMA, ROC with AUC <0.25

Number of peaks with a ROC curve showing a AUC < 0,25 ; < 0,2 ;< 0,1 respectively. Peaks derived from cHCC-CCA are compared to CT-HCC and CT-CCA.

	114		118		119		120		121		122		123		127		128		129	
AUC	CCA	HCC	iCCA	HCC	iCCA	HCC	iCCA	HCC	iCCA	HCC	iCCA	HCC	iCCA	HCC	iCCA	HCC	iCCA	HCC	iCCA	HCC
< 0,25	0	274	0	136	0	95	2	255	0	297	0	171	18	281	8	256	19	137	0	123
< 0,2	0	242	0	92	0	65	0	225	0	252	0	114	6	265	0	232	1	93	0	80
< 0,1	0	114	0	20	0	14	0	117	0	131	0	3	0	198	0	160	0	8	0	8

Table 12 indicates the number of peaks having ROC curves with an area under the curve (AUC) smaller than 0.25, 0.2, 0.1, respectively. The fact that some peaks have ROCs with AUCs below 0.25 meant that the peaks had an area under the curve corresponding to 0.75 in the second comparison term. CT-HCC showed a higher number of differential peaks when compared to cHCC-CCA. By contrast, very few peaks had ROCs with AUCs below zero 0.25 in the comparison between cHCC-CCA and CT-CCA. These data taken together suggest that HCC

are more different from cHCC-CCA than iCCA, on the other hand cHCC-CCA are more similar to iCCA.

6.2.4.4 *Further annotation of cHCC-CCA samples*

Since one single tumor core included in cHCC-CCA TMAs may display either iCCA or HCC phenotypes at the morphological analysis, we decided to re-label single cores of cHCC-CCA into MT-cHCC-CCA, MT-iCCA, MT-HCC, and non-classifiable (MT-NC) when none of the previous labeling could be applied (Annotation shown in Fig.48).

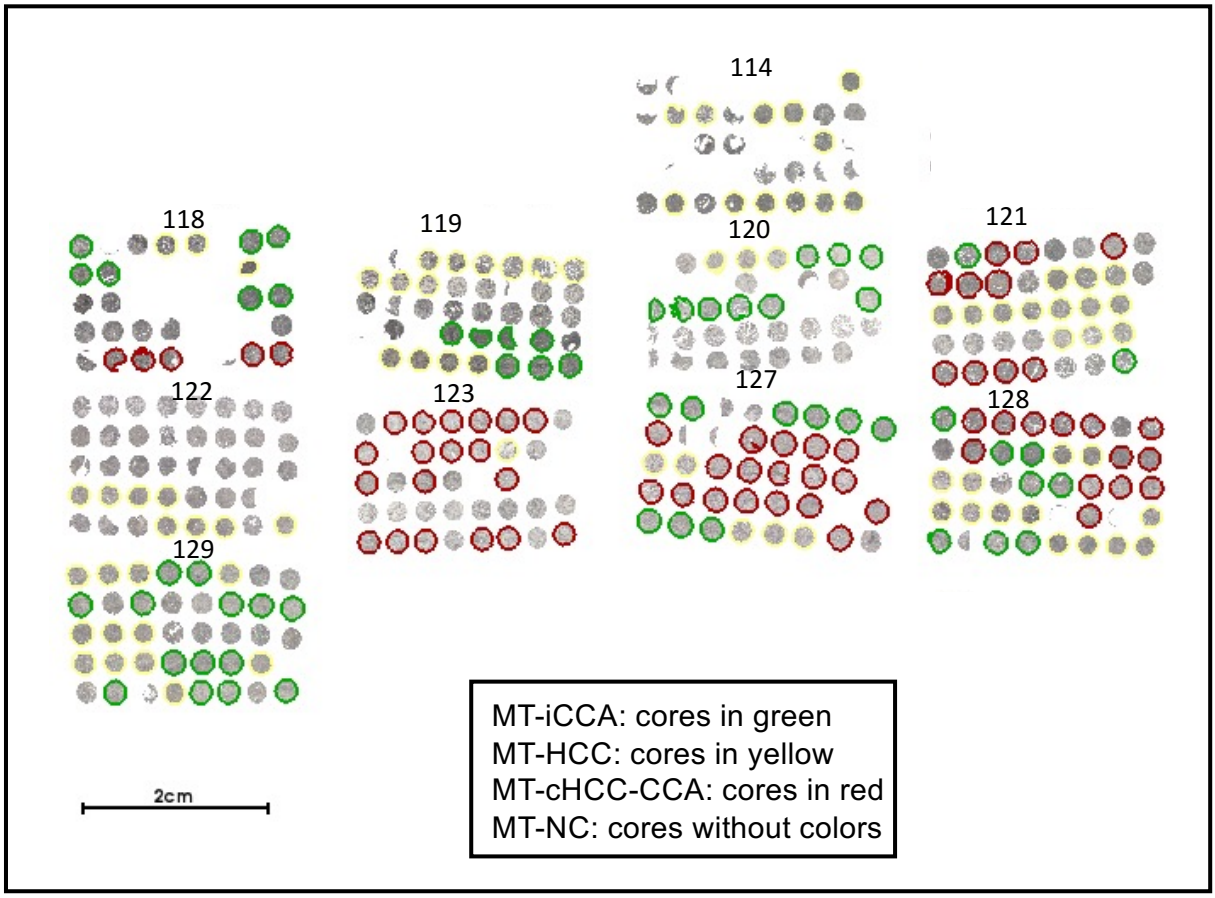


Figure 48: New annotation of cHCC-CCA on optical scanner image.

Further annotation performed in the TMAs of cHCC-CCA cases (114, 118, 119, 120,121,122,123,127,128,129) highlights the different subtypes identified. In green the purely cholangiocarcinomatous component of cHCC-CCA (MT-iCCA), in yellow the hepatocarcinomatous component of cHCC-CCA (MT-HCC) , in red the mixed cHCC-CCA component (MT-cHCC-CCA) and finally the tissues without annotation are identified as unclassifiable (MT-NC).

.

More than 500 peaks were found to be differentially expressed between all tumor categories. MT-cHCC-CCA and CT-iCCA displayed the lowest number of differential peaks, followed by MT-NC vs MT-iCCA; MT-NC vs MT-cHCC-CCA, MT-NC vs CT-iCCA. Unclassified tumors (MT-NC) and CT-HCCs, as well as MT-cHCC-CCA and CT-HCC displayed the most differential expression with over 500 peaks (Fig.49).

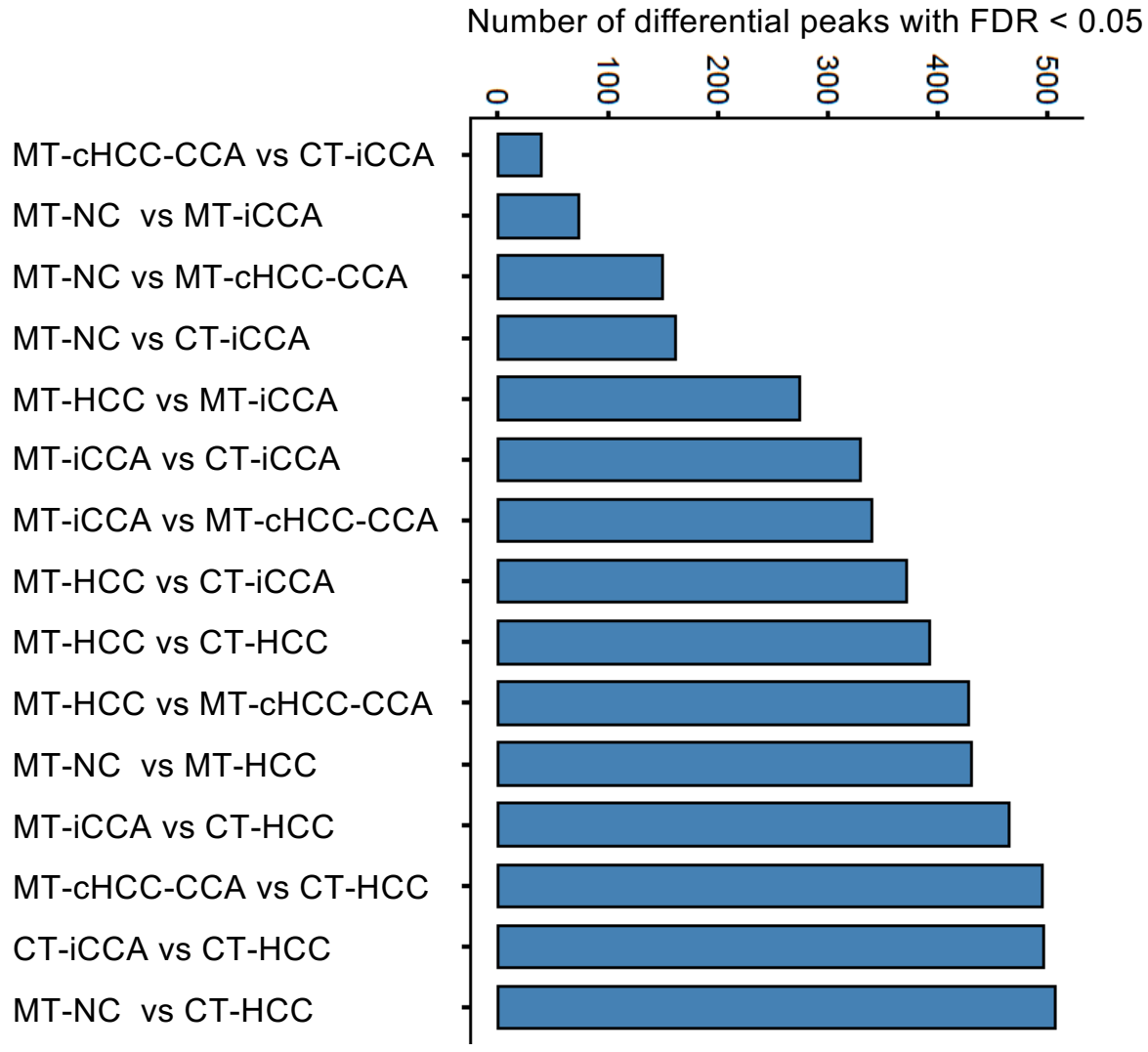


Figure 49: Number of differential peaks between the different cancer subtypes.

This figure shows the number of existing differential peaks identified with a Mann-Whitney test (FDR >0.05) calculated in comparisons between different histological subtypes. HCC and CCA controls are shown for greater precision as CT-HCC and CT-iCCA, respectively.

To illustrate this results correlation was performed for each group with the mean peak intensity of CT-HCC or CT-CCA. On average MT-NC, MT-HCC and MT-iCCA were close to zero in their correlation with iCCA showing no correlation (Fig 50 A). CT-iCCA and MT-cHCC-CCA showed a higher correlation to iCCA. CT-HCC as expected was located separately in the lower sector of the figure, showing low correlation with iCCA (Fig 50 A). In Fig 50 B, it could be seen that CT-HCC had a compact distribution and correlates strongly with HCC, similarly but less intensely, we found MT-HCC, which was strongly correlated with HCC. MT-NC, MT-iCCA, and MT-cHCC-CCA did not seem to be correlated with HCC. It should be noted in the graph that all subtypes outside of CT-HCC have a particularly wide distribution, showing that their composition is heterogeneous. In conclusion, the components of cHCC-CCA had a similar distribution, not correlated with iCCA, or HCC with the exception of MT-cHCC-CCA that showed similarity with iCCA and MT-HCC which showed a higher degree of similarity with HCC.

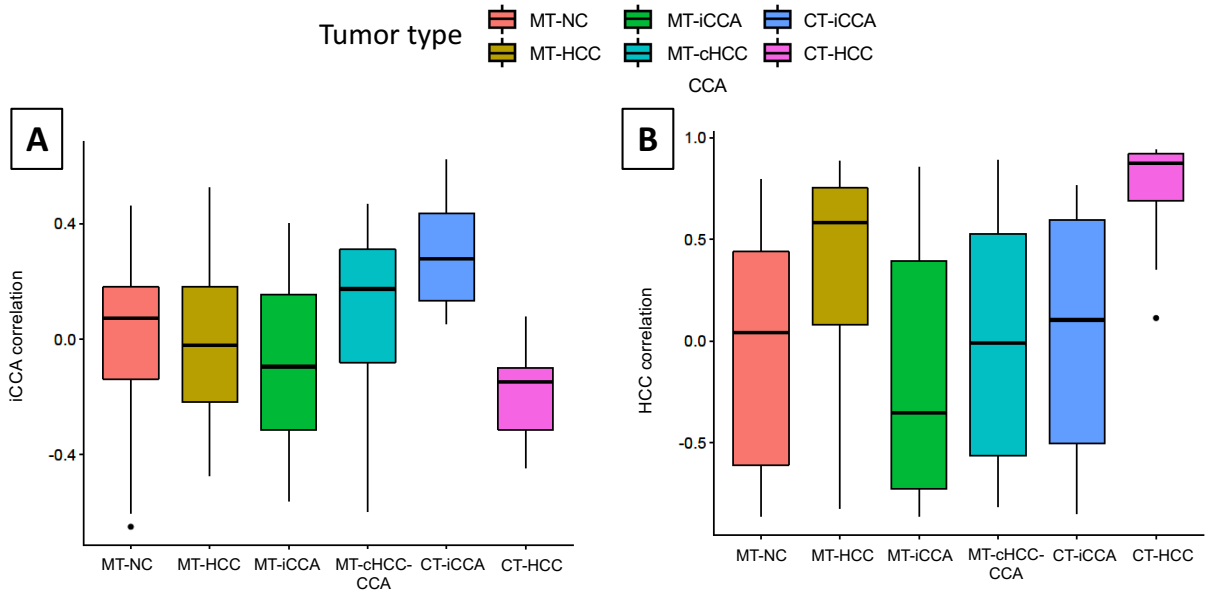


Figure 50: Correlation analysis of subtypes with HCC and iCCA, separated vision

A: Box plot showing the correlation of each histological subtype with the centroid of iCCA control
B: Box plot showing the correlation of each histologic subtype with the centroid of the control HCC
The similarity of each sample to each centroid was then calculated using Pearson's correlation.
The most similar to iCCA are CT-iCCA and MT-cHCC-CCA. The most similar to HCC are CT-HCC and MT-HCC.

6.2.4.5 Addition of new controls for data validation

Considering the reduction of control samples following data verification, we decided to include an additional control TMA in an attempt to normalize the sample set. New control TMA included 10 HCCs and 10 iCCAs. The purpose of building this new TMA and acquiring it with a different MALDI machine was to increase the terms of comparison and to validate the concept that MALDI data can be made homogeneous even if they were acquired with different machines at different times. The new control TMA was constructed to reduce analytical biases related to sample homogeneity. The segmentation analysis allowed a good separation of the cores by clusters. The cores colored in red belonged rather to the iCCA group, whereas the cores in green belonged rather to HCC group (Fig.51). The combination of data acquired from different MALDI equipment at different times allowed the generation of valid data giving good confirmation of the reproducibility of the technique.

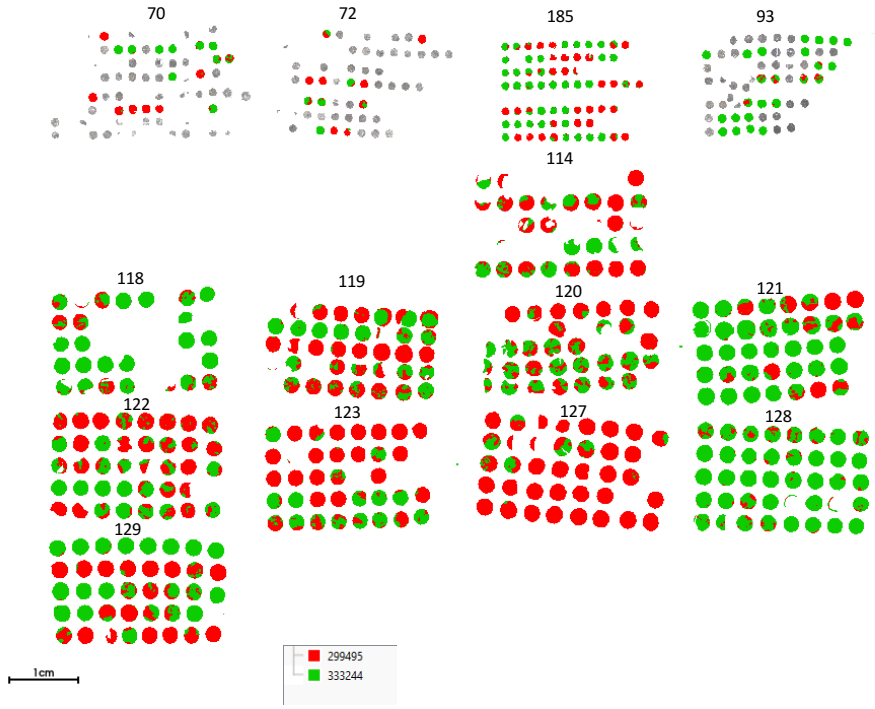


Figure 51: Segmentation analysis including TMA 185

A new TMA control composed of HCC and iCCA (185) is also included In this segmentation display, only the controls considered as typical are included, Analysis by segmentation shows results consistent with the histologic composition of the tissue; HCC-like tissue is represented in green, while iCCA tissue is represented in red. TMA 93 is correctly identified with a homogeneous color cluster, control 185 HCC-like tissue is well differentiated from iCCA tissue. In the two iCCA controls (70, 72) from cholangiocarcinoma, the tissues, on the other hand, are shown as a mixture of the two heterogeneously distributed clusters and do not clearly represent the tissue composition.

After the integration of TMA 185, about 100 additional differential peaks were identified between the different tumor subtypes. The lowest number of differential peaks was now found between MT-NC and MT-iCCA, which remained below 100 peaks. Summarizing these results, it can be stated that typical cHCC-CCAs acquired an important number of differential peaks compared to iCCA controls and also increased differential peaks with HCC controls. However, cHCC-CCA remained less different from iCCA controls than HCC controls. Unclassified tumors (MT-NC) were still the most different from control HCC. MT-cHCC-CCAs remained particularly different from control HCCs with more than 500 peaks. In conclusion, the addition of controls increased the difference in terms of number of differential peaks between cases and controls. (Fig. 52)

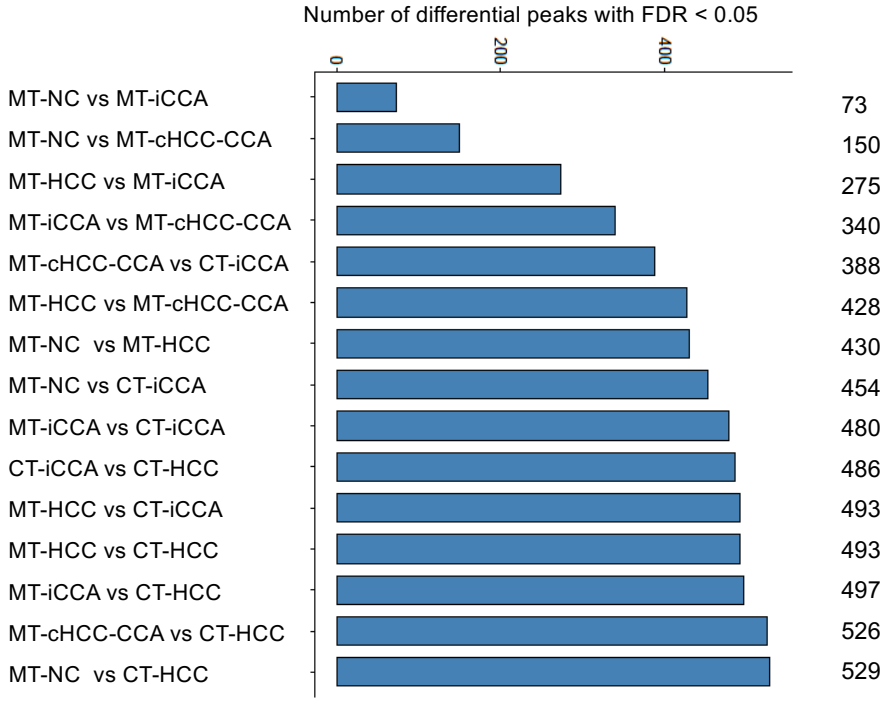


Figure 52: Number of differential peaks between with TMA 185

Figure shows the number of existing differential peaks identified with a Mann-Whitney test (FDR >0.05) calculated in comparisons between different histological subtypes after the addition of TMA 185.

Applying PCA analysis to all dataset after inclusion of TMA 185 identified two groups of ions. In yellow, the highlighted cores are more related to HCC, while in green they are more related to iCCA.

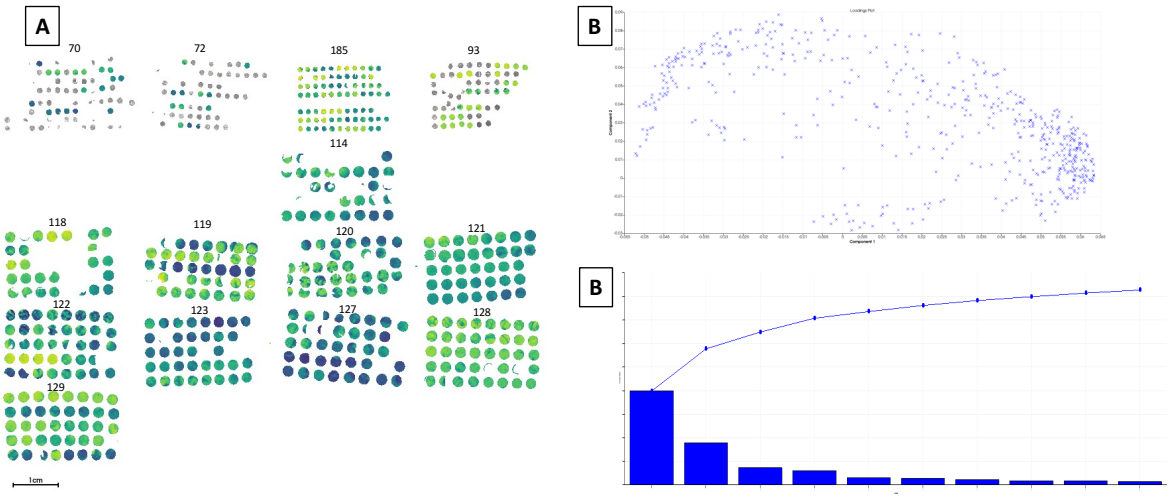


Figure 53: PCA with TMA 185

A: This figure shows the distribution of component one of PCA in the TMA data set. In yellow the highlighted tissues are more related to HCC while in green they are more related to iCCA. B: loading plot, data are scattered in two poles corresponding to HCC and iCCA. C: impact of each component on the variance.

To develop useful tools to improve correct identification, we compared all the subgroups. Here we report as an example the comparison between MT-iCCA and CT-iCCA. Some of the differential peaks showing ROC curves with AUC >0.75 were analyzed and their distribution over the whole sample was visualized. In the comparison between MT-iCCA vs CT-iCCA we found 480 peaks with a Wilcoxon test reporting an FDR value <0.05, of those 69 had a ROC curve with an AUC >0.75. Peaks 1143.541 m/z and 1145.506 m/z that had a high discriminating power between MT-iCCA vs CT-iCCA are shown (Fig. 54).

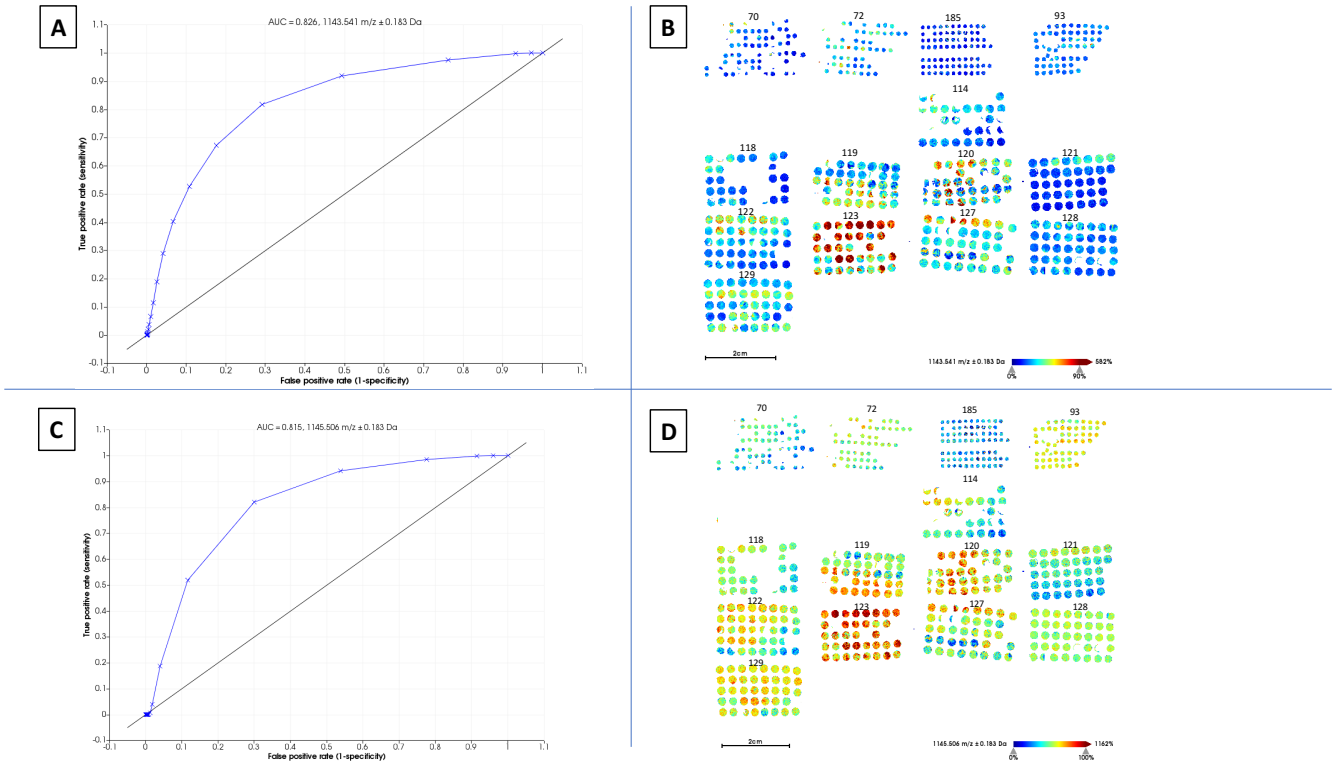


Figure 54: ROC curves of discriminant peaks between MT-iCCA vs CT-iCCA

.

A and C: Two example of peptides with a ROC curve with AUC >0.8; (1143.541 m/z and 1145.506 m/z peaks)
B and D: peak intensity displayed on TMAs: red color means overexpression blue color means underexpression.

6.2.4.6 Survival analysis

Lastly, we performed a univariable analysis to determine which factors were associated with death in our group patients. The statistically associated factors were the largest tumor size, the presence of satellite nodules and the number of tumors (Fig. 55)

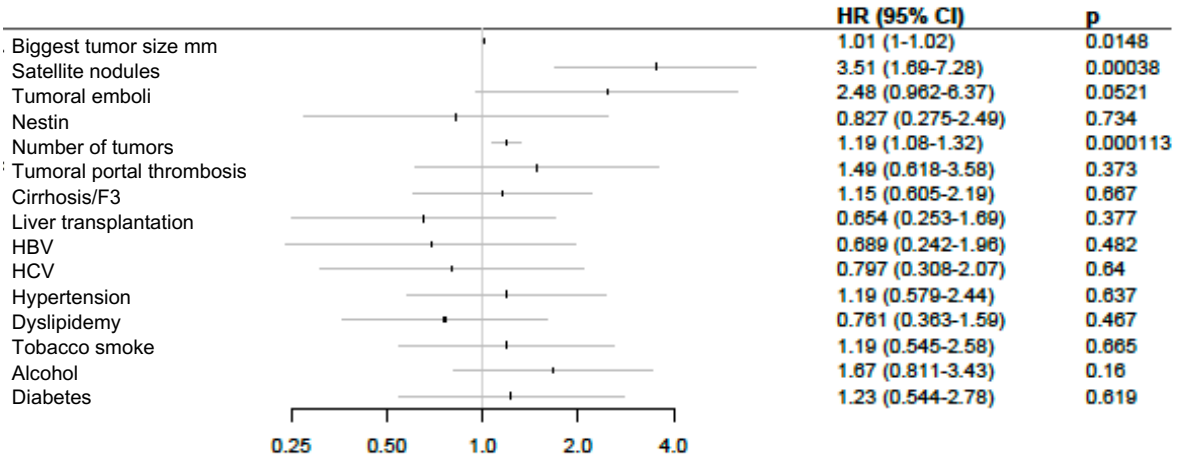


Figure 55: Univariable analysis

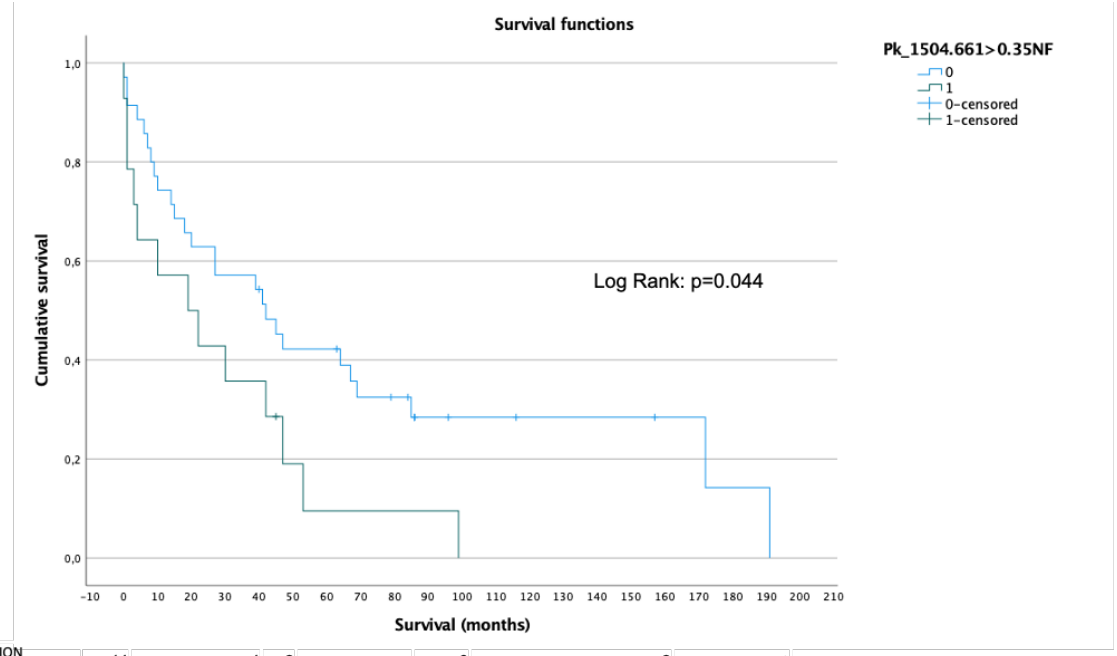
Known risk factors of poor prognosis are included in the univariable analysis. The only factors that were significant were the presence of satellite nodules, the number of tumors and tumor size.

Taking into account the positive variables according to the univariable analysis, a multivariable analysis including the peaks of interest found in the cHCC-CCA was performed, which reported 9 peaks independently associated with mortality and one protective peak for mortality (Table 13).

Table 13: Uni and multivariable analysis of peaks of interest

Peaks	Univariable p value	Univariable HR	Multivariable P value	Multivariable HR
Pk_1504.661	0,14151462	1,26480495	0,02747365	1,48369505
Pk_1884.86	0,2072127	1,20242769	0,03189466	1,38172343
Pk_1497.723	0,09806431	1,28131051	0,03773601	1,41061865
Pk_1885.901	0,29619844	1,16353112	0,04135578	1,37227864
Pk_1498.764	0,11018074	1,25341468	0,04292963	1,38303446
Pk_1866.937	0,18479336	1,23329412	0,04402094	1,35163843
Pk_1853.871	0,27928877	1,17129957	0,0455475	1,36141259
Pk_1883.935	0,23473804	1,19011122	0,0481182	1,35175528
Pk_1868.903	0,24036395	1,19847123	0,04917135	1,35087319
Pk_1140.534	0,09762636	0,78316742	0,04952728	0,69964491

Pk_1504.661 shows a HR of 1,48 with a p=0,0275. The example of a peak-related survival curve is shown in figure 56, the group expressing the peak Pk_1504.661 with higher intensity had a higher mortality than the group with Pk_1504.661 lower expression. The median survival in the two groups was 42 months (19-64) vs 19 months (0-41), respectively (Fig. 56).



HIGH EXPRESSION Pk_1504.661	14	4	2		0	2	0
LOW EXPRESSION Pk_1504.661	35	18	14		4	0	0

Figure 56: Kaplan-Meier curve of Pk_1504.661

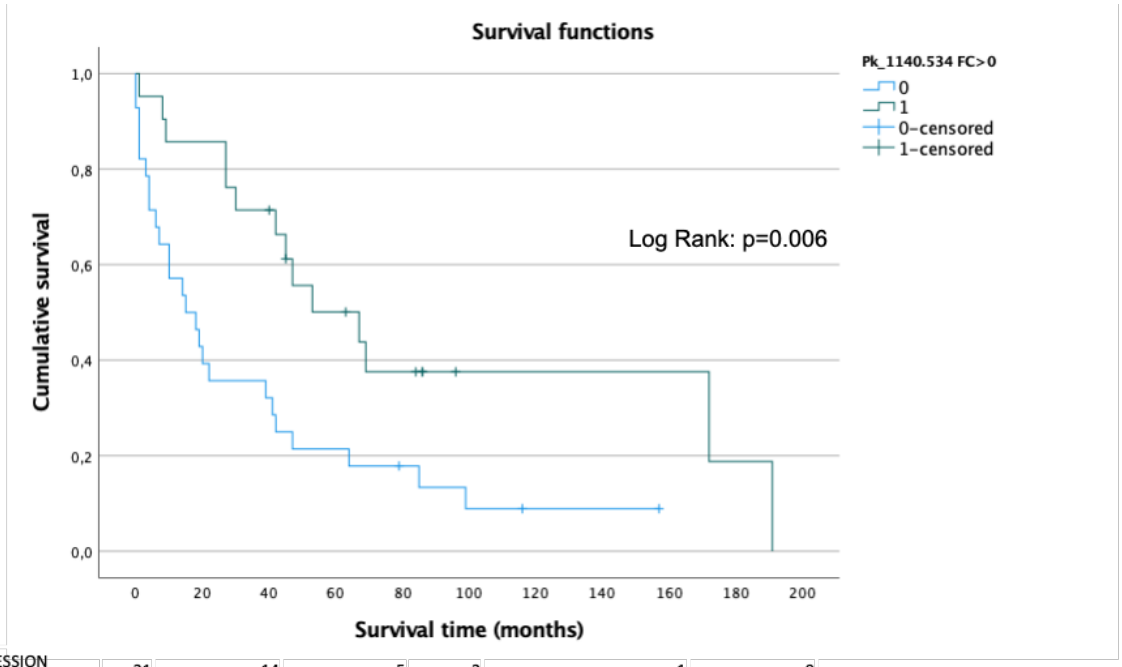
Patients with low expression of Pk_1504.661 had significantly better survival than patients with high expression of Pk_1504.661

The same approach was applied excluding transplanted patients. The analysis revealed four peaks independently associated with reduced mortality and one peak associated with mortality (Table 14).

Table 14: Uni and multivariable analysis excluding transplanted patients.

Peaks	**Univariable p value**	**Univariable HR**	**Multivariable P value**	**Multivariable HR**
Pk_1140.534	0,03711337	0,70963356	0,0235521	0,62347351
Pk_1337.688	0,04181659	0,64959891	0,02691626	0,60671912
Pk_1138.568	0,03841054	0,67303376	0,02935321	0,6180539
Pk_1139.609	0,04363868	0,68686882	0,03291445	0,63235035
Pk_1497.723	0,15277439	1,25143451	0,04420437	1,40828482

For example, the Pk_1140.534 showed a HR of 0.6 with a p= 0.023. The peak-related survival curve is shown in the figure 57, the group expressing the peak Pk_1140.534 with higher intensity had a lower mortality than the group with lower Pk_1140.534 expression. The median survival in the two groups was 67 months (29-105) vs (15 months (3-27). (Fig. 57)



HIGH EXPRESSION Pk_1140.534	21	14	5	2	1	0
LOW EXPRESSION Pk_1140.534	28	8	3	2	0	0

Figure 57: Kaplan-Meier curve of Pk 1140.534

Patients with high expression of Pk 1140.534 had significantly better survival than patients with low expression of Pk 1140.534

6.2.5 Conclusions-2

After a thorough methodological review and the addition of additional histological cases via the TMA approach, we were able to identify a number of peptide markers specific for the different subclasses of cHCC-CCA. From an etiological point of view, analyzing the results obtained, we can state that cHCC-CCA is an entity in itself from a molecular point of view, although its divergence probably does not lie in a completely different composition but rather in a more or less intense expression of certain components distributed with great heterogeneity. In our study, however, we found indications of its similarity to iCCA with respect to HCC. Thanks to the data generated by MALDI, we have been able to develop an extensive list of peptides of interest useful for diagnosis and related to prognosis. These latter data must therefore be considered with caution, as the multivariate analyses, due to the limited number of events, could only take into account a few covariables and patients, again due to the limited number of observations, were not matched according to the treatments received at the time of relapse.

7 GENERAL CONCLUSIONS

cHCC-CCA is a complex tumor in many respects. Its inherent heterogeneity underlies the difficulties encountered in classification, diagnosis and treatment planning. With our work, we have tried to answer the open questions about cHCC-CCA on different aspects, both clinical and basic research.

Regarding the diagnostic area, we described how a sequential approach based on imaging and liver biopsy, with the help of histological immunomarkers, can help to diagnose cHCC-CCA before surgery. Although not easy to propose in clinical practice, increasing the number of image-guided biopsy passages in tumors seems to us to be a recommended practice to probe all tumor components.

Through a innovative imaging *in situ* approach (MALDI imaging), we highlighted the great tumor heterogeneity of cHCC-CCA but also iCCA, and the potential of this technique for (1) better characterize PLC (improve morphological magnification and upgrade information provided by conventional immunohistochemistry), and (2) identifying new tissue diagnostic and prognostic biomarkers.

Regarding therapy of cHCC-CCA, which is poorly standardized, our nationwide multicenter retrospective study supports the treatment strategy based on TKIs or platinum-based chemotherapies in patients with advanced stages.

Although there is still a long way to go, we hope that with the data developed in this manuscript we have succeeded in increasing the general knowledge about cHCC-CCA and stimulating the research dedicated to this entity.

8 BIBLIOGRAPHY

- Abdelmoula, Walid M., Benjamin Balluff, Sonja Englert, Jouke Dijkstra, Marcel J. T. Reinders, Axel Walch, Liam A. McDonnell, et Boudewijn P. F. Lelieveldt. 2016. « Data-Driven Identification of Prognostic Tumor Subpopulations Using Spatially Mapped t-SNE of Mass Spectrometry Imaging Data ». *Proceedings of the National Academy of Sciences of the United States of America* 113 (43): 12244-49. https://doi.org/10.1073/pnas.1510227113.

- Aerni, Hans-Rudolf, Dale S. Cornett, et Richard M. Caprioli. 2006. « Automated Acoustic Matrix Deposition for MALDI Sample Preparation ». *Analytical Chemistry* 78 (3): 827-34. https://doi.org/10.1021/ac051534r.

- Agrawal, Shefali, et Jacques Belghiti. 2011. « Oncologic Resection for Malignant Tumors of the Liver ». *Annals of Surgery* 253 (4): 656-65. https://doi.org/10.1097/SLA.0b013e3181fc08ca.

- Akiba, J., O. Nakashima, S. Hattori, K. Tanikawa, M. Takenaka, M. Nakayama, R. Kondo, et al. 2013. « Clinicopathologic analysis of combined hepatocellular-cholangiocarcinoma according to the latest WHO classification ». *Am J Surg Pathol* 37 (4): 496-505. https://doi.org/10.1097/PAS.0b013e31827332b0.

- Alexandrov, Theodore, Michael Becker, Sren-Oliver Deininger, Günther Ernst, Liane Wehder, Markus Grasmair, Ferdinand von Eggeling, Herbert Thiele, et Peter Maass. 2010. « Spatial Segmentation of Imaging Mass Spectrometry Data with Edge-Preserving Image Denoising and Clustering ». *Journal of Proteome Research* 9 (12): 6535-46. https://doi.org/10.1021/pr100734z.

- Allen, Raymond A, et James R Lisa. 1949. « Combined Liver Cell ahd Bile Duct Carcinoma ». *The American Journal of Pathology* 25 (4): 647-55.

- Amstalden van Hove, Erika R., Donald F. Smith, et Ron M. A. Heeren. 2010. « A Concise Review of Mass Spectrometry Imaging ». *Journal of Chromatography. A* 1217 (25): 3946-54. https://doi.org/10.1016/j.chroma.2010.01.033.

- Bagante, Fabio, Gaya Spolverato, Matthew Weiss, Sorin Alexandrescu, Hugo P. Marques, Luca Aldrighetti, Shishir K. Maithel, et al. 2018. « Surgical Management of Intrahepatic Cholangiocarcinoma in Patients with Cirrhosis: Impact of Lymphadenectomy on Peri-Operative Outcomes ». *World Journal of Surgery* 42 (8): 2551-60. https://doi.org/10.1007/s00268-017-4453-1.

- Balluff, Benjamin, Christian K. Frese, Stefan K. Maier, Cédrik Schöne, Bernhard Kuster, Manfred Schmitt, Michaela Aubele, et al. 2015. « De Novo Discovery of Phenotypic Intratumour Heterogeneity Using Imaging Mass Spectrometry ». *The Journal of Pathology* 235 (1): 3-13. https://doi.org/10.1002/path.4436.

- Balluff, Benjamin, Sandra Rauser, Stephan Meding, Mareike Elsner, Cedrik Schöne, Annette Feuchtinger, Christoph Schuhmacher, et al. 2011. « MALDI Imaging Identifies Prognostic Seven-Protein Signature of Novel Tissue Markers in Intestinal-Type Gastric Cancer ». *The American Journal of Pathology* 179 (6): 2720-29. https://doi.org/10.1016/j.ajpath.2011.08.032.

- Basu, Sankha S., et Nathalie Y. R. Agar. 2021. « Bringing Matrix-Assisted Laser Desorption/Ionization Mass Spectrometry Imaging to the Clinics ». *Clinics in Laboratory Medicine* 41 (2): 309-24. https://doi.org/10.1016/j.cll.2021.03.009.

- Beaufrère, Aurélie, Julien Calderaro, et Valérie Paradis. 2021. « Combined Hepatocellular-Cholangiocarcinoma: An Update ». *Journal of Hepatology* 74 (5): 1212-24. https://doi.org/10.1016/j.jhep.2021.01.035.

- Berghmans, Eline, Kurt Boonen, Evelyne Maes, Inge Mertens, Patrick Pauwels, et Geert Baggerman. 2020. « Implementation of MALDI Mass Spectrometry Imaging in Cancer Proteomics Research: Applications and Challenges ». *Journal of Personalized Medicine* 10 (2). https://doi.org/10.3390/jpm10020054.

- Bich, Claudia, David Touboul, et Alain Brunelle. 2014. « Biomedical Studies by TOF-SIMS Imaging ». *Biointerphases* 10 (1): 018901. https://doi.org/10.1116/1.4901511.

- Bollwein, Christine, Juliana Pereira Lopes Gonçalves, Kirsten Utpatel, Wilko Weichert, et Kristina Schwamborn. 2022. « MALDI Mass Spectrometry Imaging for the Distinction of Adenocarcinomas of the Pancreas and Biliary Tree ». *Molecules (Basel, Switzerland)* 27 (11): 3464. https://doi.org/10.3390/molecules27113464.

- Boskamp, Tobias, Delf Lachmund, Janina Oetjen, Yovany Cordero Hernandez, Dennis Trede, Peter Maass, Rita Casadonte, et al. 2017. « A New Classification Method for MALDI Imaging Mass Spectrometry Data Acquired on Formalin-Fixed Paraffin-Embedded Tissue Samples ». *Biochimica Et Biophysica Acta. Proteins and Proteomics* 1865 (7): 916-26. https://doi.org/10.1016/j.bbapap.2016.11.003.

- Brunt, Elizabeth, Shinichi Aishima, Pierre-Alain Clavien, Kathryn Fowler, Zachary Goodman, Gregory Gores, Annette Gouw, et al. 2018. « cHCC-CCA: Consensus terminology for primary liver carcinomas with both hepatocytic and cholangiocytic differentation ». *Hepatology* 68 (1): 113-26. https://doi.org/10.1002/hep.29789.

- Brunt, Elizabeth M., Valerie Paradis, Christine Sempoux, et Neil D. Theise. 2015. « Biphenotypic (Hepatobiliary) Primary Liver Carcinomas: The Work in Progress ». *Hepatic Oncology* 2 (3): 255-73. https://doi.org/10.2217/hep.15.8.

- Calderaro, Julien, Luca Di Tommaso, Pascale Maillé, Aurélie Beaufrère, Cong Trung Nguyen, Lara Heij, Viviane Gnemmi, et al. 2022a. « Nestin as a Diagnostic and Prognostic Marker for Combined Hepatocellular-Cholangiocarcinoma ». *Journal of Hepatology*,août,S0168-8278(22)02983-X. https://doi.org/10.1016/j.jhep.2022.07.019.

- Campos, Rafael O. P. de, Richard C. Semelka, Rafael M. Azevedo, Miguel Ramalho, Vasco Heredia, Diane M. Armao, et John T. Woosley. 2012. « Combined Hepatocellular Carcinoma-Cholangiocarcinoma: Report of MR Appearance in Eleven Patients ». *Journal of Magnetic Resonance Imaging: JMRI* 36 (5): 1139-47. https://doi.org/10.1002/jmri.23754.

- Caprioli, Richard M. 2016. « Imaging Mass Spectrometry: Molecular Microscopy for the New Age of Biology and Medicine ». *Proteomics* 16 (11-12): 1607-12. https://doi.org/10.1002/pmic.201600133.

- Caprioli, Richard M., Terry B. Farmer, et Jocelyn Gile. 1997. « Molecular Imaging of Biological Samples: Localization of Peptides and Proteins Using MALDI-TOF MS ». *Analytical Chemistry* 69 (23): 4751-60. https://doi.org/10.1021/ac970888i.

- Casadonte, R., R. Longuespée, J. Kriegsmann, et M. Kriegsmann. 2017. « MALDI IMS and Cancer Tissue Microarrays ». *Applications of Mass Spectrometry Imaging to Cancer* 134 (janvier): 173-200. https://doi.org/10.1016/bs.acr.2016.11.007.

- Casadonte, Rita, Mark Kriegsmann, Friederike Zweynert, Katrin Friedrich, Gustavo Bretton, Mike Otto, Sören-Oliver Deininger, et al. 2014. « Imaging mass spectrometry to discriminate breast from pancreatic cancer metastasis in formalin-fixed paraffin-embedded tissues ». *PROTEOMICS* 14 (7-8): 956-64. https://doi.org/10.1002/pmic.201300430.

- Castaing, Raimond, et Georges Slodzian. 2021. « Microanalysis Using Secondary Ion Emission ». *Journal of Mass Spectrometry: JMS* 56 (12): e4800. https://doi.org/10.1002/jms.4800.

- Cazier, Hélène ; Junot, Christophe ; Afonso, Carlos ; Fournier, Isabelle ; Brunelle, Alain ; Taran, Frédéric. 2019. « Développement d'une nouvelle approche combinant la radioimagerie et l'imagerie par spectrométrie de masse pour l'analyse de nanoparticules ». http://www.theses.fr/2019SACLS399.

- Chen, Jiu, Youdi Li, et Guoyou Yu. 2020. « Diagnostic Value of Serum Biomarkers in Combined Hepatocelluar-Cholangiocarcinoma ». *Journal of the College of Physicians andSurgeonsPakistan:JCPSP*30(3):263-67.https://doi.org/10.29271/jcpsp.2020.03.263

- Chen, Xiaoyuan, Shiquan Sun, Yiwei Lu, Xiaoli Shi, Ziyi Wang, Xuejiao Chen, Guoyong Han, Jie Zhao, Yun Gao, et Xuehao Wang. 2022. « Promising Role of Liver Transplantation in Patients with Combined Hepatocellular-Cholangiocarcinoma: A Propensity Score Matching Analysis ». *Annals of Translational Medicine* 10 (8): 434. https://doi.org/10.21037/atm-21-5391.

- Chughtai, Kamila, et Ron M. A. Heeren. 2010. « Mass Spectrometric Imaging for Biomedical Tissue Analysis ». *Chemical Reviews* 110 (5): 3237-77. https://doi.org/10.1021/cr100012c.

- Cornett, Dale S., Michelle L. Reyzer, Pierre Chaurand, et Richard M. Caprioli. 2007. « MALDI Imaging Mass Spectrometry: Molecular Snapshots of Biochemical Systems ». *Nature Methods* 4 (10): 828-33. https://doi.org/10.1038/nmeth1094.

- Coulouarn, C., C. Cavard, L. Rubbia-Brandt, A. Audebourg, F. Dumont, S. Jacques, P. A. Just, et al. 2012. « Combined hepatocellular-cholangiocarcinomas exhibit progenitor features and activation of Wnt and TGFbeta signaling pathways ». *Carcinogenesis* 33 (9): 1791-96. https://doi.org/10.1093/carcin/bgs208.

- Cucchetti, Alessandro, Fabio Piscaglia, Antonia D'Errico Grigioni, Matteo Ravaioli, Matteo Cescon, Matteo Zanello, Gian Luca Grazi, Rita Golfieri, Walter Franco Grigioni, et Antonio Daniele Pinna. 6. « Preoperative prediction of hepatocellular carcinoma tumour grade and micro-vascular invasion by means of artificial neural network: A pilot study ». *Journal of Hepatology* 52 (6): 880-88. https://doi.org/10.1016/j.jhep.2009.12.037.

- Cutolo, Carmen, Federica Dell'Aversana, Roberta Fusco, Giulia Grazzini, Giuditta Chiti, Igino Simonetti, Federico Bruno, et al. 2022. « Combined Hepatocellular-Cholangiocarcinoma: What the Multidisciplinary Team Should Know ». *Diagnostics (Basel, Switzerland)* 12 (4): 890. https://doi.org/10.3390/diagnostics12040890.

- Dageforde, Leigh Anne, Neeta Vachharajani, Parissa Tabrizian, Vatche Agopian, Karim Halazun, Erin Maynard, Kristopher Croome, et al. 2021. « Multi-Center Analysis of Liver Transplantation for Combined Hepatocellular Carcinoma-Cholangiocarcinoma Liver Tumors ». *Journal of the American College of Surgeons* 232 (4): 361-71. https://doi.org/10.1016/j.jamcollsurg.2020.11.017.

- De Hoffman, Edmond, et Vincent Stroobant. s. d. *Mass Spectrometry: Principles and Applications, 3rd Edition, Third edition*.

- De Martin, Eleonora, Michael Rayar, Nicolas Golse, Margot Dupeux, Maximiliano Gelli, Viviane Gnemmi, Marc Antoine Allard, et al. 2020. « Analysis of Liver Resection versus Liver Transplantation on Outcome of Small Intrahepatic Cholangiocarcinoma and Combined Hepatocellular-Cholangiocarcinoma in the Setting of Cirrhosis ». *Liver Transplantation: Official Publication of the American Association for the Study of Liver Diseases and the International Liver Transplantation Society*, février. https://doi.org/10.1002/lt.25737.

- De mestier du bourg, Louis. s. d. « Caractérisation clinico-pathologique et moléculaire de l'hétérogénéité des tumeurs neuroendocrines digestives : hétérogénéité intertumorale, intratumorale et chimioinduite ». These en préparation, Université Paris Cité. Consulté le 23 octobre 2022. https://www.theses.fr/s215663.

- Deininger, Sören-Oliver, Christine Bollwein, Rita Casadonte, Petra Wandernoth, Juliana Pereira Lopes Gonçalves, Katharina Kriegsmann, Mark Kriegsmann, et al. 2022. « Multicenter Evaluation of Tissue Classification by Matrix-Assisted Laser Desorption/Ionization Mass Spectrometry Imaging ». *Analytical Chemistry* 94 (23): 8194-8201. https://doi.org/10.1021/acs.analchem.2c00097.

- Deininger, Sören-Oliver, Matthias P. Ebert, Arne Fütterer, Marc Gerhard, et Christoph Röcken. 2008. « MALDI Imaging Combined with Hierarchical Clustering as a New Tool for the Interpretation of Complex Human Cancers ». *Journal of Proteome Research* 7 (12): 5230-36. https://doi.org/10.1021/pr8005777.

- Delcourt, Vivian, Julien Franck, Jusal Quanico, Jean-Pascal Gimeno, Maxence Wisztorski, Antonella Raffo-Romero, Firas Kobeissy, Xavier Roucou, Michel Salzet, et Isabelle Fournier. 2018. « Spatially-Resolved Top-down Proteomics Bridged to MALDI MS Imaging Reveals the Molecular Physiome of Brain Regions ». *Molecular & Cellular Proteomics: MCP* 17 (2): 357-72. https://doi.org/10.1074/mcp.M116.065755.

- Delvolve, Alice M., et Amina S. Woods. 2011. « Optimization of Automated Matrix Deposition for Biomolecular Mapping Using a Spotter ». *Journal of Mass Spectrometry: JMS* 46 (10): 1046-50. https://doi.org/10.1002/jms.1986.

- « EASL Clinical Practice Guidelines: Management of hepatocellular carcinoma ». 2018. *Journal of Hepatology* 69 (1): 182-236. https://doi.org/10.1016/j.jhep.2018.03.019.

- Edeline, Julien, Yann Touchefeu, Boris Guiu, Olivier Farge, David Tougeron, Isabelle Baumgaertner, Ahmet Ayav, et al. 2019. « Radioembolization Plus Chemotherapy for First-Line Treatment of Locally Advanced Intrahepatic Cholangiocarcinoma: A Phase 2 Clinical Trial ». *JAMA Oncology*, octobre. https://doi.org/10.1001/jamaoncol.2019.3702.

- Edmondson, H. A., et P. E. Steiner. 1954. « Primary Carcinoma of the Liver: A Study of 100 Cases among 48,900 Necropsies ». *Cancer* 7 (3): 462-503. https://doi.org/10.1002/1097-0142(195405)7:3<462::aid-cncr2820070308>3.0.co;2-e.

- Fenaille, François, Pierre Barbier Saint-Hilaire, Kathleen Rousseau, et Christophe Junot. 2017. « Data Acquisition Workflows in Liquid Chromatography Coupled to High Resolution Mass Spectrometry-Based Metabolomics: Where Do We Stand? » *Journal of Chromatography. A* 1526 (décembre): 1-12. https://doi.org/10.1016/j.chroma.2017.10.043.

- Fernández, Roberto, Jone Garate, Lucia Martín-Saiz, Igor Galetich, et José A. Fernández. 2019. « Matrix Sublimation Device for MALDI Mass Spectrometry Imaging ». *Analytical Chemistry* 91 (1): 803-7. https://doi.org/10.1021/acs.analchem.8b04765.

- Fonville, Judith M., Claire Carter, Olivier Cloarec, Jeremy K. Nicholson, John C. Lindon, Josephine Bunch, et Elaine Holmes. 2012. « Robust Data Processing and Normalization Strategy for MALDI Mass Spectrometric Imaging ». *Analytical Chemistry* 84 (3): 1310-19. https://doi.org/10.1021/ac201767g.

- Fowler, Kathryn J., Arman Sheybani, Rex A. Parker, Sean Doherty, Elizabeth M. Brunt, William C. Chapman, et Christine O. Menias. 2013. « Combined Hepatocellular and Cholangiocarcinoma (Biphenotypic) Tumors: Imaging Features and Diagnostic Accuracy of Contrast-Enhanced CT and MRI ». *American Journal of Roentgenology* 201 (2): 332-39. https://doi.org/10.2214/AJR.12.9488.

- Fujii, H., X. G. Zhu, T. Matsumoto, M. Inagaki, Y. Tokusashi, N. Miyokawa, T. Fukusato, et al. 2000. « Genetic classification of combined hepatocellular-cholangiocarcinoma ». *Hum Pathol* 31 (9): 1011-17. https://doi.org/10.1053/hupa.2000.9782.

- Fujimoto, A., M. Furuta, Y. Shiraishi, K. Gotoh, Y. Kawakami, K. Arihiro, T. Nakamura, et al. 2015. « Whole-genome mutational landscape of liver cancers displaying biliary phenotype reveals hepatitis impact and molecular diversity ». *Nat Commun* 6: 6120. https://doi.org/10.1038/ncomms7120.

- Fujimura, Yoshinori, et Daisuke Miura. 2014. « MALDI Mass Spectrometry Imaging for Visualizing In Situ Metabolism of Endogenous Metabolites and Dietary Phytochemicals ». *Metabolites* 4 (2): 319-46. https://doi.org/10.3390/metabo4020319.

- Gaowa, Siqin, Manabu Futamura, Masayuki Tsuneki, Hiroki Kamino, Jesse Y. Tajima, Ryutaro Mori, Hirofumi Arakawa, et Kazuhiro Yoshida. 2018. « Possible role of p53/Mieap-regulated mitochondrial quality control as a tumor suppressor in human

breast cancer ». *Cancer Science* 109 (12): 3910-20. https://doi.org/10.1111/cas.13824.

- Garancini, Mattia, Paolo Goffredo, Fabio Pagni, Fabrizio Romano, Sanziana Roman, Julie Ann Sosa, et Vittorio Giardini. 2014. « Combined Hepatocellular-Cholangiocarcinoma: A Population-Level Analysis of an Uncommon Primary Liver Tumor ». *Liver Transplantation: Official Publication of the American Association for the Study of Liver Diseases and the International Liver Transplantation Society* 20 (8): 952-59. https://doi.org/10.1002/lt.23897.

- Garza, Kyana Y., Clara L. Feider, Dustin R. Klein, Jake A. Rosenberg, Jennifer S. Brodbelt, et Livia S. Eberlin. 2018. « Desorption Electrospray Ionization Mass Spectrometry Imaging of Proteins Directly from Biological Tissue Sections ». *Analytical Chemistry* 90 (13): 7785-89. https://doi.org/10.1021/acs.analchem.8b00967.
- Gentile, Damiano, Matteo Donadon, Ana Lleo, Alessio Aghemo, Massimo Roncalli, Luca di Tommaso, et Guido Torzilli. 2020. « Surgical Treatment of Hepatocholangiocarcinoma: A Systematic Review ». *Liver Cancer* 9 (1): 15-27. https://doi.org/10.1159/000503719.

- Gerlinger, Marco, Andrew J. Rowan, Stuart Horswell, M. Math, James Larkin, David Endesfelder, Eva Gronroos, et al. 2012. « Intratumor Heterogeneity and Branched Evolution Revealed by Multiregion Sequencing ». *The New England Journal of Medicine* 366 (10): 883-92. https://doi.org/10.1056/NEJMoa1113205.

- Gigante, Elia, Valérie Paradis, Maxime Ronot, François Cauchy, Olivier Soubrane, Nathalie Ganne-Carrié, et Jean-Charles Nault. 2021. « New Insights into the Pathophysiology and Clinical Care of Rare Primary Liver Cancers ». *JHEP Reports: Innovation in Hepatology* 3 (1): 100174. https://doi.org/10.1016/j.jhepr.2020.100174.

- Gigante, Elia, Maxime Ronot, Caroline Bertin, Maria Ciolina, Mohamed Bouattour, Federica Dondero, François Cauchy, Olivier Soubrane, Valérie Vilgrain, et Valérie Paradis. 2019. « Combining Imaging and Tumour Biopsy Improves the Diagnosis of Combined Hepatocellular-Cholangiocarcinoma ». *Liver International: Official Journal of the International Association for the Study of the Liver* 39 (12): 2386-96. https://doi.org/10.1111/liv.14261.

- Gleiberman, Anatoli S., Juan M. Encinas, John L. Mignone, Tatyana Michurina, Michael G. Rosenfeld, et Grigori Enikolopov. 2005. « Expression of nestin–green fluorescent protein transgene marks oval cells in the adult liver ». *Developmental Dynamics* 234 (2): 413-21. https://doi.org/10.1002/dvdy.20536.

- Gonçalves, Juliana P., Christine Bollwein, Anna M. Schlitter, Mark Kriegsmann, Anne Jacob, Wilko Weichert, et Kristina Schwamborn. 2022. « MALDI-MSI: A Powerful Approach to Understand Primary Pancreatic Ductal Adenocarcinoma and Metastases ». *Molecules* 27 (15). https://doi.org/10.3390/molecules27154811.

- Gonçalves, Juliana P. L., Christine Bollwein, et Kristina Schwamborn. 2022. « Mass Spectrometry Imaging Spatial Tissue Analysis toward Personalized Medicine ». *Life (Basel, Switzerland)* 12 (7): 1037. https://doi.org/10.3390/life12071037.

- Gonçalves, Juliana Pereira Lopes, Christine Bollwein, Anna Melissa Schlitter, Benedikt Martin, Bruno Märkl, Kirsten Utpatel, Wilko Weichert, et Kristina Schwamborn. 2021. « The Impact of Histological Annotations for Accurate Tissue Classification Using Mass Spectrometry Imaging ». *Metabolites* 11 (11): 752. https://doi.org/10.3390/metabo11110752.

- Goodman, Z. D., K. G. Ishak, J. M. Langloss, I. A. Sesterhenn, et L. Rabin. 1985. « Combined Hepatocellular-Cholangiocarcinoma. A Histologic and Immunohistochemical Study ». *Cancer* 55 (1): 124-35. https://doi.org/10.1002/1097-0142(19850101)55:1<124::aid-cncr2820550120>3.0.co;2-z.

- Groseclose, M. R., P. P. Massion, P. Chaurand, et R. M. Caprioli. 2008. « High-throughput proteomic analysis of formalin-fixed paraffin-embedded tissue microarrays using MALDI imaging mass spectrometry ». *Proteomics* 8 (18): 3715-24. https://doi.org/10.1002/pmic.200800495.

- Hamada, Koichiro, Tomomi Kurashige, Mika Shimamura, Hirofumi Arakawa, Yasuyuki Nakamura, et Yuji Nagayama. 2022. « MIEAP and ATG5 Are Tumor Suppressors in a Mouse Model of BRAFV600E-Positive Thyroid Cancer ». *Frontiers in Endocrinology* 13: 932754. https://doi.org/10.3389/fendo.2022.932754.

- Hoffmann, Edmond de. 2005. « Mass Spectrometry ». In *Kirk-Othmer Encyclopedia of ChemicalTechnology*.https://doi.org/10.1002/0471238961.1301191913151518.a01.pub2.

- Holzner, Matthew L., Parissa Tabrizian, Fatemeh P. Parvin-Nejad, Kezhen Fei, Ganesh Gunasekaran, Chiara Rocha, Marcelo E. Facciuto, Sander Florman, et Myron E. Schwartz. 2020. « Resection of Mixed Hepatocellular-Cholangiocarcinoma, Hepatocellular Carcinoma, and Intrahepatic Cholangiocarcinoma: A Western Center Experience ». *Liver Transplantation: Official Publication of the American Association for the Study of Liver Diseases and the International Liver Transplantation Society*, avril. https://doi.org/10.1002/lt.25786.

- Hu, Zheng, Zan Li, Zhicheng Ma, et Christina Curtis. 2020. « Multi-Cancer Analysis of Clonality and the Timing of Systemic Spread in Paired Primary Tumors and Metastases ». *Nature Genetics* 52 (7): 701-8. https://doi.org/10.1038/s41588-020-0628-z.

- Hunter, Mandana, Nicholas J. Demarais, Richard L. M. Faull, Angus C. Grey, et Maurice A. Curtis. 2018. « Layer-Specific Lipid Signatures in the Human Subventricular Zone Demonstrated by Imaging Mass Spectrometry ». *Scientific Reports* 8 (1): 2551. https://doi.org/10.1038/s41598-018-20793-4.

- Hwang, Jiyoung, Young Kon Kim, Min Jung Park, Mi Hee Lee, Seong Hyun Kim, Won Jae Lee, et Hyun Chul Rhim. 2012. « Differentiating combined hepatocellular and cholangiocarcinoma from mass-forming intrahepatic cholangiocarcinoma using gadoxetic acid-enhanced MRI ». *Journal of Magnetic Resonance Imaging* 36 (4): 881-89. https://doi.org/10.1002/jmri.23728.

- Ikeda, Hiroko, Kenichi Harada, Yasunori Sato, Motoko Sasaki, Norihide Yoneda, Seiko Kitamura, Yoshiko Sudo, Akishi Ooi, et Yasuni Nakanuma. 2013. « Clinicopathologic Significance of Combined Hepatocellular-Cholangiocarcinoma With Stem Cell Subtype Components With Reference to the Expression of Putative Stem Cell Markers ». *American Journal of Clinical Pathology* 140 (3): 329-40. https://doi.org/10.1309/ajcp66avbanvntqj.

- Janßen, Charlotte, Tobias Boskamp, Lena Hauberg-Lotte, Jens Behrmann, Sören-Oliver Deininger, Mark Kriegsmann, Katharina Kriegsmann, et al. 2022. « Robust Subtyping of Non-Small Cell Lung Cancer Whole Sections through MALDI Mass Spectrometry Imaging ». *Proteomics. Clinical Applications* 16 (4): e2100068. https://doi.org/10.1002/prca.202100068.

- Jarnagin, William R., Sharon Weber, Satish K. Tickoo, Jonathan B. Koea, Sam Obiekwe, Yuman Fong, Ronald P. DeMatteo, Leslie H. Blumgart, et David Klimstra. 2002. « Combined Hepatocellular and Cholangiocarcinoma: Demographic, Clinical, and Prognostic Factors ». *Cancer* 94 (7): 2040-46. https://doi.org/10.1002/cncr.10392.

- Jeon, Sun Kyung, Ijin Joo, Dong Ho Lee, Sang Min Lee, Hyo-Jin Kang, Kyoung-Bun Lee, et Jeong Min Lee. 2019. « Combined hepatocellular cholangiocarcinoma: LI-RADS v2017 categorisation for differential diagnosis and prognostication on gadoxetic acid-enhanced MR imaging ». *European Radiology* 29 (1): 373-82. https://doi.org/10.1007/s00330-018-5605-x.

- Johnson, Philip, Qing Zhou, Doan Y. Dao, et Y. M. Dennis Lo. 2022. « Circulating Biomarkers in the Diagnosis and Management of Hepatocellular Carcinoma ». *Nature Reviews. Gastroenterology & Hepatology* 19 (10): 670-81. https://doi.org/10.1038/s41575-022-00620-y.

- Jolliffe, Ian T., et Jorge Cadima. 2016. « Principal Component Analysis: A Review and Recent Developments ». *Philosophical Transactions. Series A, Mathematical, Physical, and Engineering Sciences* 374 (2065): 20150202. https://doi.org/10.1098/rsta.2015.0202.

- Jones, Emrys A., Sören-Oliver Deininger, Pancras C. W. Hogendoorn, André M. Deelder, et Liam A. McDonnell. 2012. « Imaging Mass Spectrometry Statistical Analysis ». *Journal of Proteomics* 75 (16): 4962-89. https://doi.org/10.1016/j.jprot.2012.06.014.

- Joseph, Nancy M., Christos G. Tsokos, Sarah E. Umetsu, A. Hunter Shain, Robin K. Kelley, Courtney Onodera, Sarah Bowman, et al. 2019. « Genomic Profiling of Combined Hepatocellular-Cholangiocarcinoma Reveals Similar Genetics to Hepatocellular Carcinoma ». *The Journal of Pathology* 248 (2): 164-78. https://doi.org/10.1002/path.5243.

- Karas, M., D. Bachmann, U. Bahr, et F. Hillenkamp. 1987. « Matrix-assisted ultraviolet laser desorption of non-volatile compounds ». *International Journal of Mass Spectrometry and Ion Processes* 78 (septembre): 53-68. https://doi.org/10.1016/0168-1176(87)87041-6.

- Katz, Sarah-Fee, André Lechel, Anna C. Obenauf, Yvonne Begus-Nahrmann, Johann M. Kraus, Eva M. Hoffmann, Johanna Duda, et al. 2012. « Disruption of Trp53 in Livers of Mice Induces Formation of Carcinomas with Bilineal Differentiation ». *Gastroenterology* 142 (5): 1229-1239.e3. https://doi.org/10.1053/j.gastro.2012.02.009.

- Kim, Eo Jin, Changhoon Yoo, Hyo Jeong Kang, Kyu-Pyo Kim, Min-Hee Ryu, Sook Ryun Park, Danbi Lee, et al. 2021. « Clinical Outcomes of Systemic Therapy in Patients with Unresectable or Metastatic Combined Hepatocellular-Cholangiocarcinoma ». *Liver International: Official Journal of the International Association for the Study of the Liver* 41 (6): 1398-1408. https://doi.org/10.1111/liv.14813.

- Kim, Jin Hyoung, Hyun-Ki Yoon, Gi-Young Ko, Dong Il Gwon, Cheol Soo Jang, Ho-Young Song, Ji Hoon Shin, et Kyu-Bo Sung. 2010. « Nonresectable Combined Hepatocellular Carcinoma and Cholangiocarcinoma: Analysis of the Response and Prognostic Factors after Transcatheter Arterial Chemoembolization ». *Radiology* 255 (1): 270-77. https://doi.org/10.1148/radiol.09091076.

- Kirchberger-Tolstik, Tatiana, Oleg Ryabchykov, Thomas Bocklitz, Olaf Dirsch, Utz Settmacher, Juergen Popp, et Andreas Stallmach. 2021. « Nondestructive molecular imaging by Raman spectroscopy vs. marker detection by MALDI IMS for an early diagnosis of HCC ». *Analyst* 146 (4): 1239-52. https://doi.org/10.1039/D0AN01555E.

- Kleinfeld, Alan M., J. Patrick Kampf, et Claude Lechene. 2004. « Transport of 13C-Oleate in Adipocytes Measured Using Multi Imaging Mass Spectrometry ». *Journal of the American Society for Mass Spectrometry* 15 (11): 1572-80. https://doi.org/10.1016/j.jasms.2004.07.010.

- Kobayashi, Satoshi, Takeshi Terashima, Satoshi Shiba, Yukio Yoshida, Ikuhiro Yamada, Shouta Iwadou, Shigeru Horiguchi, et al. 2018. « Multicenter Retrospective Analysis of Systemic Chemotherapy for Unresectable Combined Hepatocellular and Cholangiocarcinoma ». *Cancer Science* 109 (8): 2549-57. https://doi.org/10.1111/cas.13656.

- Koster, Harry, et Louis P. Kasman. 1932. « Primary Duplex Liver Carcinoma ». *The American Journal of Surgery* 17 (2): 237-41. https://doi.org/10.1016/S0002-9610(32)90487-5.

- Kriegsmann, Mark, Rita Casadonte, Jörg Kriegsmann, Hendrik Dienemann, Peter Schirmacher, Jan Hendrik Kobarg, Kristina Schwamborn, Albrecht Stenzinger, Arne Warth, et Wilko Weichert. 2016. « Reliable Entity Subtyping in Non-small Cell Lung Cancer by Matrix-assisted Laser Desorption/Ionization Imaging Mass Spectrometry on Formalin-fixed Paraffin-embedded Tissue Specimens * ». *Molecular & Cellular Proteomics* 15 (10): 3081-89. https://doi.org/10.1074/mcp.M115.057513.

- Kriegsmann, Mark, Christiane Zgorzelski, Rita Casadonte, Kristina Schwamborn, Thomas Muley, Hauke Winter, Martin Eichhorn, et al. 2020. « Mass Spectrometry Imaging for Reliable and Fast Classification of Non-Small Cell Lung Cancer Subtypes ». *Cancers* 12 (9). https://doi.org/10.3390/cancers12092704.

- Kubo, Shoji, Hiroji Shinkawa, Yoshinari Asaoka, Tatsuya Ioka, Hiroshi Igaki, Namiki Izumi, Takao Itoi, et al. 2022. « Liver Cancer Study Group of Japan Clinical Practice Guidelines for Intrahepatic Cholangiocarcinoma ». *Liver Cancer* 11 (4): 290-314. https://doi.org/10.1159/000522403.

- Kubota, Yoshiko, Kazumi Nomura, Yasutake Katoh, Rina Yamashita, Kiriko Kaneko, et Kazumichi Furuyama. 2016. « Novel Mechanisms for Heme-Dependent Degradation of ALAS1 Protein as a Component of Negative Feedback Regulation of Heme Biosynthesis ». *The Journal of Biological Chemistry* 291 (39): 20516-29. https://doi.org/10.1074/jbc.M116.719161.

- Kudo, Masatoshi, Namiki Izumi, Shoji Kubo, Norihiro Kokudo, Michiie Sakamoto, Shuichiro Shiina, Ryosuke Tateishi, et al. 2020. « Report of the 20th Nationwide Follow-up Survey of Primary Liver Cancer in Japan ». *Hepatology Research: The Official Journal of the Japan Society of Hepatology* 50 (1): 15-46. https://doi.org/10.1111/hepr.13438.

- Laouirem, Samira, Julie Le Faouder, Theodore Alexandrov, Denis Mestivier, Thibaut Léger, Xavier Baudin, Mouniya Mebarki, Valérie Paradis, Jean-Michel Camadro, et Pierre Bedossa. 2014. « Progression from Cirrhosis to Cancer Is Associated with Early Ubiquitin Post-Translational Modifications: Identification of New Biomarkers of Cirrhosis at Risk of Malignancy ». *The Journal of Pathology* 234 (4): 452-63. https://doi.org/10.1002/path.4398.

- Lazova, Rossitza, Erin H. Seeley, Heinz Kutzner, Richard A. Scolyer, Glynis Scott, Lorenzo Cerroni, Isabella Fried, et al. 2016. « Imaging mass spectrometry assists in the classification of diagnostically challenging atypical Spitzoid neoplasms ». *Journal of the American Academy of Dermatology* 75 (6): 1176-1186.e4. https://doi.org/10.1016/j.jaad.2016.07.007.

- Le Faouder, Julie, Elia Gigante, Thibaut Léger, Miguel Albuquerque, Aurélie Beaufrère, Olivier Soubrane, Safi Dokmak, Jean-Michel Camadro, Jérôme Cros, et Valérie Paradis. 2019. « Proteomic Landscape of Cholangiocarcinomas Reveals Three Different Subgroups According to Their Localization and the Aspect of Non-Tumor Liver ». *Proteomics. Clinical Applications* 13 (1): e1800128. https://doi.org/10.1002/prca.201800128.

- Le Faouder, Julie, Samira Laouirem, Theodore Alexandrov, Soundes Ben-Harzallah, Thibaut Léger, Miguel Albuquerque, Pierre Bedossa, et Valérie Paradis. 2014. « Tumoral Heterogeneity of Hepatic Cholangiocarcinomas Revealed by MALDI Imaging Mass Spectrometry ». *Proteomics* 14 (7-8): 965-72. https://doi.org/10.1002/pmic.201300463.

- Lee, Won-Suk, Kwang-Woong Lee, Jin-Seok Heo, Sung-Ju Kim, Seong-Ho Choi, Yong-Il Kim, et Jae-Won Joh. 2006. « Comparison of Combined Hepatocellular and Cholangiocarcinoma with Hepatocellular Carcinoma and Intrahepatic Cholangiocarcinoma ». *Surgery Today* 36 (10): 892-97. https://doi.org/10.1007/s00595-006-3276-8.

- Li, Chao-Qun, Xin Zheng, Huan-Ling Guo, Mei-Qing Cheng, Yang Huang, Xiao-Yan Xie, Ming-de Lu, Ming Kuang, Wei Wang, et Li-da Chen. 2022. « Differentiation between Combined Hepatocellular Carcinoma and Hepatocellular Carcinoma: Comparison of Diagnostic Performance between Ultrasomics-Based Model and CEUS LI-RADS V2017 ». *BMC Medical Imaging* 22 (1): 36. https://doi.org/10.1186/s12880-022-00765-x.

- Li, Rui, Dan Yang, Chun-Lin Tang, Ping Cai, Kuan-Sheng Ma, Shi-Yi Ding, Xiao-Hang Zhang, De-Yu Guo, et Xiao-Chu Yan. 2016. « Combined Hepatocellular Carcinoma and Cholangiocarcinoma (Biphenotypic) Tumors: Clinical Characteristics, Imaging Features of Contrast-Enhanced Ultrasound and Computed Tomography ». *BMC Cancer* 16 (février): 158. https://doi.org/10.1186/s12885-016-2156-x.

- Liu, Chi-Leung, Sheung-Tat Fan, Chung-Mau Lo, Irene Oi-Lin Ng, Chi-Ming Lam, Ronnie Tung-Ping Poon, et John Wong. 2003. « Hepatic Resection for Combined Hepatocellular and Cholangiocarcinoma ». *Archives of Surgery (Chicago, Ill.: 1960)* 138 (1): 86-90.

- Liu, Xin, Jessica K. Lukowski, Colin Flinders, Seungil Kim, Rebecca A. Georgiadis, Shannon M. Mumenthaler, et Amanda B. Hummon. 2018. « MALDI-MSI of Immunotherapy: Mapping the EGFR-Targeting Antibody Cetuximab in 3D Colon-Cancer Cell Cultures ». *Analytical Chemistry* 90 (24): 14156-64. https://doi.org/10.1021/acs.analchem.8b02151.

- Liu, Xinai, Xiaoyan Ni, Yubo Li, Chun Yang, Yi Wang, Chunzheng Ma, Changwu Zhou, et Xin Lu. 2022. « Diagnostic Performance of LI-RADS Version 2018 for Primary Liver Cancer in Patients With Liver Cirrhosis on Enhanced MRI ». *Frontiers in Oncology* 12: 934045. https://doi.org/10.3389/fonc.2022.934045.

- Liu, Zhen-Hao, Bao-Feng Lian, Qiong-Zhu Dong, Han Sun, Jin-Wang Wei, Yuan-Yuan Sheng, Wei Li, et al. 2018. « Whole-Exome Mutational and Transcriptional Landscapes of Combined Hepatocellular Cholangiocarcinoma and Intrahepatic Cholangiocarcinoma Reveal Molecular Diversity ». *Biochimica Et Biophysica Acta. Molecular Basis of Disease* 1864 (6 Pt B): 2360-68. https://doi.org/10.1016/j.bbadis.2018.01.027.

- Llovet, Josep M., Sergio Ricci, Vincenzo Mazzaferro, Philip Hilgard, Edward Gane, Jean-Frédéric Blanc, Andre Cosme de Oliveira, et al. 2008. « Sorafenib in Advanced Hepatocellular Carcinoma ». *The New England Journal of Medicine* 359 (4): 378-90. https://doi.org/10.1056/NEJMoa0708857.

- Loch, Florian N., Oliver Klein, Katharina Beyer, Frederick Klauschen, Christian Schineis, Johannes C. Lauscher, Georgios A. Margonis, Claudius E. Degro, Wael Rayya, et Carsten Kamphues. 2021. « Peptide Signatures for Prognostic Markers of Pancreatic Cancer by MALDI Mass Spectrometry Imaging ». *Biology* 10 (10): 1033. https://doi.org/10.3390/biology10101033.

- Lunsford, Keri E., Colin Court, Yong Seok Lee, David S. Lu, Bita V. Naini, Michael P. Harlander-Locke, Ronald W. Busuttil, et Vatche G. Agopian. 2018. « Propensity-Matched Analysis of Patients with Mixed Hepatocellular-Cholangiocarcinoma and Hepatocellular Carcinoma Undergoing Liver Transplantation ». *Liver Transplantation: Official Publication of the American Association for the Study of Liver Diseases and the International Liver Transplantation Society* 24 (10): 1384-97. https://doi.org/10.1002/lt.25058.

- Ly, Alice, Rémi Longuespée, Rita Casadonte, Petra Wandernoth, Kristina Schwamborn, Christine Bollwein, Christian Marsching, et al. 2019. « Site-to-Site Reproducibility and Spatial Resolution in MALDI–MSI of Peptides from Formalin-Fixed Paraffin-Embedded Samples ». *PROTEOMICS – Clinical Applications* 13 (1): 1800029. https://doi.org/10.1002/prca.201800029.

- Ma, Ka Wing, et Kenneth Siu Ho Chok. 2017. « Importance of Surgical Margin in the Outcomes of Hepatocholangiocarcinoma ». *World Journal of Hepatology* 9 (13): 635-41. https://doi.org/10.4254/wjh.v9.i13.635.

- Malone, Christopher D., Wendell Gibby, Richard Tsai, Seung Kwon Kim, Samantha Lancia, Olaguoke Akinwande, et Raja S. Ramaswamy. 2020. « Outcomes of Yttrium-90 Radioembolization for Unresectable Combined Biphenotypic Hepatocellular-Cholangiocarcinoma ». *Journal of Vascular and Interventional Radiology: JVIR*, février. https://doi.org/10.1016/j.jvir.2019.09.028.

- Malvi, Deborah, Dario de Biase, Silvia Fittipaldi, Marco Grillini, Michela Visani, Annalisa Pession, Antonia D'Errico, et Francesco Vasuri. 2020. « Immunomorphology and molecular biology of mixed primary liver cancers: is Nestin a marker of intermediate-cell carcinoma? » *Histopathology* 76 (2): 265-74. https://doi.org/10.1111/his.13966.

- Marrero, Jorge A., Laura M. Kulik, Claude B. Sirlin, Andrew X. Zhu, Richard S. Finn, Michael M. Abecassis, Lewis R. Roberts, et Julie K. Heimbach. 2018. « Diagnosis, Staging, and Management of Hepatocellular Carcinoma: 2018 Practice Guidance by the American Association for the Study of Liver Diseases ». *Hepatology* 68 (2): 723-50. https://doi.org/10.1002/hep.29913.

- Marusyk, Andriy, Vanessa Almendro, et Kornelia Polyak. 2012. « Intra-Tumour Heterogeneity: A Looking Glass for Cancer? » *Nature Reviews. Cancer* 12 (5): 323-34. https://doi.org/10.1038/nrc3261.

- Meier, Michael A. R., Berend-Jan de Gans, Antje M. J. van den Berg, et Ulrich S. Schubert. 2003. « Automated Multiple-Layer Spotting for Matrix-Assisted Laser Desorption/Ionization Time-of-Flight Mass Spectrometry of Synthetic Polymers Utilizing Ink-Jet Printing Technology ». *Rapid Communications in Mass Spectrometry: RCM* 17 (20): 2349-53. https://doi.org/10.1002/rcm.1195.

- Mitchell, Donald G., Jordi Bruix, Morris Sherman, et Claude B. Sirlin. 2015. « LI-RADS (Liver Imaging Reporting and Data System): Summary, Discussion, and Consensus of the LI-RADS Management Working Group and Future Directions ». *Hepatology (Baltimore, Md.)* 61 (3): 1056-65. https://doi.org/10.1002/hep.27304.

- Mittal, Paul, Mark R. Condina, Manuela Klingler-Hoffmann, Gurjeet Kaur, Martin K. Oehler, Oliver M. Sieber, Michelle Palmieri, et al. 2021. « Cancer Tissue Classification Using Supervised Machine Learning Applied to MALDI Mass Spectrometry Imaging ». *Cancers* 13 (21): 5388. https://doi.org/10.3390/cancers13215388.

- Moeini, Agrin, Daniela Sia, Zhongyang Zhang, Genis Camprecios, Ashley Stueck, Hui Dong, Robert Montal, et al. 2017. « Mixed hepatocellular cholangiocarcinoma tumors: Cholangiolocellular carcinoma is a distinct molecular entity ». *Journal of Hepatology* 66 (5): 952-61. https://doi.org/10.1016/j.jhep.2017.01.010.

- Mulder, Inge A., Clara Esteve, Marieke J. H. Wermer, Mathias Hoehn, Else A. Tolner, Arn M. J. M. van den Maagdenberg, et Liam A. McDonnell. 2016. « Funnel-Freezing versus Heat-Stabilization for the Visualization of Metabolites by Mass Spectrometry Imaging in a Mouse Stroke Model ». *Proteomics* 16 (11-12): 1652-59. https://doi.org/10.1002/pmic.201500402.

- Murtagh, Fionn, et Pedro Contreras. 2012. « Algorithms for hierarchical clustering: an overview ». *WIREs Data Mining and Knowledge Discovery* 2 (1): 86-97. https://doi.org/10.1002/widm.53.

- Murugesan, Karthikeyan, Radwa Sharaf, Meagan Montesion, Jay A. Moore, James Pao, Dean C. Pavlick, Garrett M. Frampton, et al. 2021. « Genomic Profiling of Combined Hepatocellular Cholangiocarcinoma Reveals Genomics Similar to Either Hepatocellular Carcinoma or Cholangiocarcinoma ». *JCO Precision Oncology* 5 (août): PO.20.00397. https://doi.org/10.1200/PO.20.00397.

- Na, Seong Kyun, Gwang Hyeon Choi, Han Chu Lee, Yong Moon Shin, Jihyun An, Danbi Lee, Ju Hyun Shim, et al. 2018. « The Effectiveness of Transarterial Chemoembolization in Recurrent Hepatocellular-Cholangiocarcinoma after Resection ». *PloS One* 13 (6): e0198138. https://doi.org/10.1371/journal.pone.0198138.

- Nagtegaal, Iris D., Robert D. Odze, David Klimstra, Valerie Paradis, Massimo Rugge, Peter Schirmacher, Mary K. Washington, Fatima Carneiro, et Ian A. Cree. 2019. « The 2019 WHO classification of tumours of the digestive system ». *Histopathology* 0 (ja). https://doi.org/10.1111/his.13975.

- Ng, I. O., T. W. Shek, J. Nicholls, et L. T. Ma. 1998. « Combined Hepatocellular-Cholangiocarcinoma: A Clinicopathological Study ». *Journal of Gastroenterology and Hepatology* 13 (1): 34-40. https://doi.org/10.1111/j.1440-1746.1998.tb00542.x.

- Nguyen, Cong Trung, Stefano Caruso, Pascale Maille, Aurélie Beaufrère, Jérémy Augustin, Loetitia Favre, Anaïs Pujals, et al. 2022. « Immune Profiling of Combined Hepatocellular- Cholangiocarcinoma Reveals Distinct Subtypes and Activation of Gene

Signatures Predictive of Response to Immunotherapy ». *Clinical Cancer Research: An Official Journal of the American Association for Cancer Research* 28 (3): 540-51. https://doi.org/10.1158/1078-0432.CCR-21-1219.

- Nimptsch, Ariane, Stephanie Schibur, Matthias Schnabelrauch, Beate Fuchs, Daniel Huster, et Jürgen Schiller. 2009. « Characterization of the Quantitative Relationship between Signal-to-Noise (S/N) Ratio and Sample Amount on-Target by MALDI-TOF MS: Determination of Chondroitin Sulfate Subsequent to Enzymatic Digestion ». *Analytica Chimica Acta* 635 (2): 175-82. https://doi.org/10.1016/j.aca.2009.01.025.

- Nishie, Akihiro, Kengo Yoshimitsu, Yoshiki Asayama, Hiroyuki Irie, Hitoshi Aibe, Tsuyoshi Tajima, Kenji Shinozaki, et al. 2005. « Detection of Combined Hepatocellular and Cholangiocarcinomas on Enhanced CT: Comparison with Histologic Findings ». *American Journal of Roentgenology* 184 (4): 1157-62. https://doi.org/10.2214/ajr.184.4.01841157.

- Nowell, P. C. 1986. « Mechanisms of Tumor Progression ». *Cancer Research* 46 (5): 2203-7.

- Oetjen, Janina, Delf Lachmund, Andrew Palmer, Theodore Alexandrov, Michael Becker, Tobias Boskamp, et Peter Maass. 2016. « An Approach to Optimize Sample Preparation for MALDI Imaging MS of FFPE Sections Using Fractional Factorial Design of Experiments ». *Analytical and Bioanalytical Chemistry* 408 (24): 6729-40. https://doi.org/10.1007/s00216-016-9793-4.

- Paradis, Valérie, et Jessica Zucman-Rossi. 2022. « Pathogenesis of Primary Liver Carcinomas ». *Journal of Hepatology*, septembre, S0168-8278(22)00361-0. https://doi.org/10.1016/j.jhep.2022.05.037.

- Peng, Yuting, Peng Lin, Linyong Wu, Da Wan, Yujia Zhao, Li Liang, Xiaoyu Ma, et al. 2020. « Ultrasound-Based Radiomics Analysis for Preoperatively Predicting Different Histopathological Subtypes of Primary Liver Cancer ». *Frontiers in Oncology* 10: 1646. https://doi.org/10.3389/fonc.2020.01646.

- Phillips, Leo, Anthony J. Gill, et Robert C. Baxter. 2019. « Novel Prognostic Markers in Triple-Negative Breast Cancer Discovered by MALDI-Mass Spectrometry Imaging ». *Frontiers in Oncology* 9: 379. https://doi.org/10.3389/fonc.2019.00379.

- Porcari, Andreia M., Jialing Zhang, Kyana Y. Garza, Raquel M. Rodrigues-Peres, John Q. Lin, Jonathan H. Young, Robert Tibshirani, et al. 2018. « Multicenter Study Using Desorption-Electrospray-Ionization-Mass-Spectrometry Imaging for Breast-Cancer Diagnosis ». *Analytical Chemistry* 90 (19): 11324-32. https://doi.org/10.1021/acs.analchem.8b01961.

- Porta Siegel, Tiffany, Gregory Hamm, Josephine Bunch, Jo Cappell, John S. Fletcher, et Kristina Schwamborn. 2018. « Mass Spectrometry Imaging and Integration with Other Imaging Modalities for Greater Molecular Understanding of Biological Tissues ». *Molecular Imaging and Biology* 20 (6): 888-901. https://doi.org/10.1007/s11307-018-1267-y.

- Poté, Nicolas, Theodore Alexandrov, Julie Le Faouder, Samira Laouirem, Thibaut Léger, Mouniya Mebarki, Jacques Belghiti, Jean-Michel Camadro, Pierre Bedossa, et Valérie Paradis. 2013. « Imaging Mass Spectrometry Reveals Modified Forms of Histone H4 as New Biomarkers of Microvascular Invasion in Hepatocellular Carcinomas ». *Hepatology (Baltimore, Md.)* 58 (3): 983-94. https://doi.org/10.1002/hep.26433.

- Poté, Nicolas, François Cauchy, Miguel Albuquerque, Jérôme Cros, Olivier Soubrane, Pierre Bedossa, et Valérie Paradis. 2018. « Contribution of Virtual Biopsy to the Screening of Microvascular Invasion in Hepatocellular Carcinoma: A Pilot Study ». *Liver International: Official Journal of the International Association for the Study of the Liver* 38 (4): 687-94. https://doi.org/10.1111/liv.13585.

- Potretzke, Theodora A., Benjamin R. Tan, Maria B. Doyle, Elizabeth M. Brunt, Jay P. Heiken, et Kathryn J. Fowler. 2016. « Imaging Features of Biphenotypic Primary Liver Carcinoma (Hepatocholangiocarcinoma) and the Potential to Mimic Hepatocellular Carcinoma: LI-RADS Analysis of CT and MRI Features in 61 Cases ». *AJR. American Journal of Roentgenology* 207 (1): 25-31. https://doi.org/10.2214/AJR.15.14997.

- Ramai, Daryl, Andrew Ofosu, Jonathan K. Lai, Madhavi Reddy, et Douglas G. Adler. 2019. « Combined Hepatocellular Cholangiocarcinoma: A Population-Based Retrospective Study ». *The American Journal of Gastroenterology* 114 (9): 1496-1501. https://doi.org/10.14309/ajg.0000000000000326.

- Rebours, Vinciane, Julie Le Faouder, Samira Laouirem, Mounya Mebarki, Miguel Albuquerque, Jean-Michel Camadro, Thibaut Léger, et al. 2014. « In Situ Proteomic Analysis by MALDI Imaging Identifies Ubiquitin and Thymosin-B4 as Markers of Malignant Intraductal Pancreatic Mucinous Neoplasms ». *Pancreatology: Official Journal of the International Association of Pancreatology (IAP) ... [et Al.]* 14 (2): 117-24. https://doi.org/10.1016/j.pan.2013.12.001.

- Renzulli, Matteo, Daryl Ramai, Jameel Singh, Samridhi Sinha, Nicolò Brandi, Anna Maria Ierardi, Elisa Albertini, Rodolfo Sacco, Antonio Facciorusso, et Rita Golfieri. 2021. « Locoregional Treatments in Cholangiocarcinoma and Combined Hepatocellular Cholangiocarcinoma ». *Cancers* 13 (13): 3336. https://doi.org/10.3390/cancers13133336.

- Rizvi, Sumera, Shahid A. Khan, Christopher L. Hallemeier, Robin K. Kelley, et Gregory J. Gores. 2017. « Cholangiocarcinoma — evolving concepts and therapeutic strategies ». *Nature Reviews Clinical Oncology* 15 (octobre): 95.

- Rosenberg, Nofar, Matthias Van Haele, Tali Lanton, Neta Brashi, Zohar Bromberg, Hanan Adler, Hilla Giladi, et al. 2022. « Combined Hepatocellular-Cholangiocarcinoma Derives from Liver Progenitor Cells and Depends on Senescence and IL6 Trans-Signaling ». *Journal of Hepatology*, août, S0168-8278(22)02995-6. https://doi.org/10.1016/j.jhep.2022.07.029.

- Roskams, Tania A., Louis Libbrecht, et Valeer J. Desmet. 2003. « Progenitor Cells in Diseased Human Liver ». *Seminars in Liver Disease* 23 (4): 385-96. https://doi.org/10.1055/s-2004-815564.

- Roth, Lee, Swati Srivastava, Moshit Lindzen, Aldema Sas-Chen, Michal Sheffer, Mattia Lauriola, Yehoshua Enuka, et al. 2018. « SILAC Identifies LAD1 as a Filamin-Binding Regulator of Actin Dynamics in Response to EGF and a Marker of Aggressive Breast Tumors ». *Science Signaling* 11 (515): eaan0949. https://doi.org/10.1126/scisignal.aan0949.

- Sagrini, Elisabetta, Massimo Iavarone, Federico Stefanini, Francesco Tovoli, Sara Vavassori, Marco Maggioni, Matteo Renzulli, et al. 2019. « Imaging of Combined Hepatocellular-Cholangiocarcinoma in Cirrhosis and Risk of False Diagnosis of Hepatocellular Carcinoma ». *United European Gastroenterology Journal* 7 (1): 69-77. https://doi.org/10.1177/2050640618815378.

- Salimon, Maëva, Caroline Prieux-Klotz, David Tougeron, Vincent Hautefeuille, Morgane Caulet, Jérôme Gournay, Tamara Matysiak-Budnik, et al. 2018. « Gemcitabine plus Platinum-Based Chemotherapy for First-Line Treatment of Hepatocholangiocarcinoma: An AGEO French Multicentre Retrospective Study ». *British Journal of Cancer* 118 (3): 325-30. https://doi.org/10.1038/bjc.2017.413.

- Sangro, Bruno, Ignacio Melero, Samir Wadhawan, Richard S. Finn, Ghassan K. Abou-Alfa, Ann-Lii Cheng, Thomas Yau, et al. 2020. « Association of Inflammatory Biomarkers with Clinical Outcomes in Nivolumab-Treated Patients with Advanced Hepatocellular Carcinoma ». *Journal of Hepatology* 73 (6): 1460-69. https://doi.org/10.1016/j.jhep.2020.07.026.

- Sano, Hitoya, Manabu Futamura, Siqin Gaowa, Hiroki Kamino, Yasuyuki Nakamura, Kazuya Yamaguchi, Yoshihiro Tanaka, et al. 2020. « P53/Mieap-Regulated Mitochondrial Quality Control Plays an Important Role as a Tumor Suppressor in Gastric and Esophageal Cancers ». *Biochemical and Biophysical Research Communications* 529 (3): 582-89. https://doi.org/10.1016/j.bbrc.2020.05.168.

- Sapisochin, G., C. Rodríguez de Lope, M. Gastaca, J. Ortiz de Urbina, R. López-Andujar, F. Palacios, E. Ramos, et al. 2014. « Intrahepatic Cholangiocarcinoma or Mixed Hepatocellular-Cholangiocarcinoma in Patients Undergoing Liver Transplantation: A Spanish Matched Cohort Multicenter Study ». *Annals of Surgery* 259(5).https://journals.lww.com/annalsofsurgery/Fulltext/2014/05000/Intrahepatic_Cholangiocarcinoma_or_Mixed.17.aspx.

- Sapisochin, Gonzalo, Milind Javle, Jan Lerut, Masayuki Ohtsuka, Mark Ghobrial, Taizo Hibi, Nancy Man Kwan, et Julie Heimbach. 2020. « Liver Transplantation for Cholangiocarcinoma and Mixed Hepatocellular-Cholangiocarcinoma. Working Group Report from the ILTS Transplant Oncology Consensus Conference ». *Transplantation*, mars. https://doi.org/10.1097/TP.0000000000003212.

- Sasaki, M, Y Sato, et Y Nakanuma. 2022. « Is nestin a diagnostic marker for combined hepatocellular–cholangiocarcinoma? » *Histopathology* 80 (5): 859-68. https://doi.org/10.1111/his.14622.

- Sasaki, Motoko, Hirohide Sato, Yuko Kakuda, Yasunori Sato, Joon Hyuk Choi, et Yasuni Nakanuma. 2015. « Clinicopathological significance of 'subtypes with stem-cell feature' in combined hepatocellular-cholangiocarcinoma ». *Liver International* 35 (3): 1024-35. https://doi.org/10.1111/liv.12563.

- Sasaki, Motoko, Yasunori Sato, et Yasuni Nakanuma. 2017. « Mutational Landscape of Combined Hepatocellular Carcinoma and Cholangiocarcinoma, and Its Clinicopathological Significance ». *Histopathology* 70 (3): 423-34. https://doi.org/10.1111/his.13084.

- Sasaki, Motoko, Yasunori Sato, et Yasuni Nakanuma. 2019. « Cholangiolocellular Carcinoma With "Ductal Plate Malformation" Pattern May Be Characterized by ARID1A Genetic Alterations ». *The American Journal of Surgical Pathology* 43 (3): 352-60. https://doi.org/10.1097/PAS.0000000000001201.

- Sempoux, C. s. d. « Kakar S, Kondo F, Schirmacher P. Combined hepatocellular-cholangiocarcinoma and undifferentiated primary liver carcinoma. In: WHO Classification of Tumours: Digestive System Tumours, 5th, Arends MJ, Fukuyama M, Klimstra DS, et al (Eds), IARC, Lyon 2019. p.260. » .

- Smith, Andrew, Isabella Piga, Manuel Galli, Martina Stella, Vanna Denti, Marina Del Puppo, et Fulvio Magni. 2017. « Matrix-Assisted Laser Desorption/Ionisation Mass Spectrometry Imaging in the Study of Gastric Cancer: A Mini Review ». *International Journal of Molecular Sciences* 18 (12). https://doi.org/10.3390/ijms18122588.

- Sohoni, Sagar, Poorva Ghosh, Tianyuan Wang, Sarada Preeta Kalainayakan, Chantal Vidal, Sanchareeka Dey, Purna Chaitanya Konduri, et Li Zhang. 2019. « Elevated Heme Synthesis and Uptake Underpin Intensified Oxidative Metabolism and Tumorigenic Functions in Non-Small Cell Lung Cancer Cells ». *Cancer Research* 79 (10): 2511-25. https://doi.org/10.1158/0008-5472.CAN-18-2156.

- Stopka, Sylwia A., Laith Z. Samarah, Jared B. Shaw, Andrey V. Liyu, Dušan Veličković, Beverly J. Agtuca, Caroline Kukolj, et al. 2019. « Ambient Metabolic Profiling and Imaging of Biological Samples with Ultrahigh Molecular Resolution Using Laser Ablation Electrospray Ionization 21 Tesla FTICR Mass Spectrometry ». *Analytical Chemistry* 91 (8): 5028-35. https://doi.org/10.1021/acs.analchem.8b05084.

- Taguchi, J., O. Nakashima, M. Tanaka, T. Hisaka, T. Takazawa, et M. Kojiro. 1996. « A Clinicopathological Study on Combined Hepatocellular and Cholangiocarcinoma ». *Journal of Gastroenterology and Hepatology* 11 (8): 758-64. https://doi.org/10.1111/j.1440-1746.1996.tb00327.x.

- Takáts, Zoltán, Justin M. Wiseman, et R. Graham Cooks. 2005. « Ambient Mass Spectrometry Using Desorption Electrospray Ionization (DESI): Instrumentation, Mechanisms and Applications in Forensics, Chemistry, and Biology ». *Journal of Mass Spectrometry: JMS* 40 (10): 1261-75. https://doi.org/10.1002/jms.922.

- Tanaka, Koichi, Hiroaki Waki, Yutaka Ido, Satoshi Akita, Yoshikazu Yoshida, Tamio Yoshida, et Takekiyo Matsuo. 1988. « Protein and polymer analyses up to m/z 100 000 by laser ionization time-of-flight mass spectrometry ». *Rapid Communications in Mass Spectrometry* 2: 151-53.

- Tang, You-Yin, Yu-Nuo Zhao, Tao Zhang, Zhe-Yu Chen, et Xue-Lei Ma. 2021. « Comprehensive Radiomics Nomogram for Predicting Survival of Patients with Combined Hepatocellular Carcinoma and Cholangiocarcinoma ». *World Journal of Gastroenterology* 27 (41): 7173-89. https://doi.org/10.3748/wjg.v27.i41.7173.

- Theise, N., Nakashima, O., Park, Y.N., Nakanuma, Y. 2010. « Combined hepatocellular-cholangiocarcinoma ». *in: F.T. Bosman, F. Carnoiro, R.H. Hruba, N.D. Theise (Eds.) WHO classification of tumors of the digestive system.* IARC Press, Lyon; 2010:225–227.

- Trikalinos, Nikolaos A., Amy Zhou, Maria B. Majella Doyle, Kathryn J. Fowler, Ashley Morton, Neeta Vachharajani, Manik Amin, et al. 2018. « Systemic Therapy for Combined Hepatocellular-Cholangiocarcinoma: A Single-Institution Experience ». *Journal of the National Comprehensive Cancer Network: JNCCN* 16 (10): 1193-99. https://doi.org/10.6004/jnccn.2018.7053.

- Tschaharganeh, Darjus F., Wen Xue, Diego F. Calvisi, Matthias Evert, Tatyana V. Michurina, Lukas E. Dow, Ana Banito, et al. 2016. « P53-Dependent Nestin Regulation Links Tumor Suppression to Cellular Plasticity in Liver Cancer ». *Cell* 165 (6): 1546-47. https://doi.org/10.1016/j.cell.2016.05.058.

- Wang, Anqiang, Liangcai Wu, Jianzhen Lin, Longzhe Han, Jin Bian, Yan Wu, Simon C. Robson, et al. 2018. « Whole-exome sequencing reveals the origin and evolution of hepato-cholangiocarcinoma ». *Nature Communications* 9 (1): 894. https://doi.org/10.1038/s41467-018-03276-y.

- Wang, Xiaodong, Jun Han, Jingxi Pan, et Christoph H. Borchers. 2014. « Comprehensive Imaging of Porcine Adrenal Gland Lipids by MALDI-FTMS Using Quercetin as a Matrix ». *Analytical Chemistry* 86 (1): 638-46. https://doi.org/10.1021/ac404044k.

- Wells, H Gideon. 1903. « PRIMARY CARCINOMA OF THE LIVER. » *The American Journal of the Medical Sciences (1827-1924)* 126 (3): 403.

- Wells, Michael L., Sudhakar K. Venkatesh, Vishal S. Chandan, Jeff L. Fidler, Joel G. Fletcher, Geoffrey B. Johnson, David M. Hough, et Lewis R. Roberts. 2015. « Biphenotypic hepatic tumors: imaging findings and review of literature ». *Abdominal Imaging* 40 (7): 2293-2305. https://doi.org/10.1007/s00261-015-0433-9.

- Willekens, Inneke, Anne Hoorens, Caroline Geers, Bart Op de Beeck, Frederik Vandenbroucke, et Johan de Mey. 2009. « Combined hepatocellular and cholangiocellular carcinoma presenting with radiological characteristics of focal nodular hyperplasia ». *World Journal of Gastroenterology : WJG* 15 (31): 3940-43. https://doi.org/10.3748/wjg.15.3940.

- Xue, Ruidong, Lu Chen, Chong Zhang, Masashi Fujita, Ruoyan Li, Shu-Mei Yan, Choon Kiat Ong, et al. 2019. « Genomic and Transcriptomic Profiling of Combined Hepatocellular and Intrahepatic Cholangiocarcinoma Reveals Distinct Molecular Subtypes ». *Cancer Cell* 35 (6): 932-947.e8. https://doi.org/10.1016/j.ccell.2019.04.007.

- Yano, H., A. Iemura, M. Haramaki, S. Momosaki, S. Ogasawara, K. Higaki, et M. Kojiro. 1996. « A Human Combined Hepatocellular and Cholangiocarcinoma Cell Line (KMCH-2) That Shows the Features of Hepatocellular Carcinoma or Cholangiocarcinoma under Different Growth Conditions ». *Journal of Hepatology* 24 (4): 413-22. https://doi.org/10.1016/s0168-8278(96)80161-9.

- Yeh, Matthew M. 2010. « Pathology of Combined Hepatocellular-Cholangiocarcinoma ». *Journal of Gastroenterology and Hepatology* 25 (9): 1485-92. https://doi.org/10.1111/j.1440-1746.2010.06430.x.

- Yoh, Tomoaki, François Cauchy, et Olivier Soubrane. 2020. « Oncological Resection for Liver Malignancies: Can the Laparoscopic Approach Provide Benefits? » *Annals of Surgery*, mars. https://doi.org/10.1097/SLA.0000000000003851.

- Yoon, Young-In, Shin Hwang, Young-Joo Lee, Ki-Hun Kim, Chul-Soo Ahn, Deok-Bog Moon, Tae-Yong Ha, et al. 2016. « Postresection Outcomes of Combined Hepatocellular Carcinoma-Cholangiocarcinoma, Hepatocellular Carcinoma and Intrahepatic Cholangiocarcinoma ». *Journal of Gastrointestinal Surgery: Official Journal of the Society for Surgery of the Alimentary Tract* 20 (2): 411-20. https://doi.org/10.1007/s11605-015-3045-3.

- Zen, Chikako, Yoh Zen, Ragai R. Mitry, Denis Corbeil, Jana Karbanová, John O'Grady, John Karani, et al. 2011. « Mixed Phenotype Hepatocellular Carcinoma after Transarterial Chemoembolization and Liver Transplantation ». *Liver Transplantation: Official Publication of the American Association for the Study of Liver Diseases and the International Liver Transplantation Society* 17 (8): 943-54. https://doi.org/10.1002/lt.22314.

- Zhao, Yalei, Xiaoyun Zhang, Yabin Liu, Yiping Ma, Pong Kong, Tianliang Bai, Mei Han, et Binghui Li. 2020. « Inhibition of ALAS1 Activity Exerts Anti-Tumour Effects on Colorectal Cancer in Vitro ». *Saudi Journal of Gastroenterology: Official Journal of the Saudi Gastroenterology Association* 26 (3): 144-52. https://doi.org/10.4103/sjg.SJG_477_19.

- Zhou, Yan, Shanshan Yin, Lin Zhao, Xiang Zhang, Meng Li, Jianmin Ding, Kun Yan, et Xiang Jing. 2022. « CEUS and CT/MRI LI-RADS in Association With Serum Biomarkers for Differentiation of Combined Hepatocellular-Cholangiocarcinoma From Hepatocellular Carcinoma ». *Frontiers in Oncology* 12: 897090. https://doi.org/10.3389/fonc.2022.897090.

- Zhou, Yan-Ming, Xiao-Feng Zhang, Lu-Peng Wu, Cheng-Jun Sui, et Jia-Mei Yang. 2014. « Risk factors for combined hepatocellular-cholangiocarcinoma: A hospital-based case-control study ». *World Journal of Gastroenterology : WJG* 20 (35): 12615-20. https://doi.org/10.3748/wjg.v20.i35.12615.

- Zou, Xianlun, Yan Luo, John N. Morelli, Xuemei Hu, Yaqi Shen, et Daoyu Hu. 2021. « Differentiation of Hepatocellular Carcinoma from Intrahepatic Cholangiocarcinoma and Combined Hepatocellular-Cholangiocarcinoma in High-Risk Patients Matched to MR Field Strength: Diagnostic Performance of LI-RADS Version 2018 ». *Abdominal Radiology (New York)* 46 (7): 3168-78. https://doi.org/10.1007/s00261-021-02996-y.

9 FIGURES AND TABLES LIST

Figure list

Figure 1: Prevalence and macroscopical appearance of cHCC-CCA 16
Figure 2: Macroscopic and microscopic features of iCCA and HCC. 19
Figure 3: Macroscopic and microscopic features of cHCC-CCA. 20
Figure 4: Combined liver cells and bile ducts carcinoma 21
Figure 5: Combined liver cells and bile ducts carcinoma. 22
Figure 6: Type I combined Hepatocellular-choangiocarcinoma 23
Figure 7: Histological relationships between PLCs. 25
Figure 8: Immunohistochemistry. 28
Figure 9: Nestin as a diagnostic marker. 28
Figure 10: Imaging features of cHCC-CCA 31
Figure 11: Mutational spectrum of cHCC-CCA, courtesy of Pr. Paradis 45
Figure 12: Mechanisms of tumor heterogeneity, from Hu et al. 46
Figure 13: Prognostic impact of cHCC-CCA immune subtype. 47
Figure 14: cHCC-CCA derives from liver progenitor cells 48
Figure 15: Combined Hepato-Cholangiocarcinoma in a glimpse 50
Figure 16: Different Ionization Techniques 53
Figure 17: Ionization process in MALDI acquisitions 56
Figure 18: Time-of-flight principle 57
Figure 19: Hierarchical clustering analysis (Segmentation) 60
Figure 20: Principal component analysis (PCA) 61
Figure 21: t-SNE. 61
Figure 22: Mass spectrometry imaging (MSI) data elaboration workflow. 62
Figure 23: MALDI workflow. 69
Figure 24: Graphical abstract. 103
Figure 25: Segmentation analysis. 108
Figure 26: Segmentation, division in four clusters. 108
Figure 27: Pathological labelling of 5 cHCC-CCA 109
Figure 28: Principal component analysis. Component 1 and 2. 110
Figure 29: Comparison of tryptic peptides derived from current IHC markers 111
Supplementary Figure 30: Segmentation, division in four clusters. All cases 115
Supplementary Figure 31: Comparison of a selection of tryptic peptides 116
Supplementary Figure 32: Mascot Score Histogram 117
Figure 33: Tissue selection 122
Figure 34: Tissue microarray construction 123
Figure 35: RapifleX MALDI Proteopath Laboratory, Trier, Germany 125
Figure 36: AutofleX III MALDI Inserm U1149, Clichy, France 127
Figure 37: TMA analysis. Complete dataset. Optical scanner image. 132
Figure 38: Clustering analysis, segmentation 133
Figure 39: Linear Discriminant Analysis (LDA) Classification Model applied to data 134
Figure 40: Correlation between PCA and segmentation in controls TMA 135
Figure 41: PCA of TMA 92 and 93 136
Figure 42: Peak alignment and segmentation 137
Figure 43: TMA layout after revisions. 138
Figure 44: Exhaustive review of controls and identification of subtypes of interest 139
Figure 45: Analysis of controls spectra distribution after revision and 2D PCA 140

Figure 46: PCA of iCCA subtypes 141
Figure 47: PCA in HCC controls 141
Figure 48: New annotation of cHCC-CCA on optical scanner image. 143
Figure 49: Number of differential peaks between the different cancer subtypes. 144
Figure 50: Correlation analysis of subtypes with HCC and iCCA, separated vision 145
Figure 51: Segmentation analysis including TMA 185 146
Figure 52: Number of differential peaks between with TMA 185 147
Figure 53: PCA with TMA 185 148
Figure 54: ROC curves of discriminant peaks between MT-iCCA vs CT-iCCA 149
Figure 55: Univariable analysis 150
Figure 56: Kaplan-Meier curve of Pk_1504.661 151
Figure 57: Kaplan-Meier curve of Pk 1140.534 152

Table list

Table 1: Risk factors of hepatocholangiocarcinoma. Adapted from (Gigante et al. 2021).. 18
Table 2: Different classifications of hepatocholangiocarcinoma 26
Table 3: Genomic alterations in hepatocholangiocarcinomas 49
Table 4: Comparison of histology, immunohistochemistry, and MALDI imaging. 65
Table 5: Clinical and pathological features of patients 107
Supplementary Table 6: Immunoistochemistry list 117
Supplementary Table 7: List of proteins with a protein score > 56 117
Table 8: Patients characteristics and relative percentage 129
Table 9: Immunohistochemistry staining and relative percentage of positivity 131
Table 10: Immunohistochemistry staining, relative positivity 131
Table 11: Discriminating ROC curve shown for cHCC-HCC TMA, ROC with AUC >0.75 142
Table 12: Discriminating ROC curve shown for cHCC-HCC TMA, ROC with AUC <0.25 142
Table 13: Uni and multivariable analysis of peaks of interest 150
Table 14: Uni and multivariable analysis excluding transplanted patients. 151

10 LISTE DES ÉLÉMENTS SOUS DROITS

Liste de **tous les éléments retirés** de la version complète de la thèse faute d'en détenir les droits

Figure list

Figure 1: Prevalence and macroscopical appearance of cHCC-CCA 16
Figure 2: Macroscopic and microscopic features of iCCA and HCC. 19
Figure 3: Macroscopic and microscopic features of cHCC-CCA. 20
Figure 4: Combined liver cells and bile ducts carcinoma 21
Figure 5: Combined liver cells and bile ducts carcinoma. 22
Figure 6: Type I combined Hepatocellular-choangiocarcinoma 23
Figure 7: Histological relationships between PLCs. 25
Figure 8: Immunohistochemistry. 28
Figure 9: Nestin as a diagnostic marker. 28
Figure 10: Imaging features of cHCC-CCA 31
Figure 12: Mechanisms of tumor heterogeneity, from Hu et al. 46
Figure 13: Prognostic impact of cHCC-CCA immune subtype. 47
Figure 14: cHCC-CCA derives from liver progenitor cells 48
Figure 15: Combined Hepato-Cholangiocarcinoma in a glimpse 50
Figure 16: Different Ionization Techniques 53
Figure 17: Ionization process in MALDI acquisitions 56
Figure 18: Time-of-flight principle 57
Figure 21: t-SNE. 61
Figure 22: Mass spectrometry imaging (MSI) data elaboration workflow. 62
Figure 23: MALDI workflow. 69

Articles list

Article 1: Combining imaging and tumor biopsy improves the diagnosis of combined hepatocellular-cholangiocarcinoma (Published) 76-86

Article 2: Systemic treatments with tyrosine kinase inhibitor and platinum based chemotherapy in patients with unresectable or metastatic hepatocholangiocarcinoma (Published) 88-101

11 TABLE OF CONTENTS

1 LIST OF ABBREVIATIONS 5

2 ABSTRACTS 6

2.1 Résumé en Français 6

2.2 Abstract in English 8

2.3 Résumé détaillé en Français 10

3 INTRODUCTION 16

3.1 Epidemiology, classification and diagnosis of combined hepatocellular-cholangiocarcinoma 16

3.1.1 Epidemiology 16

3.1.1.1 Incidence and prevalence 17

3.1.1.2 Risk factors 17

3.1.2 Pathological characterization of cHCC-CCA 19

3.1.2.1 Histological diagnosis 27

3.1.2.2 Pathological tools useful for diagnosis 27

3.1.3 Main clinical manifestations of cHCC-CCA 29

3.1.4 Biochemical elements of the characterization of cHCC-CCA 30

3.1.4.1 Alpha-phoetoprotein and CA 19.9 30

3.1.5 cHCC-CCA characterization by imaging 30

3.1.5.1 Computed tomography (CT) and Magnetic Resonance Imaging (MRI) 30

3.1.5.2 Contrast-enhanced ultrasound 33

3.1.5.3 Artificial intelligence in radiology 33

3.2 Treatment of cHCC-CCA 34

3.2.1 Surgery 34

3.2.1.1 Liver resection. 34

3.2.1.2 Liver transplantation 37

3.2.2 Locoregional treatments 38

3.2.2.1 Intra-arterial treatments and percutaneous ablations 38

3.2.3 Treatment of advanced or metastatic cHCC-CCA 39

3.2.3.1 Platinum based chemotherapy 40

3.2.3.2 Oral targeted therapies 40

3.3 Conclusion, clinical aspects. 41

3.4 Heterogeneity of cHCC-CCA 42

3.4.1 Genetic landscape of cHCC-CCA 42

3.4.1.1 Molecular alterations 42

3.4.2 Intratumoral heterogeneity 43

3.4.3 Heterogeneity and cancer 45

3.4.4 New insights in cHCC-CCAs pathological mechanisms 46

3.5 General conclusions (genetics) 48

3.6 Mass spectrometry 51

3.6.1 Technological aspects 51

3.6.2 Treatment of biological samples 53

3.6.3 Matrix 55

3.6.4 The analyzers 56

3.6.5 Time-of-flight principle 56

3.6.6 Detectors in mass spectrometry 57

3.6.7 Data processing 58

3.6.8 Normalization of raw data. 58

3.6.9 Mathematical approaches in data analysis 59

3.7 MALDI imaging and tumors 63
3.7.1 MALDI imaging applications in oncology 64
3.7.2 MALDI imaging in heterogenous tissues 66
3.7.3 MALDI imaging in less heterogenous tissues, TMA approach 67
3.7.4 MALDI imaging approach in digestive cancers 70
3.7.5 Unsolved issues 73

3.8 Conclusion about MALDI and cancers 74

4 RESULTS FIRST AXIS: Improving the diagnosis of cHCC-CCA 75

Article 1: Combining imaging and tumor biopsy improves the diagnosis of combined hepatocellular-cholangiocarcinoma (Published) 75

5 RESULTS SECOND AXIS: Improving the management of systemic therapy of unresectable or metastatic cHCC-CCAs. 87

Article 2: Systemic treatments with tyrosine kinase inhibitor and platinum-based chemotherapy in patients with unresectable or metastatic hepatocholangiocarcinoma (Published) 87

6 RESULTS THIRD AXIS: Exhaustive molecular characterization of cHCC-CCA by MALDI imaging 102

6.1 Article: MALDI imaging, a multiplex approach without a priori, is a powerful tool for deciphering intra-tumoral heterogeneity: combined hepato-cholangiocarcinomas as proof of concept (In preparation) 102

6.2 MSI on TMAs of cHCC-CCA 119
6.2.1 Objectives 119
6.2.2 Materials and methods 119
6.2.2.1 Patients and Tumors 119
6.2.2.2 Case selection and pathological analysis 120
6.2.2.3 Immunohistochemistry 120
6.2.2.4 TMA construction 121
6.2.2.5 TMA analysis by mass spectrometry imaging 123
6.2.2.6 Statistical analysis 127
6.2.3 Results: 129
6.2.3.1 Clinical and histological data. 129
6.2.3.2 MALDI dataset analysis 132
6.2.4 Conclusion-1 134
6.2.4.1 Quality control of MALDI dataset 135
6.2.4.2 New tissue revision 138
6.2.4.3 Differential peaks (cHCC-CCA, HCC and iCCA after quality control and new labelling) 142
6.2.4.4 Further annotation of cHCC-CCA samples 143
6.2.4.5 Addition of new controls for data validation 146
6.2.4.6 Survival analysis 150
6.2.5 Conclusions-2 153

7 GENERAL CONCLUSIONS 154

8 BIBLIOGRAPHY 155

9 FIGURES AND TABLES LIST 177

10 LISTE DES ÉLÉMENTS SOUS DROITS 179

11 TABLE OF CONTENTS 180